

**CALCULATION OF THE DROOP PARAMETERS FOR  
MICROGRIDS WITH DIFFERENT INVERTERS' RATINGS AND  
FEEDERS' LENGTHS**

**Mohammad Ali Aghasafari**

**A Thesis  
in  
The Department  
of  
Electrical and Computer Engineering**

**Presented in Partial Fulfillment of the Requirements  
for the Degree of Master of Applied Science at  
Concordia University  
Montréal, Québec, Canada**

**April 2010**

**© Mohammad Ali Aghasafari, 2010**



Library and Archives  
Canada

Published Heritage  
Branch

395 Wellington Street  
Ottawa ON K1A 0N4  
Canada

Bibliothèque et  
Archives Canada

Direction du  
Patrimoine de l'édition

395, rue Wellington  
Ottawa ON K1A 0N4  
Canada

*Your file* *Votre référence*  
ISBN: 978-0-494-67222-8  
*Our file* *Notre référence*  
ISBN: 978-0-494-67222-8

**NOTICE:**

The author has granted a non-exclusive license allowing Library and Archives Canada to reproduce, publish, archive, preserve, conserve, communicate to the public by telecommunication or on the Internet, loan, distribute and sell theses worldwide, for commercial or non-commercial purposes, in microform, paper, electronic and/or any other formats.

The author retains copyright ownership and moral rights in this thesis. Neither the thesis nor substantial extracts from it may be printed or otherwise reproduced without the author's permission.

**AVIS:**

L'auteur a accordé une licence non exclusive permettant à la Bibliothèque et Archives Canada de reproduire, publier, archiver, sauvegarder, conserver, transmettre au public par télécommunication ou par l'Internet, prêter, distribuer et vendre des thèses partout dans le monde, à des fins commerciales ou autres, sur support microforme, papier, électronique et/ou autres formats.

L'auteur conserve la propriété du droit d'auteur et des droits moraux qui protègent cette thèse. Ni la thèse ni des extraits substantiels de celle-ci ne doivent être imprimés ou autrement reproduits sans son autorisation.

---

In compliance with the Canadian Privacy Act some supporting forms may have been removed from this thesis.

While these forms may be included in the document page count, their removal does not represent any loss of content from the thesis.

Conformément à la loi canadienne sur la protection de la vie privée, quelques formulaires secondaires ont été enlevés de cette thèse.

Bien que ces formulaires aient inclus dans la pagination, il n'y aura aucun contenu manquant.

  
**Canada**

# ABSTRACT

---

## **Calculation of Droop Parameters for Microgrids with Different Inverter Ratings and Feeder Lengths**

**Mohammad Ali Aghasafari**

A microgrid is a local electricity network with several distributed energy systems. Different strategies of power sharing in distributed generation are reviewed and the droop control approach for inverter based distributed generators is selected for further investigation due to its low cost and potential for performance enhancement. The inverters in a microgrid with droop control use a wireless control system which doesn't have any intercommunication cost and is not distorted by electromagnetic interferences. The control system is extendable to any number of distributed sources. Proper power sharing, which enables the energy sources (with energy storage units) to provide powers proportional to their apparent rated powers, is a very important property of the system. Hence, the collection of the distributed sources can deliver their maximum powers when there is full load demand, without overloading some and underutilizing others. The conventional droop control doesn't result in proper power sharing; especially when the sources have different rated powers or the feeders are unbalanced (have different impedances). This drawback has not been fixed in the other publications; either by using the power sources with equal apparent power or by ignoring the improper power sharing ratio. Also in some publications, there have been some poor load voltage regulations. In this thesis, a modified droop system has been used which will result in appropriate power sharing and load voltage regulation. Furthermore, the effects of the sources' voltages'

magnitude, phase angle, and frequency on the system power sharing are considered. Moreover, the influences of the droop system's parameters on system's behaviour were evaluated in different cases of sources' apparent powers ratio and feeders' lengths ratio and a general rule is presented which shows how to choose the droop parameters for any isolated microgrid's control system.

## ACKNOWLEDGMENTS

---

The author would like to express his sincere gratitude to his supervisors, Dr. Luiz A. C. Lopes and Dr. Sheldon S. Williamson, for their invaluable guidance, and advice throughout the course of this research. The author would also like to thank them for their arrangements for financial support from the Natural Science and Engineering Research Council (NSERC) and the Solar Buildings Research Network (SBRN). The author would like to thank these organizations too.

The author would like to sincerely thank Mr. Joseph Woods for his technical support and dedication. The author would also like to thank his colleagues in the P. D. Ziogas Power Electronics Laboratory, Maged Barsom, Naeem Ninad, Arbi Gharakhani, and Reinaldo Tonkoski, for their helpful suggestions.

Last but not least, the author is very thankful towards his parents whose constant financial and spiritual supports made it possible to finish the project.

# TABLE OF CONTENTS

---

<b>LIST OF FIGURES .....</b>	<b>VIII</b>
<b>LIST OF TABLES.....</b>	<b>XII</b>
<b>LIST OF ACRONYMS.....</b>	<b>XIII</b>
<b>LIST OF PRINCIPAL SYMBOLS.....</b>	<b>XV</b>
<b>CAPTER 1 INTRODUCTION .....</b>	<b>1</b>
1.1 BACKGROUND.....	1
1.2 INTEGRATION OF ENERGY SOURCES.....	3
1.2.1 DISTRIBUTED GENERATION CONTROL CHEMES .....	4
1.3 OBJECTIVES AND CHALLENGES.....	6
1.4 CONTRIBUTION OF THE THESIS.....	7
<b>CHAPTER 2 SYSTEM WITH THE BASIC DROOP TECHNIQUE .....</b>	<b>10</b>
2.1 INTRODUCTION.....	10
2.2 SYSTEM POWERS' DEPENDENCY ON SYSTEM PARAMETERS .....	10
2.2.1 SYSTEM POWER EQUATIONS .....	11
2.2.2 EVALUATION OF THE EFFECTS OF SOURCES' PARAMETERS ON SYSTEM POWERS.....	12
2.2.2.1 SYSTEM POWER FLOW GRAPHS FOR THE PLANE OF $(\mathbf{E}_1 _{,1})$ .....	12
2.2.2.2 SYSTEM POWER FLOW GRAPHS FOR THE $(\mathbf{E}_1, \mathbf{E}_2)$ PLANE.....	21
2.2.2.3 SYSTEM POWER FLOW GRAPHS FOR THE PLANE OF $(\varphi_1, F)$ .....	25
2.3. BASIC DROOP LOOP.....	30
2.4 SYSTEM TRANSIENT AND STEADY STATE BEHAVIOR.....	32
2.5 CONCLUSION.....	36
<b>CHAPTER 3 PROPOSED DROOP SYSTEM .....</b>	<b>38</b>
3.1 INTRODUCTION.....	38
3.2 THE STRUCTURE OF THE PROPOSED DROOP SYSTEM.....	39
3.3 EVALUATION OF THE EFFECTS OF DROOP PARAMETERS ON SYSTEM TRANSIENT AND STEADY STATE BEHAVIOR.....	41
3.4 OPTIMUM DROOP COEFFICIENTS FOR DIFFERENT SYSTEM TYPES.....	47
3.4.1 SYSTEM BEHAVIOR ( $LENGTH2 = (LENGTH1), S1=S2$ ).....	47

3.4.2 SYSTEM WITH ( $LENGTH2 = LENGTH1, S1=2S2$ ) .....	51
3.4.3 SYSTEM WITH $LENGTH2 = (LENGTH1)/3, S1=2S2$ .....	57
3.4.4 SYSTEM WITH ( $LENGTH2 = (LENGTH1)/3, S1=S2$ ) .....	62
3.5 CONCLUSION.....	68
<b>CHAPTER 4 SYSTEM WITH COMPLETE BENCHMARK AND CONTROL ELEMENTS.....</b>	<b>70</b>
4.1 INTRODUCTION.....	70
4.3 CONTROL ELEMENTS.....	74
4.3.1 GATING SYSTEM .....	75
4.3.2 CURRENT LOOP.....	75
4.3.3 VOLTAGE LOOP .....	76
4.3.3.1 DESIGN OF THE VOLTAGE CONTROLLER.....	76
4.3.4 DROOP LOOP .....	80
4.3.5 POWER CALCULATORS .....	80
4.4 SIMULATION RESULTS FOR THE COMPLETE SYSTEM.....	81
4.4.1 TWO SOURCES WITH A LINEAR LOAD WHICH CHANGES.....	82
<b>CHAPTER 5 CONCLUSION.....</b>	<b>90</b>
5.1 SUMMARY.....	90
5.2 SUGGESTIONS FOR FUTURE WORK.....	93
<b>REFERENCES.....</b>	<b>94</b>

## LIST OF FIGURES

<b>Fig. 1-1</b> A microgrid .....	2
<b>Fig. 2-1</b> Simplified power stage of the system .....	11
<b>Fig. 2-2</b> Changes in Q1 (VAR) as the peak magnitude and phase angle of the first source change.. .....	13
<b>Fig. 2-3</b> Three dimensional view of changes in Q1(VAR) as the magnitude and phase angle of the first source change.....	14
<b>Fig. 2-4</b> Three dimensional view of changes in Q2(VAR) as the magnitude and phase angle of the first source change .....	14
<b>Fig. 2-5</b> Changes in Q2(VAR) as the magnitude and phase angle of the first source change .....	15
<b>Fig. 2-6</b> Three dimensional view of changes in Q1 & Q2 (VAR) as the magnitude and phase angle of the first source change.....	16
<b>Fig. 2-7</b> Three dimensional curve of the region in which $Q1=Q2$ , ( $ E_2  = 120V$ , $\varphi_2=0$ )...17	17
<b>Fig. 2-8</b> Two dimensional curve of the region in which $Q1=Q2$ with $ E_2  = 120V$ and $\varphi_2=0$ .....	17
<b>Fig. 2-9</b> Changes in P1 (W) as the magnitude and phase angle of the first source change.....	18
<b>Fig. 2-10</b> Changes in P2 (W) as the magnitude and phase angle of the first source change.....	19
<b>Fig. 2-11</b> Changes in P1 & P2 (W) as the magnitude and phase angle of the first source change.....	19
<b>Fig. 2-12</b> Three dimensional curve of the region in which $P1=P2$ .....	20
<b>Fig. 2-13</b> Two dimensional curve of the region in which $P1=P2$ .....	20
<b>Fig. 2-14</b> Changes in Q1 (VAR) as the magnitudes of sources' voltages change.....	21
<b>Fig. 2-15</b> Changes in Q2 (VAR) as the magnitudes of sources' voltages change.....	22
<b>Fig. 2-16</b> Changes in Q1 & Q2 (VAR) as the magnitudes of sources' voltages change...23	23
<b>Fig. 2-17</b> Changes in P1 (W) as the magnitudes of sources' voltages change .....	23
<b>Fig. 2-18</b> Changes in P2 (W) as the magnitudes of sources' voltages change .....	24
<b>Fig. 2-19</b> Changes in P1 & P2 (W) as the magnitudes of sources' voltages change.....	25

<b>Fig. 2-20</b> Changes in Q1(VAR) as the system's frequency and the first source' phase angle change.....	26
<b>Fig. 2-21</b> Changes in Q2(VAR) as the system's frequency and the first source's phase angle change.....	26
<b>Fig. 2-22</b> Changes in Q1 & Q2(VAR) as the system's frequency and the first source's phase angle change .....	27
<b>Fig. 2-23</b> Changes in P1(W) as the system's frequency and the first source's phase angle change.....	28
<b>Fig. 2-24</b> Changes in P2(W) as the system's frequency and the first source's phase angle change.....	28
<b>Fig. 2-25</b> Changes in P1 & P2(W) as the system's frequency and the first source's phase angle change.....	29
<b>Fig. 2-26</b> Power system schematic.....	33
<b>Fig. 2-27</b> Control system schematic.....	33
<b>Fig. 2-28</b> System powers changes as the load decreases by 20% at t= 0.8s.....	34
<b>Fig. 2-29</b> System voltages' changes as the load decrease by 20% at t=0.8s .....	35
<b>Fig. 2-30</b> Sources' frequencies' changes as the load decreases by 20% at t=0.8s .....	35
<b>Fig. 3-1</b> Simplified split system's circuit using the equivalent loads .....	40
<b>Fig. 3-2</b> System's powers as the load decreases by 20%.....	42
<b>Fig. 3-3</b> Effect of $\beta$ on system over shoot.....	43
<b>Fig. 3-4</b> Very small changes in settling time vs. changes in $\beta$ .....	44
<b>Fig. 3-5</b> Effect of $\beta$ on reactive power sharing .....	44
<b>Fig. 3-6</b> Changes in settling time vs. changes in $\alpha$ .....	45
<b>Fig. 3-7</b> Effect of $\alpha$ on system over shoot .....	46
<b>Fig. 3-8</b> System frequencies response as the load decreases by 20% at t=1s.....	48
<b>Fig. 3-9</b> Effect of $\beta$ on system's over(under)shoot.....	49
<b>Fig. 3-10</b> Effect of $\beta$ on system's settling time.....	49
<b>Fig. 3-11</b> Effects of $\alpha$ on system's overshoot percentage .....	50
<b>Fig. 3-12</b> System frequencies response as the load decreases by 20%.....	52
<b>Fig. 3-13</b> Effects of $\beta$ on system's over(under)shoot .....	53
<b>Fig. 3-14</b> Effects of $\beta$ on system's settling time .....	53
<b>Fig. 3-15</b> Effects of $\beta$ on system's Q sharing ratio .....	54

<b>Fig. 3-16</b> Effects of $\alpha$ on the system's settling time .....	55
<b>Fig. 3-17</b> Effects of $\alpha$ on the system's overshoot percentage .....	55
<b>Fig. 3-18</b> The effects of $CF_1$ on the system's settling time and Q sharing ratio .....	56
<b>Fig. 3-19</b> System voltages as the load decreases by 20% at $t=1s$ .....	58
<b>Fig. 3-20</b> The influence of $\beta$ on system's settling time .....	59
<b>Fig. 3-21</b> The influence of $\beta$ on system's Q sharing ratio .....	59
<b>Fig. 3-22</b> Effect of $\alpha$ on the system's settling time .....	60
<b>Fig. 3-23</b> Effect of $\alpha$ on the system's overshoot percentage .....	61
<b>Fig. 3-24</b> System's frequency's overshoot percentage as $\beta$ changes .....	63
<b>Fig. 3-25</b> System's settling time as $\beta$ changes .....	64
<b>Fig. 3-26</b> System's Q sharing ratio as $\beta$ changes .....	64
<b>Fig. 3-27</b> The influences of $\alpha$ on the system's settling time .....	65
<b>Fig. 3-28</b> The influences of $\alpha$ on the system's overshoot percentage .....	66
<b>Fig. 4-1</b> Power stage of the system. ....	71
<b>Fig. 4-2</b> Magnitude (on top) and phase (at the bottom) of the LPF's output voltage's main harmonic's transfer function .....	72
<b>Fig. 4-3</b> Schematic diagram of control system .....	73
<b>Fig. 4-4</b> Voltage open and closed loop control systems characteristics .....	77
<b>Fig. 4-5</b> Sources' reference and actual voltages before and after a change in $V_{ref1}$ .....	78
<b>Fig. 4-6</b> Sources' output voltages' errors .....	79
<b>Fig. 4-7</b> Active Power Calculator .....	80
<b>Fig. 4-8</b> Steady state system results before the load change .....	81
<b>Fig. 4-9</b> System's transient behavior after the 20% load decrement (for the graph on top, waveforms from the top to the bottom: P1, Q1, P2, Q2), (for the graph at the middle: $f_{ref1}$ has overshoot and $f_{ref2}$ has undershoot at the beginning) .....	82
<b>Fig. 4-10</b> System's powers (on top) and sources' voltage's peaks (at the bottom) before and after the disconnection of source2 from the network .....	84
<b>Fig. 4-11</b> System's sources' frequencies .....	85
<b>Fig. 4-12</b> Sources' output voltages and load voltage (on top) and also feeders' currents (at the bottom) .....	85
<b>Fig. 4-13</b> The variations of the peak value of the load voltage .....	86

**Fig. 4-14** Load and feeders' currents (on top) and also sources output and load voltages  
(at the bottom).....87

## LIST OF TABLES

---

Table 2-1 Benchmark Model Power parameters .....	10
Table 3-1 Power system Characteristics .....	39
Table 3-2 Effects of $\beta$ on system's behavior .....	42
Table 3-3 Effects of $\alpha$ on system's behavior .....	45
Table 3-4 Power system Characteristics .....	47
Table 3-5 The effects of $\beta$ on system behavior .....	48
Table 3-6 Effects of $\alpha$ on system's behavior .....	50
Table 3-7 Power system Characteristics .....	51
Table 3-8 System simulation results when $\beta$ changes .....	52
Table 3-9 Effects of $\alpha$ on system behavior ... ..	54
Table 3-10 Effects of the correction factor1 on the system behavior .....	56
Table 3-11 Power system Characteristics .....	57
Table 3-12 Simulation results as $\beta$ changes .....	58
Table 3-13 System results as $\alpha$ is changed .....	60
Table 3-14 System's behavior when $CF_1$ varies .....	61
Table 3-15 Power system Characteristics .....	62
Table 3-16 Effects of $\beta$ on system's behavior .....	63
Table 3-17 Effects of changes in $\alpha$ on system behavior .....	65
Table 3-18 Effects of $CF_2$ on the system's Q sharing and load voltage .....	66
Table 4-1 Power system's steady state parameters' values .....	82

## LIST OF ACRONYMS

---

A	Ampere
AC	Alternating Current
dB	Decibel
CF	Correction Factor
CVLTF	Closed Voltage Loop Transfer Function
DC	Direct Current
DG	Distributed Generation
ES	Energy Source
Hz	Hertz
LPF	Low Pass Filter
PF	Power Factor
PI	Proportional Integral
PM	Phase Margin
PR	Proportional Resonant
PV	Photovoltaic
PWM	Pulse Width Modulation
RES	Renewable Energy Sources
RL	Resistive Inductive
RMS	Root-Mean-Square value
SPWM	Sinusoidal Pulse Width Modulation
V	Volt

VA	Volt-Ampere
VAR	Variable Reactive Power
$V_{DF}$	Voltage Drop Factor
VLTF	Voltage Loop Transfer Function
VSI	Voltage Source Inverter
W	Watt

## LIST OF PRINCIPAL SYMBOLS

---

$C_{fil}$	Low Pass Filter's capacitance
$\vec{E}_l$	Source voltage phasor
$E_{0i}$	No reactive load voltage magnitude
$f_e, f$	System frequency
$f_{e0}$	No active load frequency
$f_{sw}$	Switching Frequency
$C_v(s)$	Transfer function of voltage controller
$J$	the ratio between the sources' apparent powers
$K_{PWM}$	PWM gating gain
$L$	Inductance
$L_{fil}$	Low Pass Filter's inductance
$m_{0i}$	The reference $m_i$
$m, n$	droop coefficients
$n_{0i}$	The reference $n_i$
$P$	Active Power
$\varphi$	Phase angle
$Q$	Reactive Power
$R$	Resistance
$S_i$	Source's apparent power
$s$	Laplace variable
$t$	Time
$T_s$	Settling Time

$V_{dc}$	DC Bus Voltage
$V_{st}$	Peak saw tooth waveform magnitude
$V_T$	Generator Output Voltage
$V_{To}$	Generator no reactive load output voltage
$\vec{V}_{load}$	Load voltage phasor
$\omega$	Angular frequency
$\omega_c$	Angular cross-over frequency
$Z_{load_{eq}}$	Equivalent load impedances
$Z_{base}$	Base Impedance

# CHAPTER 1

## INTRODUCTION

---

### 1.1 BACKGROUND

The renewable energies produced by sources such as wind turbines, solar panels, biomass, and fuel cells, are used more and more compared to the fossil fuel based energy sources nowadays. The reason is that the renewable sources cause reduced environmental impact and their resources won't run out. Besides, because of the limitation of the resources of fossil based and nuclear fuels, and the growing need of energy in the world, the average of their prices are expected to increase in the next years. That's why Canada (like many other countries) has started to increase its amount of electric energy produced by renewable energy sources (RESs).

Distributed generation (DG) is the application of parallel small (up to 10MVA) electric sources (renewable or non-renewable) which could include hydropower turbines, wind turbines, photovoltaic panels, diesel generators, fuel cells, or gas turbines. The distributed sources are located as close as possible to the main load to decrease the power loss in the distribution lines [1]. A small DG system with small sources and loads in a limited area is called microgrid. In a microgrid, there is usually a cluster of loads and microsources, overall operating as a single controllable system that can provide power and heat to the local facilities [2]. The electrical connection of sources and loads can be done through a DC (Direct Current), or an AC (Alternating Current) bus link.

Power converters interfacing electric sources to the grid are usually connected in parallel, although series arrangements of sources are possible to allow better use of high voltages and currents (e.g. in photovoltaic cell arrays). All configurations require a controlled voltage at the load bus and controlled sources' active power (P) and reactive power (Q) flows. (Note that for DC currents, there is no Q)

An AC link microgrid can be seen in Fig. 1-1.

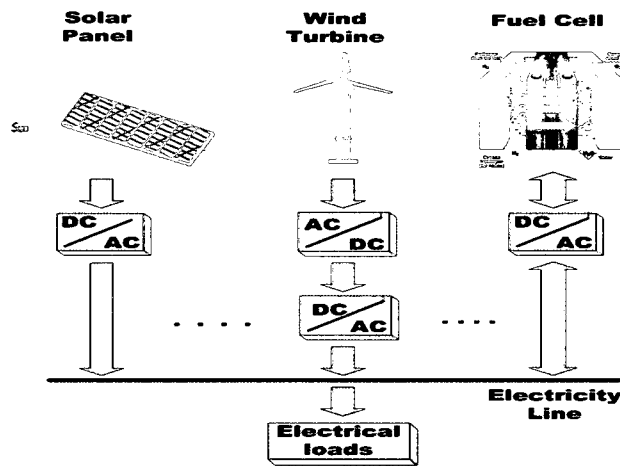


Fig. 1-1 A microgrid

In grid connected DG systems, the main grid can supply the lack of produced energy by the energy sources (ESs) to be delivered to the load or can absorb the extra energy produced by ESs. In this case, the DG units don't need an energy storage device but there would be the cost of connecting the microgrid to the utility grid network (especially when the loads are far from the grid; e.g. a remote village); and also there would be the energy loss in the grid connecting feeders (which increase as the load gets further from the grid network).

In isolated (non-grid connected) DG systems, the sources need the energy storage units, such as battery, ultra capacitor, hydrogen, or flywheel [3]. These storage units store extra produced energy to be delivered to the load at the time of ESs production shortage. This type of DG system is appropriate for areas far from the grid, which have some sorts of renewable or non-renewable energies enough for the consumption in that area. In this thesis this type of DG system will be addressed.

From another point of view, in a system with renewable sources (like solar panel, or wind turbine) with no or too small storage units (connected to utility grid), the sources have to transfer all the generated active power to the load or grid; where as in the isolated systems with large enough storage units the delivered  $P$  is equal to the required amount demanded by load or dispatcher operator, not necessarily the amount of  $P$  generated by the sources [4-7].

## **1.2 INTEGRATION OF ENERGY SOURCES**

When applying electrical energy conversion technology to energy systems, two classes of electrical systems must be considered: stationary and rotating. The stationary type usually provides direct current. Photovoltaic arrays and fuel cells are the main renewable energy sources in this group. The rotating type usually provides alternating current. Induction, synchronous, and permanent-magnet generators are the main drivers for hydropower, wind, and gas turbine energy sources; which all make AC voltage. If only photovoltaic and fuel cell systems are used, a dc-link bus might be used to integrate them. If only hydro or wind power is used, an AC voltage control can be used for their aggregation. But if some AC sources need to be integrated to some DC source, either all

the AC voltages should be converted to DC to have DC integration, or all the DC voltages should be converted to AC to have AC integration.

In the AC systems, it is less expensive and less complicated to change the voltage level; also it is possible to have three phase systems which have less construction's costs and feeders' losses. Moreover the frequency of the voltage in the AC integrated system can be used as wireless intersources communication signal. Besides, the galvanic isolation would be easy for AC systems. These are some reasons showing why the AC integration is better than DC integration to integrate any number of AC and DC ESs. In this thesis AC type of integration is considered.

### **1.2.1 DISTRIBUTED GENERATION CONTROL SCHEMES**

In power systems, if the sources are connected to the grid, their frequencies are constant and defined by the grid and the magnitudes and phase angles of their output voltages are adjusted to control the system's active and reactive power flows; while in islanded mode, the system frequency is adjusted instead of sources' phase angles. Note that this replacement is essential, to use system frequency as the communication signal for a seamless control of power sharing.

The power sharing schemes can be divided into to 2 hierarchical categories: dispatched and autonomous [1]. A typical dispatched hierarchical system consists of three levels. Each level can coordinate the lower-level. The lowest (first) level is the most time-demanding level of control, which is related to the switching of high-power transistors in the power electronic converters. The pulse-width modulation, current & voltage controls, and power electronic device protection are all within this layer.

The second level of control is required to manage the system; to generate sources' voltages' characteristics, to control the power flow among the energy sources (including energy storage units) and load; and to control load bus voltage;

The third level of control is responsible for the implementation of optimal power sharing policy to produce as much energy from the system as possible, or to minimize the costs of produced energy and system maintenance.

As an example of this category of systems, conventional dispatched synchronous generator based droop system adjusts  $V_T$  and  $f_e$  in (1-1) & (1-2) to control the power sharing and the load voltage. The droop equations of a rotating generator are shown below [8].

$$V_T = V_{T0} - m_G Q \quad (1-1)$$

$$f_e = f_{e0} - n_G P \quad (1-2)$$

Note that  $v_T$  is the generator output voltage;  $V_{T0}$  is the generator no reactive load output voltage;  $f_e$  is the system frequency, and  $f_{e0}$  is the no active load frequency. Also  $m_G$  &  $n_G$  are droop coefficients which are dependent on the values of the source rated power and allowed ranges of voltage and frequency changes

In the other category, the autonomous hierarchical scheme, the third level doesn't receive the orders about the power sharing policy from outside world (i.e. dispatch operator); and this level only makes the decisions about the power sharing policy based on the received information about the system sources' powers, the programmed power sharing strategy and possibly measured load voltage, and system frequency. The autonomous scheme has the advantage of no dispatching and less communication costs

compared to the dispatched scheme, but it is more difficult to change the power sharing policy in the autonomous scheme if it is needed.

In such a scheme, mostly the main system frequency (around 50Hz or 60 Hz, depending on the country) is used as the communication signal to control the power sharing [9-12]. The communication signal has rarely a frequency different than the system's main frequency as in [13].

An improved droop based system of this category will be proposed in this thesis for inverter based power networks (though it is extendable to the networks consisting of both inverter based and synchronous generator based sources). It will be shown later in chapter 2, that for very good P sharing, the  $f_{e,s}$  should be equal between the sources (which is not done in the conventional synchronous generator based droop system)

### **1.3 OBJECTIVES AND CHALLENGES**

In this thesis, an enhanced droop system for inverter based parallel distributed sources is proposed. The inverters have been used to connect distributed power sources to a microgrid with the capability of modification of the voltage amplitude and frequency. The inverters in a microgrid with droop control use a wireless control system which doesn't have any intercommunication cabling cost and is not distorted by electromagnetic interferences. The control system is extendable to any number of distributed sources.

Power sharing, which enables the energy sources to provide powers proportional to their apparent rated powers, is a very important property of the system. Hence, sources can provide their maximum powers when there is full load, without saturation in one of them and presence of some power capability in the other one. The conventional droop

control doesn't result in good power sharing, especially when the sources have different rated powers or the when feeders between sources and load(s) have different lengths. This bad power sharing has not been fixed in other relevant publications such as [14-16] and has been ignored in these references either by using some sources with equal apparent power or by ignoring the bad power sharing results; but in this thesis the improved droop system has been investigated which will result in appropriate active and reactive power sharing. Also the improved droop system makes a good load voltage regulation which is not taken care of in some publications such as [17].

## **1.4 CONTRIBUTION OF THE THESIS**

The major contributions of the thesis are:

1. Consideration of the effects of the sources' voltages (voltage magnitude and phase angle), and system frequency on the system P & Q sharing.
2. Design of an improved droop system using the new parameters of "voltage drop factor" and "correction factor" (added to the basic droop system) to have both good P & Q sharing and also to have good load voltage regulation. The comprehensive droop system design is done for cases of different ratios of the sources' apparent powers and feeders' lengths.
3. Consideration of the effects of the droop coefficients on the system P & Q sharing, load voltage magnitude, sources' voltages' magnitudes and phase angles, system overshoot, speed, stability, and steady state frequency.

## 1.5 THESIS OUTLINE

This thesis includes five chapters.

The first chapter includes an overview about renewable sources, the distributed generation, the microgrid, the advantages and disadvantages of different ways of integration of electric sources, the dispatched and autonomous hierarchical schemes, and why the modified droop system is chosen in the thesis to be used as the sources' integration method.

In the second chapter, the effects of the sources' voltages (voltage magnitudes and phase angles), and system frequency on the system P & Q sharing, are elaborated. Also the conventional inverter based droop system and its problems in providing good Q sharing and load voltage regulation, are considered.

The third chapter presents the design of an improved droop system using the new parameters "voltage drop factor" and "correction factor" (added to the basic droop system) to have both good P & Q sharing and also to have good load voltage regulation. This comprehensive droop system design is done for cases of different ratios of the sources' apparent powers and feeders' lengths. This chapter also includes the consideration of the effects of the droop coefficients on the system P & Q sharing, load voltage magnitude, sources' voltages' magnitudes and phase angles, system overshoot, speed, stability, and steady state frequency.

The fourth chapter is about the simulation results of the complete system with a benchmark and actual elements' values. The system includes the voltage loop, the real values of the elements in low pass filters after the inverters, and all the internal parasitic resistances.

The fifth chapter summarizes the work done in the thesis. Besides, it covers the conclusion of the materials in the previous chapters and suggestions for the future work on the topics in this thesis.

# CHAPTER 2

## SYSTEM WITH THE BASIC DROOP TECHNIQUE

---

### 2.1 INTRODUCTION

This chapter evaluates the effects of the system parameters (i.e. sources voltage magnitudes and phase angles, and system frequency) on the system powers. The sensibility and the change course of the real and reactive powers regarding each mentioned system parameter are considered; and the droop strategy is designed based on them. Also the sources' voltages conditions under which the system has some desired real or reactive powers sharing are obtained. The commonly used basic droop control is designed in section 2.3 based on the system behaviors shown in section 2.2 and the transient and steady state behavior of a system with this basic droop system is evaluated in section 2.4.

### 2.2 SYSTEM POWERS' DEPENDENCY ON SYSTEM PARAMETERS

The values in Table 2-1 are used for the benchmark model.

**TABLE 2-1** Benchmark Model Power parameters

	Source 1	Source 2
Power rating (VA)	1400	700
Line impedances ( $\Omega$ )	$(0.20 + j\omega * 0.00154)$	$3*(0.20 + j\omega * 0.00154)$

Full load impedance= (5.99+ jω\*0.0119) (Ω). The load has PF=0.8 lagging and also rated voltage is V<sub>rated</sub>=120V<sub>RMS</sub>. Line impedance phase angle =78.9° => Mostly inductive line. Note that the line parameters are used by NRCan (Natural Resources Canada).

## 2.2.1 SYSTEM POWER EQUATIONS

The simplified power system with two inverters and a single load is shown in Fig. 2-1 where the inverters and LPFs have been replaced by AC sources.

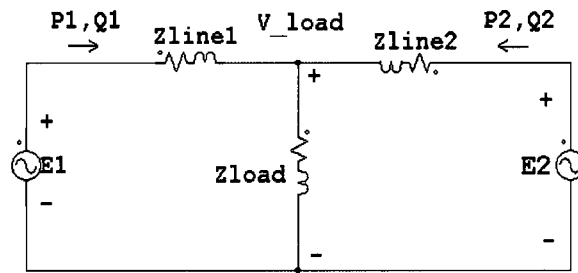


**Fig. 2-1** Simplified power stage of the system

For the Fig. 2-1 when the phasors of E<sub>1</sub> and E<sub>2</sub> have respectively the phase angles of φ<sub>1</sub>, 0 (Rad). The load voltage phasor is:

$$\vec{V}_{load} = \{ \vec{E}_1 * \left( \frac{Z_{line2} || Z_{load}}{(Z_{line2} || Z_{load}) + Z_{line1}} \right) \} + \{ \vec{E}_2 * \left( \frac{Z_{line1} || Z_{load}}{(Z_{line1} || Z_{load}) + Z_{line2}} \right) \} \quad (2-1)$$

which has the magnitude of  $|\vec{V}_{load}|$  and the phase angle of φ<sub>load</sub>.

The first source powers can be calculated as:

$$P1 = \left( \frac{|\vec{E}_1| |\vec{V}_{load}|}{|Z_{line1}|} \cos(\varphi_1 - \varphi_{load}) - \frac{|\vec{V}_{load}|^2}{|Z_{line1}|} \right) \cos(ph(Z_{line1})) + \frac{|\vec{E}_1| |\vec{V}_{load}|}{|Z_{line1}|} \sin(\varphi_1 - \varphi_{load}) \sin(ph(Z_{line1})) \quad (2-2)$$

$$Q1 = \left( \frac{|\vec{E}_1| |\vec{V}_{load}|}{|Z_{line1}|} \cos(\varphi_1 - \varphi_{load}) - \frac{|\vec{V}_{load}|^2}{|Z_{line1}|} \right) \sin(ph(Z_{line1})) - \frac{|\vec{E}_1| |\vec{V}_{load}|}{|Z_{line1}|} \sin(\varphi_1 - \varphi_{load}) \cos(ph(Z_{line1})) \quad (2-3)$$

where  $ph(Z_{line1})$  is the phase angle of the line impedance 1.

Since  $(\varphi_1 - \varphi_{load})$  is small in practical power applications, one simplifies the equations above into:

$$P1 = \left( \frac{|\vec{E}_1| |\vec{V}_{load}|}{|Z_{line1}|} - \frac{|\vec{V}_{load}|^2}{|Z_{line1}|} \right) \cos(ph(Z_{line1})) + \frac{|\vec{E}_1| |\vec{V}_{load}|}{|Z_{line1}|} * (\varphi_1 - \varphi_{load})_{(rad)} \sin(ph(Z_{line1})) \quad (2-4)$$

$$Q1 = \left( \frac{|\vec{E}_1| |\vec{V}_{load}|}{|Z_{line1}|} - \frac{|\vec{V}_{load}|^2}{|Z_{line1}|} \right) \sin(ph(Z_{line1})) -$$

$$\frac{|\vec{E}_1| |\vec{V}_{load}|}{|Z_{line1}|} * (\varphi_1 - \varphi_{load})_{(rad)} \cos(ph(Z_{line1})) \quad (2-5)$$

Note that in previous equations all the voltage magnitudes are in RMS and phase angles are in Radians.

## 2.2.2 EVALUATION OF THE EFFECTS OF SOURCES' PARAMETERS ON SYSTEM POWERS

In this section, the effects of the sources' parameters (i.e. the magnitudes of voltages, the phase angles of voltages, and the system frequency) on system powers are considered which visualizes the power equations in the previous section by the following 2 and 3 dimensional figures.

### 2.2.2.1 SYSTEM POWER FLOW GRAPHS FOR THE PLANE OF $(|\vec{E}_1|, \varphi_1)$

Using the precise power equations (2-2) & (2-3), for the system in the case of voltage source2 with reference phase angle of 0, constant frequency of 60Hz and magnitude of 120 V (source 2 can be considered as the infinite bus), with the line impedance2= 3\* line impedance1, the effects of the phase angle (difference between the

sources' phase angles) and the magnitude of the first source on powers are shown in following figures.

Fig. 2-2 shows that the maximum Q1 occurs when  $|\vec{E}_1|$  (or equivalently  $|\vec{E}_1| - |\vec{E}_2|$ ) is maximum and  $\varphi_1$  ( $\varphi_1 - \varphi_2$ ) is minimum and vice versa. Also it can be seen that Q1 is very sensitive to  $\varphi_1$ . For example, in practical systems the difference between the sources' angles is very small.

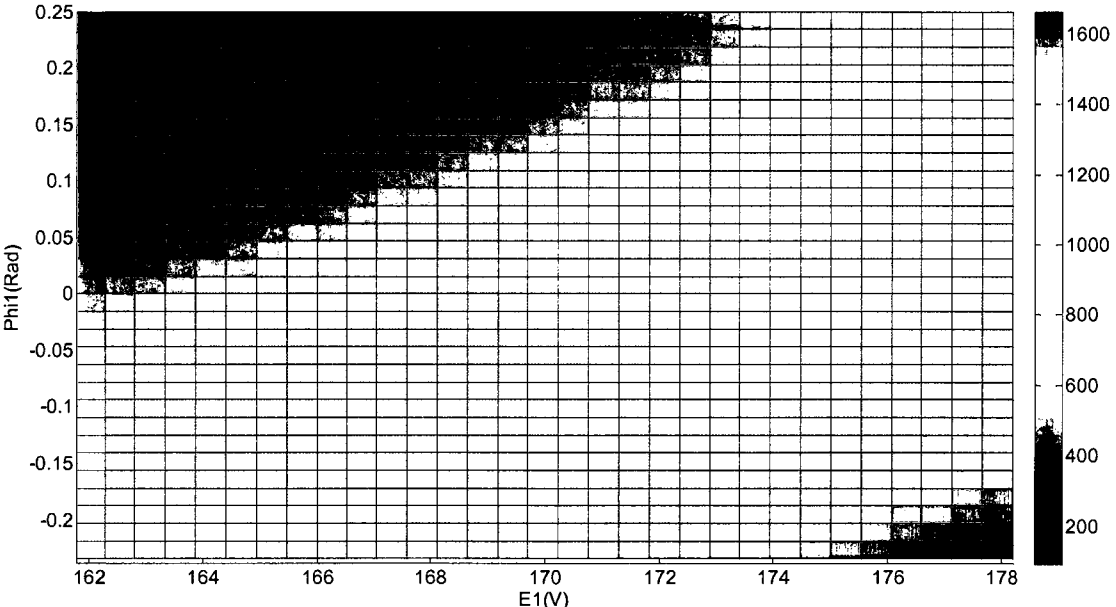


**Fig. 2-2** Changes in Q1 (VAR) as the peak magnitude and phase angle of the first source change

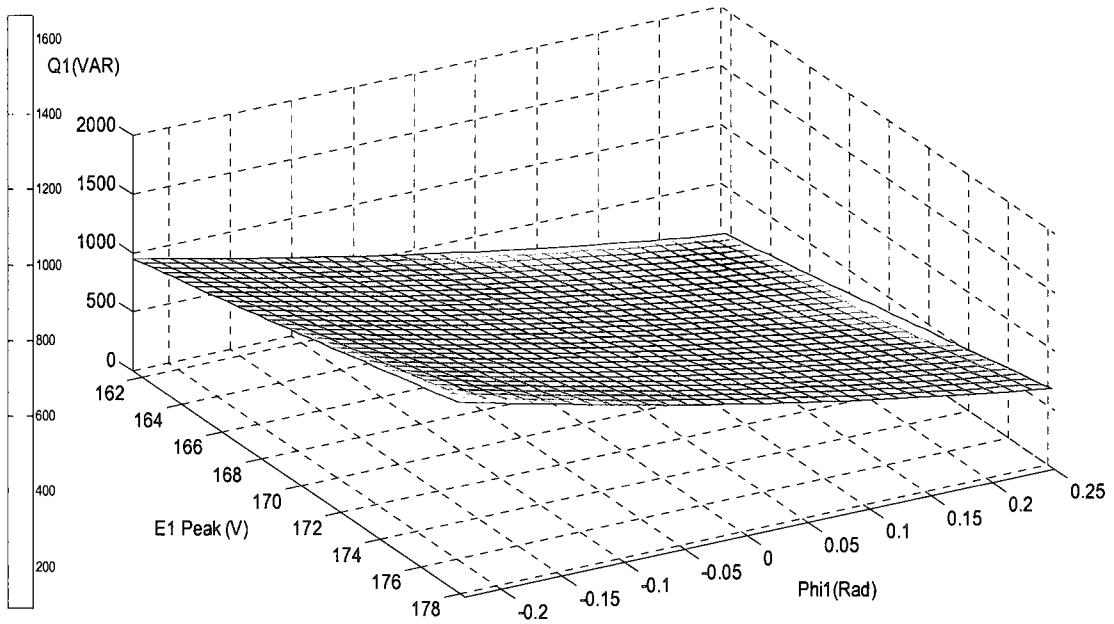


Fig. 2-3 Three dimensional view of changes in Q1(VAR) as the magnitude and phase angle of the first source change

Fig. 2-4 shows that the maximum Q2 occurs when  $|\vec{E}_1|$  is minimum and  $\phi_1$  is maximum and vice versa.

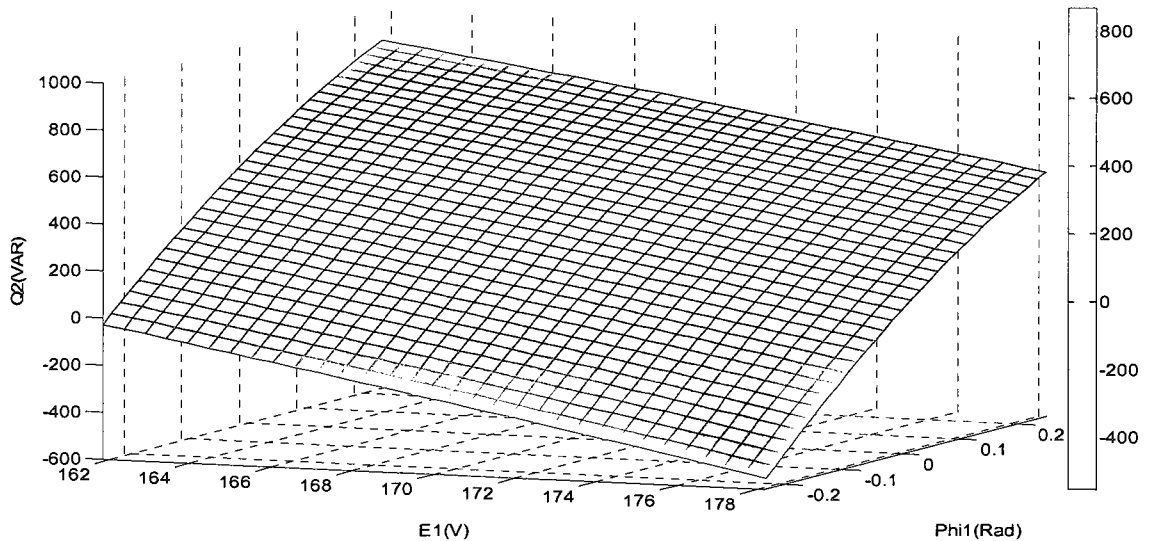
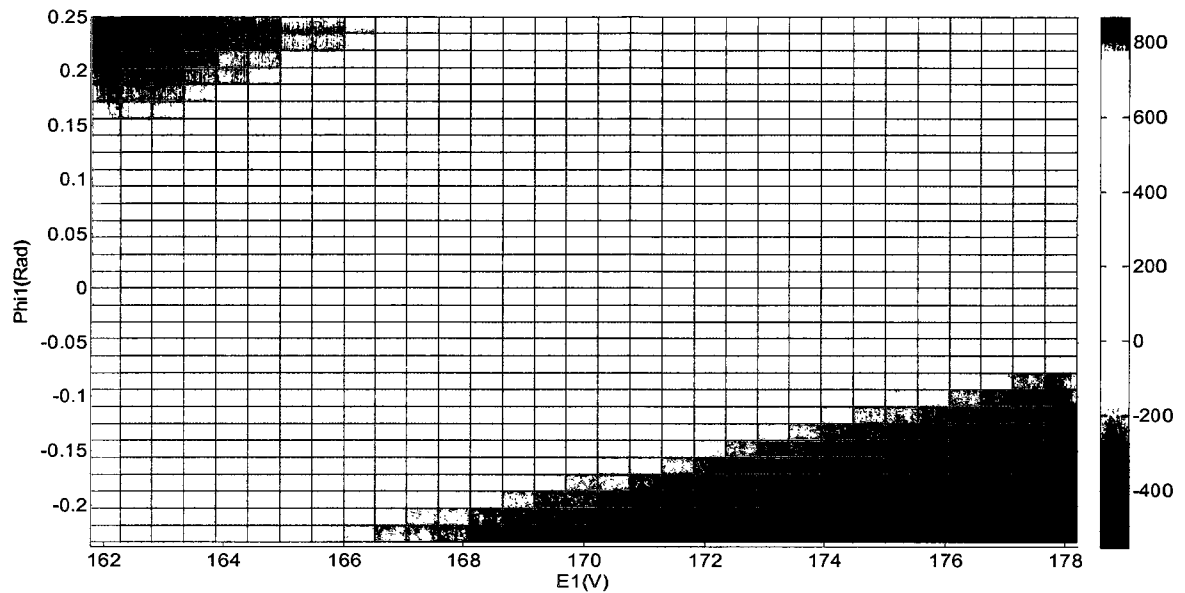


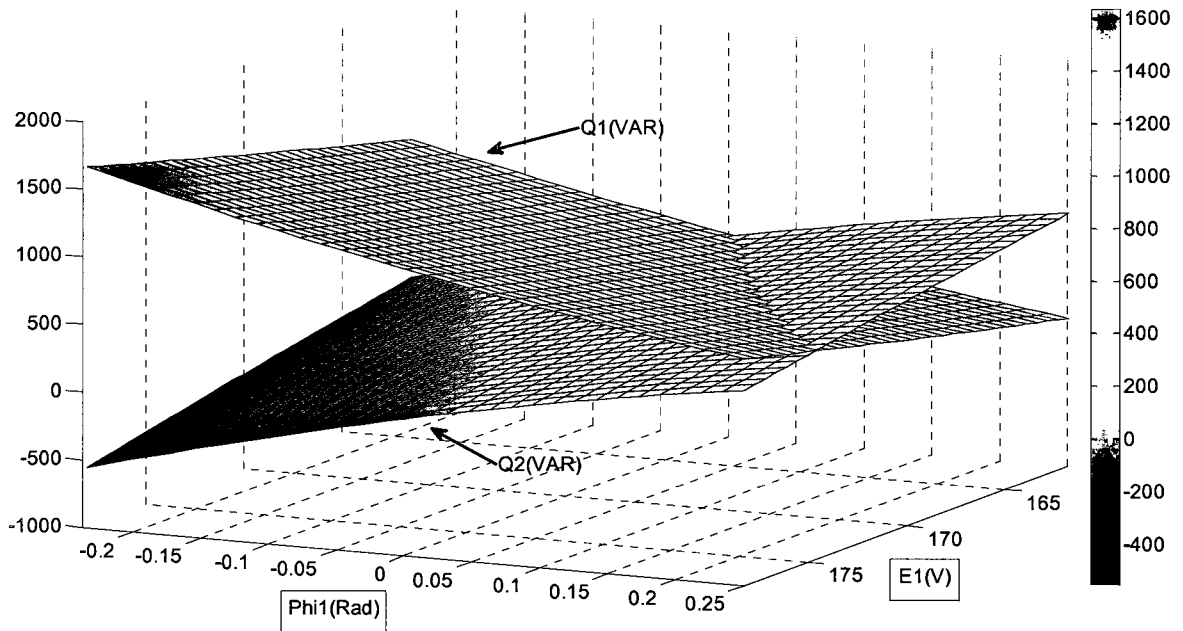
Fig. 2-4 Three dimensional view of changes in Q2(VAR) as the magnitude and phase angle of the first source change

Fig. 2-5 shows the changes in Q2(VAR) as the magnitude and phase angle of the first source change.



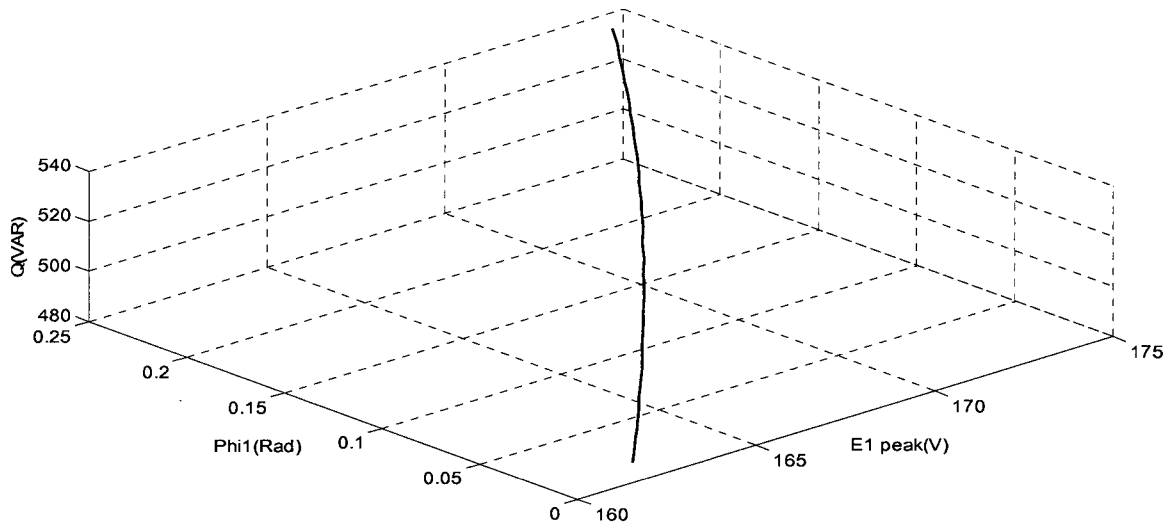
**Fig. 2-5** Changes in Q2(VAR) as the magnitude and phase angle of the first source change

It can be seen in Fig. 2-6 that Q1 and Q2 have the reverse course of change compared to each other for both changes in  $|\vec{E}_1|$  and  $\varphi_1$ . So that an increase in  $(|\vec{E}_1| - |\vec{E}_2|)$  or  $(\varphi_2 - \varphi_1)$  results in an increase in  $(Q1 - Q2)$  which is verified by the time domain simulation results as it can be seen in section 3.4.



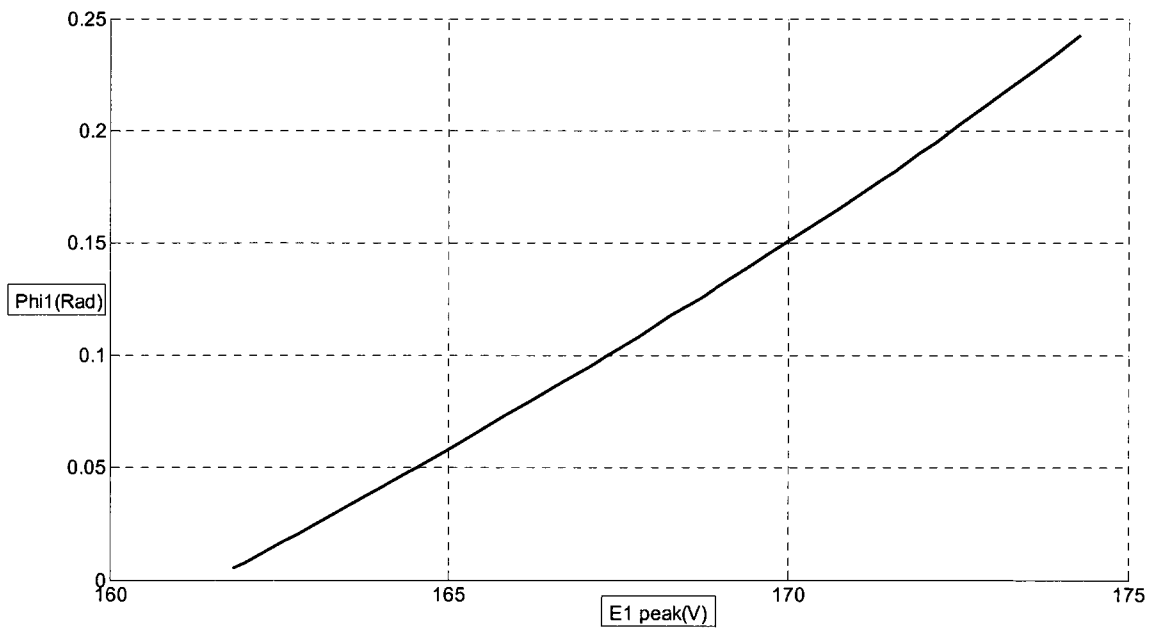
**Fig. 2-6** Three dimensional view of changes in Q1 & Q2 (VAR) as the magnitude and phase angle of the first source change

The intersection of the two surfaces on the Fig. 2-6 can be seen in Fig. 2-7. This curve shows that for having equal Q, as the magnitude of the first source increases, its phase angle should increase too. Fig. 2-7 shows that if the droop system is designed correctly to change the sources' magnitudes and phase angles, one can achieve equal Q sharing with any value of Q. Other ratios for Q sharing can be achievable as far as the multiples of the surfaces in the Fig. 2-6 (moved in vertical direction) have intersection in the allowable range of E1 and  $\varphi_1$ . For example if the desired value of  $\frac{Q_2}{Q_1}$  is 2, the surface of  $2*Q_2$  (moved up compared to initial surface of Q2) will have another intersection with the surface of Q1 which represents the desired region of Q sharing.



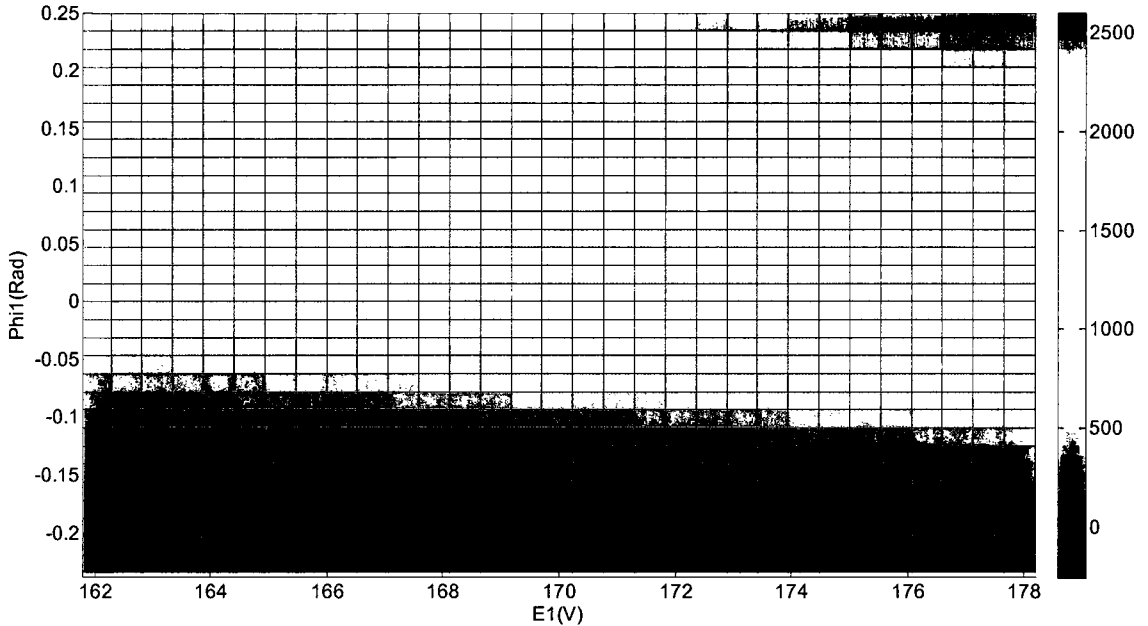
**Fig. 2-7** Three dimensional curve of the region in which  $Q_1=Q_2$ , ( $|E_2| = 120V$ ,  $\varphi_2=0$ )

Figure 2-7 shows the two dimensional curve of the region in which  $Q_1=Q_2$  with  $|E_2| = 120V$  and  $\varphi_2=0$ .



**Fig. 2-8** Two dimensional curve of the region in which  $Q_1=Q_2$  with  $|E_2| = 120V$  and  $\varphi_2=0$

It can be seen in Fig. 2-9 that the maximum P1 happens when  $|\vec{E}_1|$  and  $\phi_1$  are maximum and vice versa. As it can be seen in this figure, the phase angle variations have more impact on P than voltage variations. For example, in practical systems the difference between the sources' angles (or power angles) is very small.



**Fig. 2-9** Changes in P1 (W) as the magnitude and phase angle of the first source change

It can be seen in Fig. 2-10 that the minimum P2 occurs when  $|\vec{E}_1|$  and  $\phi_1$  are the maximum and vice versa. Also by comparing Figures 2-9 & 2-10, it can be observed that P2 has less sensitivity to  $|\vec{E}_1|$  compared to sensitivity of P1 on it, which is expected since in previous power equations, for the second source, the voltage magnitude and phase angle is constant and the change in its power flow is just dependent on the change in the load voltage.

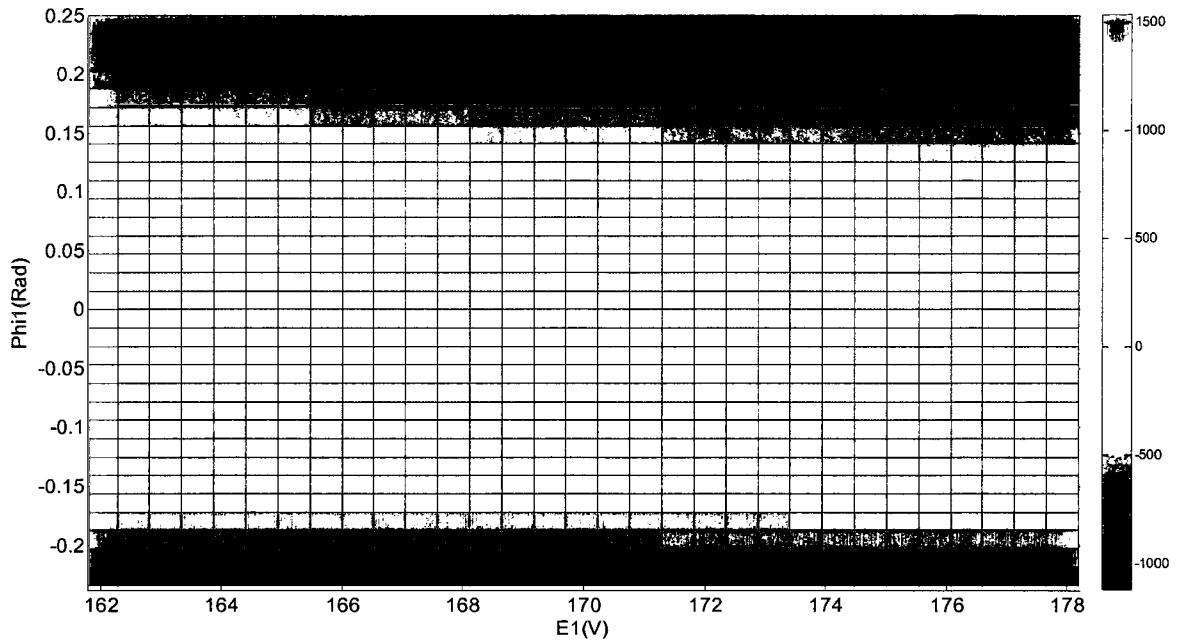


**Fig. 2-10** Changes in P2 (W) as the magnitude and phase angle of the first source change

It can be seen in Fig. 2-11 that P1 and P2 have the reverse course of change compared to each other for the changes in  $\phi_1$ .

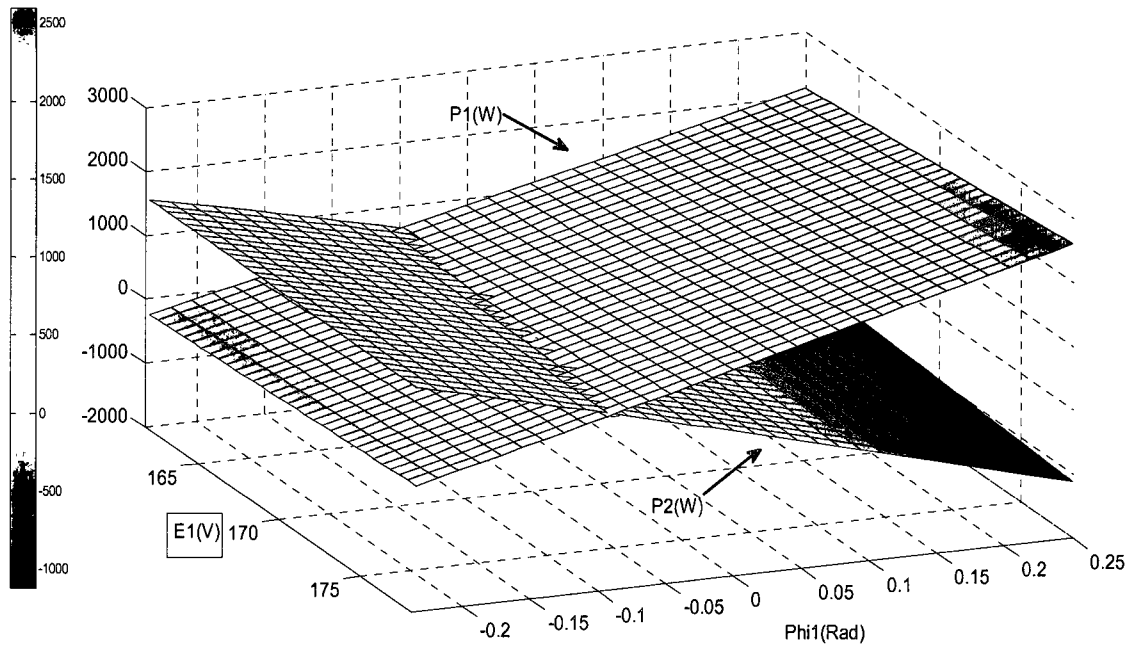


**Fig. 2-11** Changes in P1 & P2 (W) as the magnitude and phase angle of the first source change

Figures 2-12 & 2-13 show the intersection of the previous P1 & P2 surfaces where P1=P2 (equal P sharing). Other ratios for P sharing can be achievable as far as the multiples of the surfaces in the Fig. 2-11 (moved in vertical direction) have intersection in the allowable range of  $|\vec{E}_1|$  and  $\varphi_1$ .

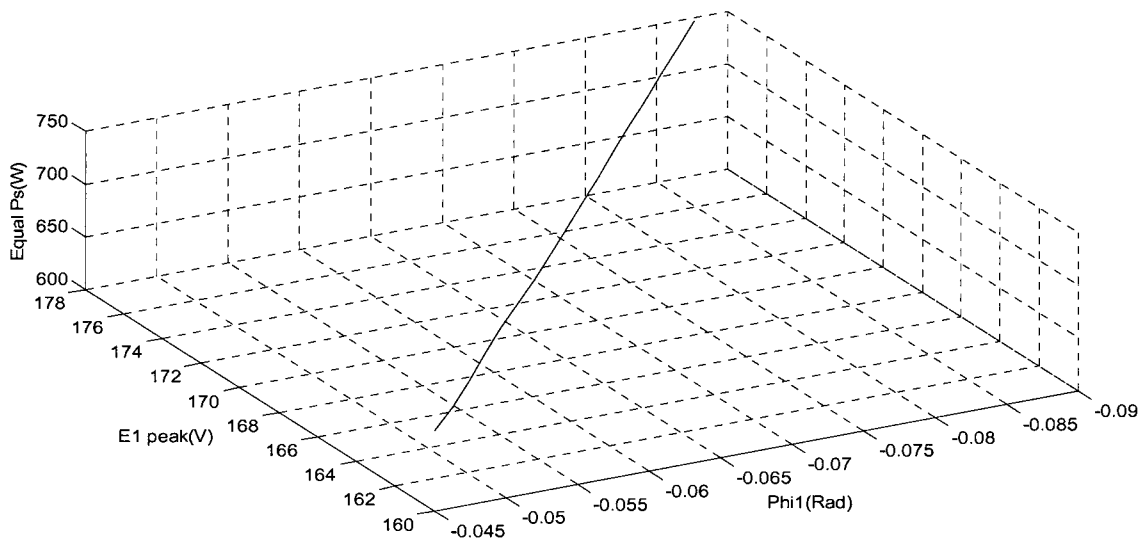


**Fig. 2-12** Three dimensional curve of the region in which P1=P2

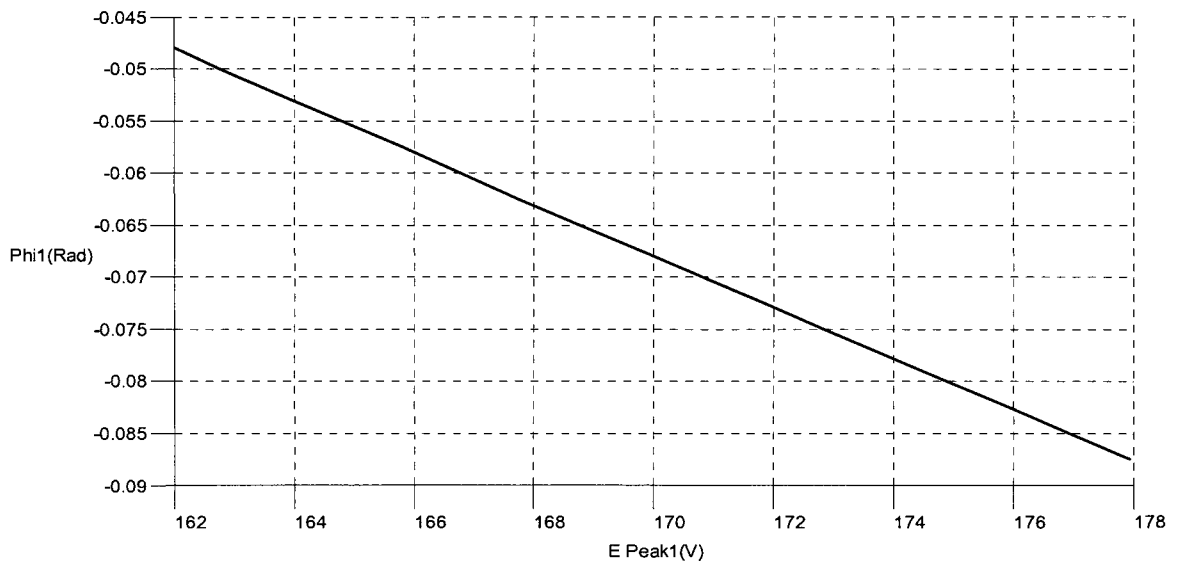


**Fig. 2-13** Two dimensional curve of the region in which P1=P2

There is another influencing parameter in power sharing which is  $|\vec{E}_2|$  whose effect will be considered in the next subsection.

### 2.2.2.2 SYSTEM POWER FLOW GRAPHS FOR THE $(\vec{E}_1, \vec{E}_2)$ PLANE

Now using the precise power equations (2-2) & (2-3) for the system in the case of voltage sources with equal constant phase angles of  $0^\circ$ , constant frequency of 60Hz, with the line impedances  $Z_2 = 3 * Z_1$ , the effects of the magnitudes of the sources voltages on powers' flows will be shown in the coming figures.

It can be seen in Fig. 2-14 that the maximum Q1 happens when maximum  $|\vec{E}_1|$  and minimum  $|\vec{E}_2|$  and vice versa. The case is reversed for Q2 which can be observed in Fig. 2-15. Also by comparing these two figures it can be seen that Q1 has more sensitivity to  $|\vec{E}_1|$  and Q2 has more sensitivity to  $|\vec{E}_2|$ .

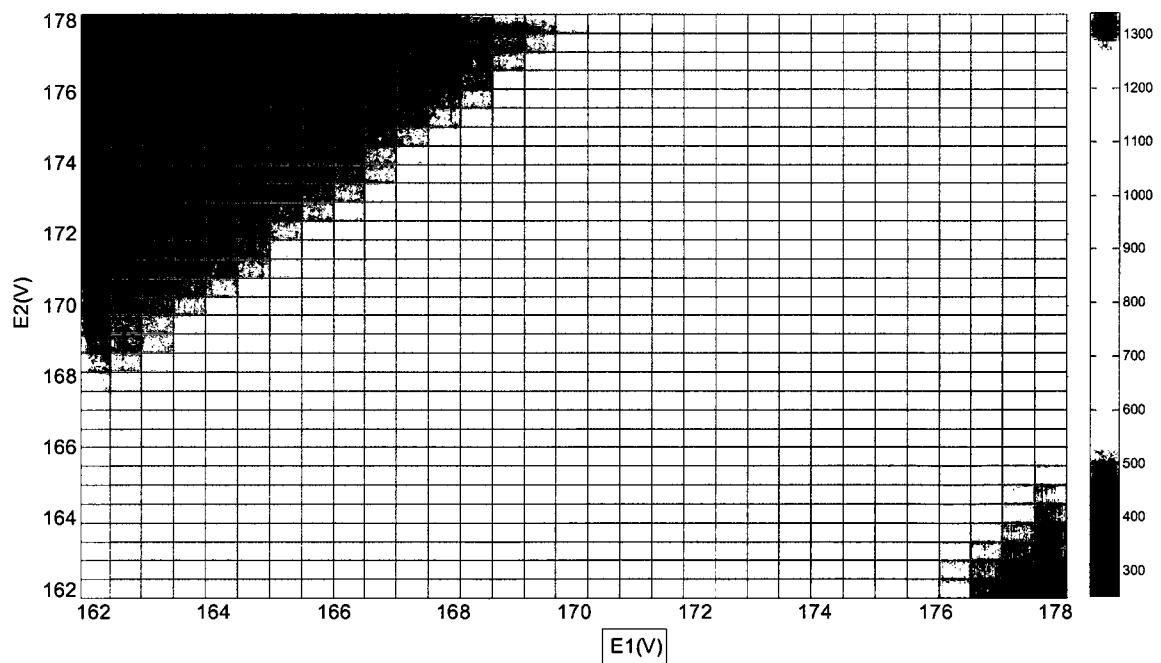


**Fig. 2-14** Changes in Q1 (VAR) as the magnitudes of sources' voltages change

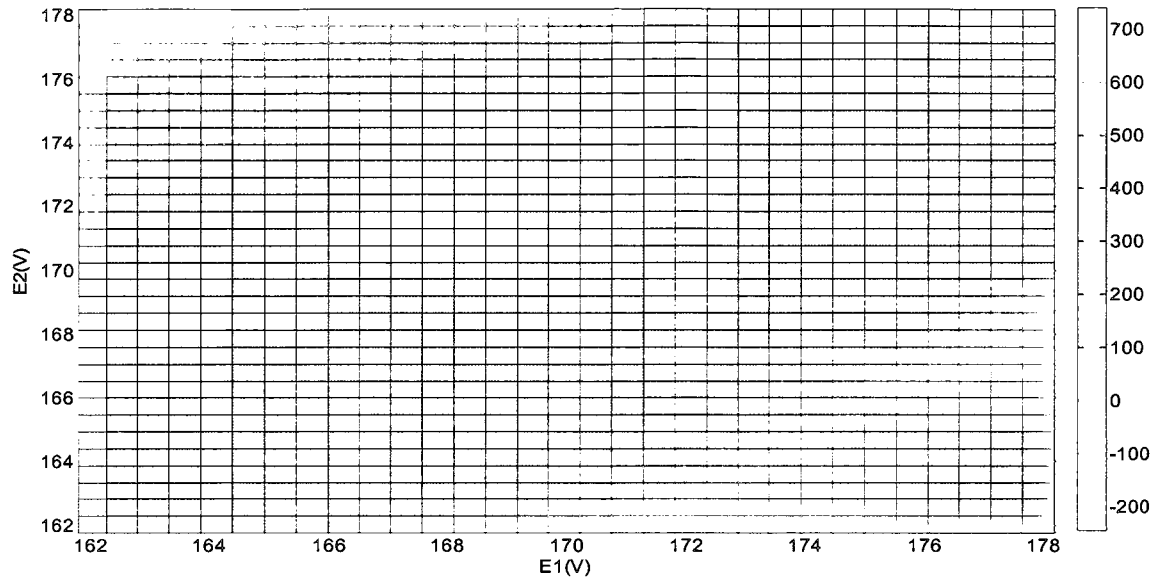


Fig. 2-15 Changes in Q2 (VAR) as the magnitudes of sources' voltages change

The reverse course of change in the values of Q1 and Q2 versus the change in voltage magnitudes can be seen in Fig. 2-16 as the partial slopes (i.e. surfaces' edges' slopes) with different signs. Also figure 2-16 shows that any desired Q sharing ratio is achievable as far as the multiples of the Q surfaces have intersection in the allowable range of  $|\vec{E}_1|$  and  $|\vec{E}_2|$ .

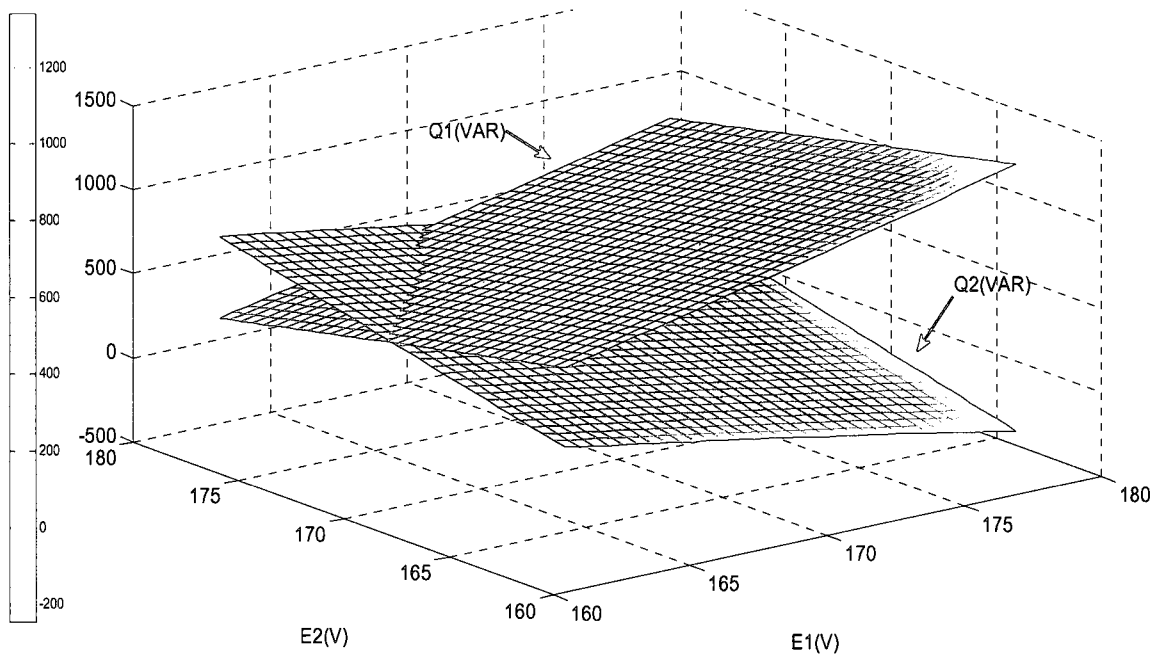


Fig. 2-16 Changes in  $Q_1$  &  $Q_2$  (VAR) as the magnitudes of sources' voltages change

Fig. 2-17 shows that  $P_1$  increases as  $|\vec{E}_1|$  increases or  $|\vec{E}_2|$  decreases. There is the reverse case for  $P_2$  as it is shown on Fig. 2-18. Also in these two figures, it can be observed that  $P_1$  is more sensitive to  $|\vec{E}_1|$ , and  $P_2$  is more sensitive to  $|\vec{E}_2|$ .

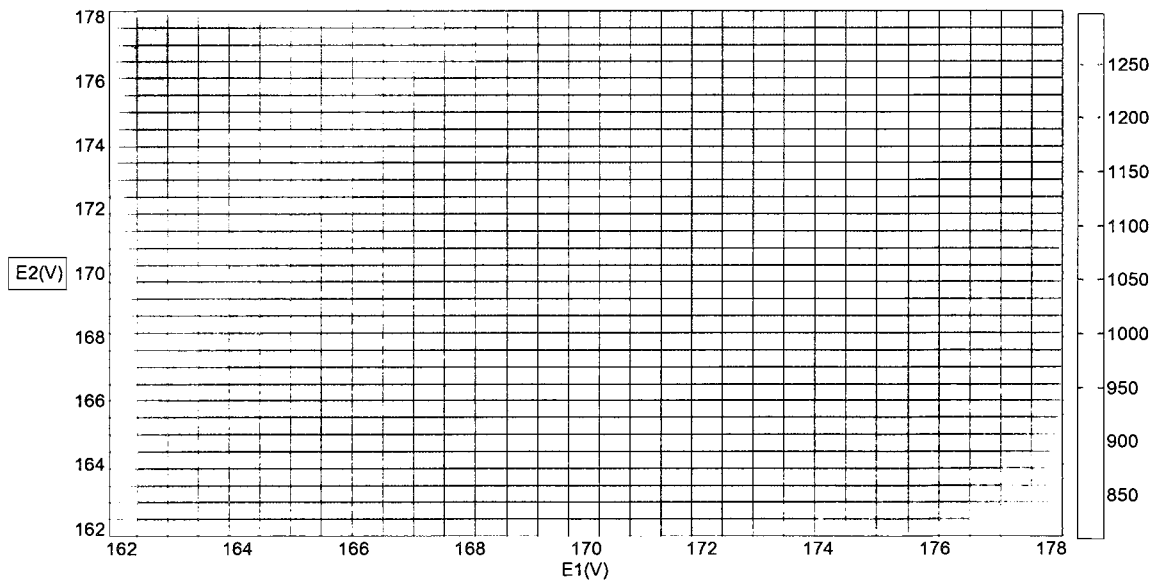


Fig. 2-17 Changes in  $P_1$  (W) as the magnitudes of sources' voltages change

Figure 2-18 shows the changes in P2 (W) as the magnitudes of sources' voltages change.

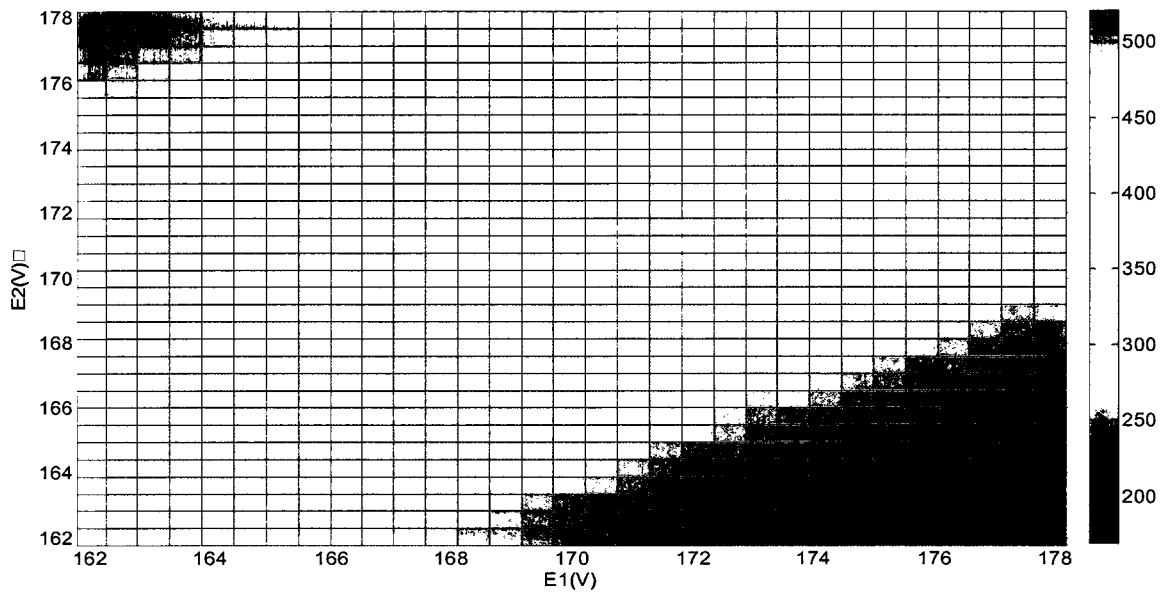
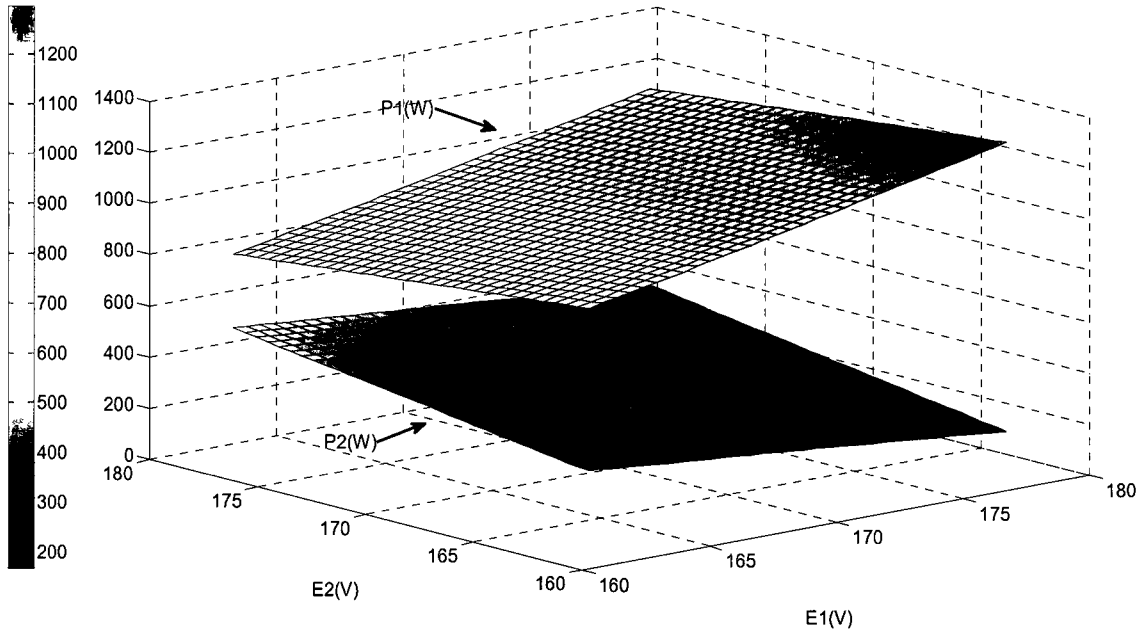


Fig. 2-18 Changes in P2 (W) as the magnitudes of sources' voltages change

The reverse course of change in the values of P1 and P2 versus the changes in voltage magnitudes can be seen in Fig. 2-19 as the partial slopes with different signs. Also it can be seen that since the line impedance 2 is 3 times larger than line impedance 1, if the sources have the same phase angles, for any choice of  $|\vec{E}_1|$  and  $|\vec{E}_2|$ , P2 will be less than P1. So that if one needs to have more P2 compared to P1 or equal power sharing, the sources' phase angles need to be adjusted too, as one can see in Fig. 2-11.



**Fig. 2-19** Changes in P1 & P2 (W) as the magnitudes of sources' voltages change

### 2.2.2.3 SYSTEM POWER FLOW GRAPHS FOR THE PLANE OF $(\varphi_1, F)$

Now for the system in the case of voltage source2 with reference phase angle of  $0^\circ$ , constant magnitudes of 120V for both sources, with the line impedances $_2 = 3 \times$  load impedances $_1$ , the effects of the phase angle $_1$  (difference between the sources' phase angles) and the system's frequency on powers are shown in following figures.

It can be seen on figures 2-20 & 2-21 that by increment in  $\varphi_1$ , Q1 decreases and Q2 increases. Also the reactive powers have very small sensitivity to the system's frequency in its allowed range (horizontal color bands).

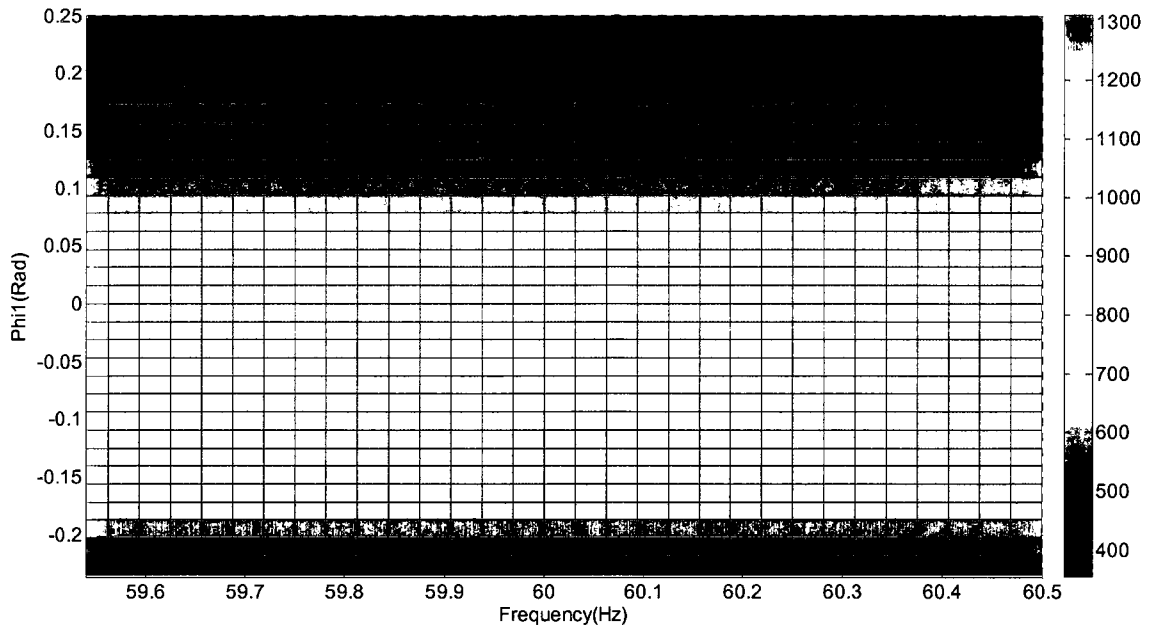


**Fig. 2-20** Changes in Q1(VAR) as the system's frequency and the first source's phase angle change

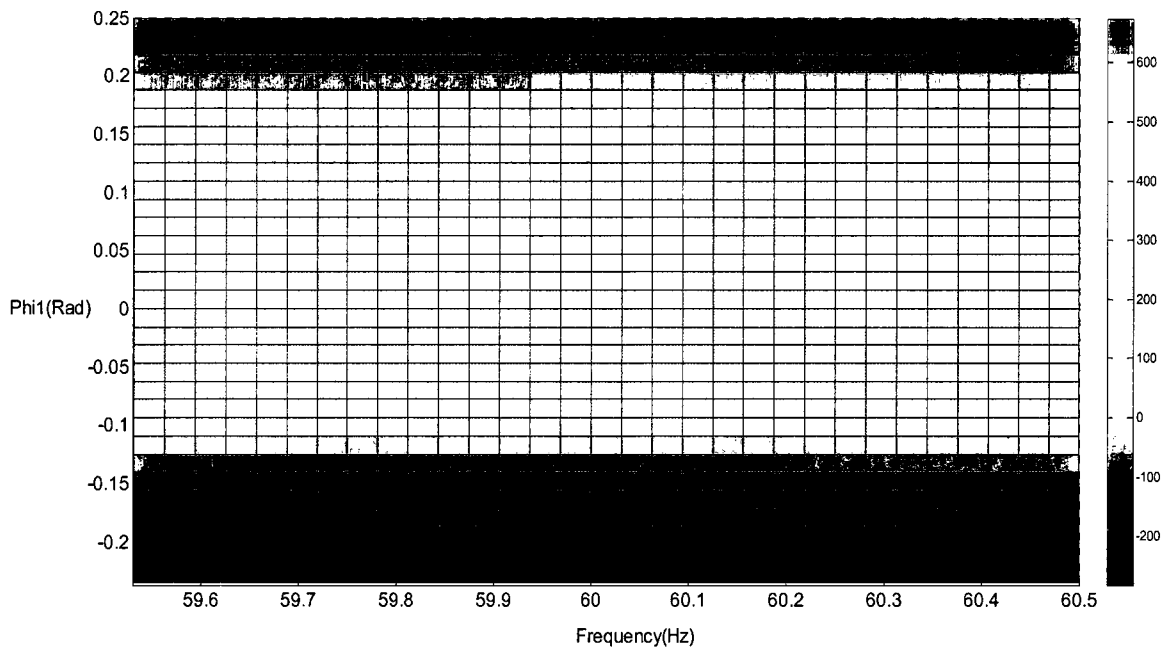


**Fig. 2-21** Changes in Q2(VAR) as the system's frequency and the first source's phase angle change

Figure 2-22 demonstrates the changes in Q1 & Q2 (VAR) as the system's frequency and the first source's phase angle change.

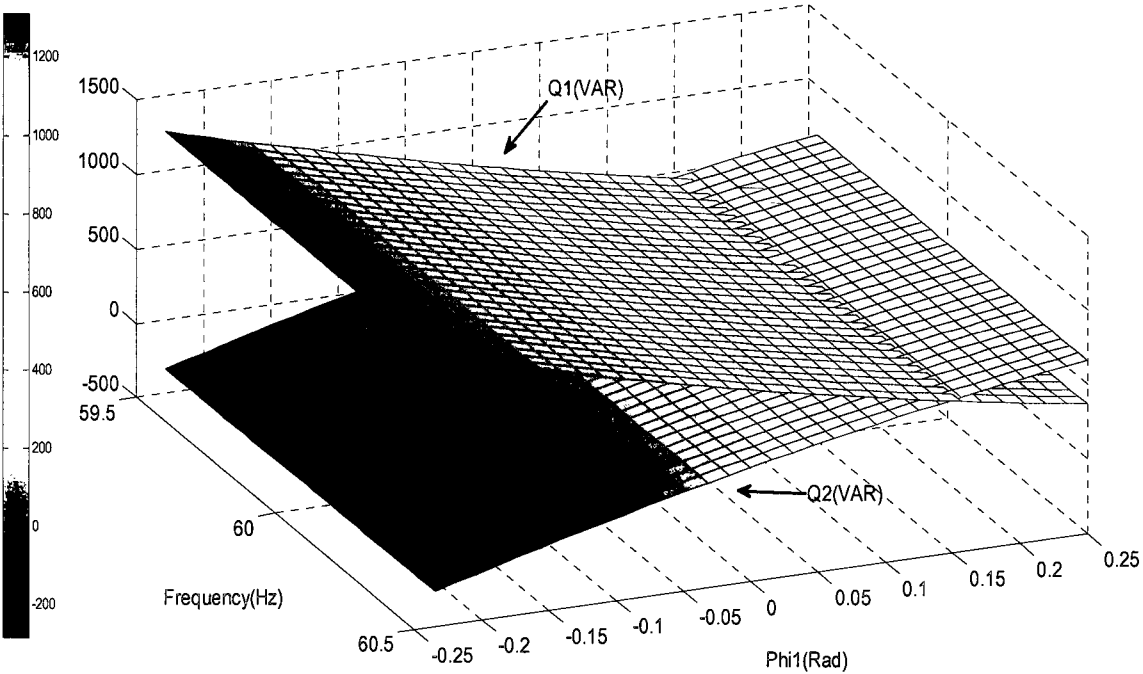


**Fig. 2-22** Changes in Q1 & Q2(VAR) as the system's frequency and the first source's phase angle change

It can be seen on the figures 2-23 and 2-24 that by increasing  $\phi_1$ , P2 decreases and P1 increases. Also the active powers have very small sensitivity to the system's frequency (horizontal color bands).

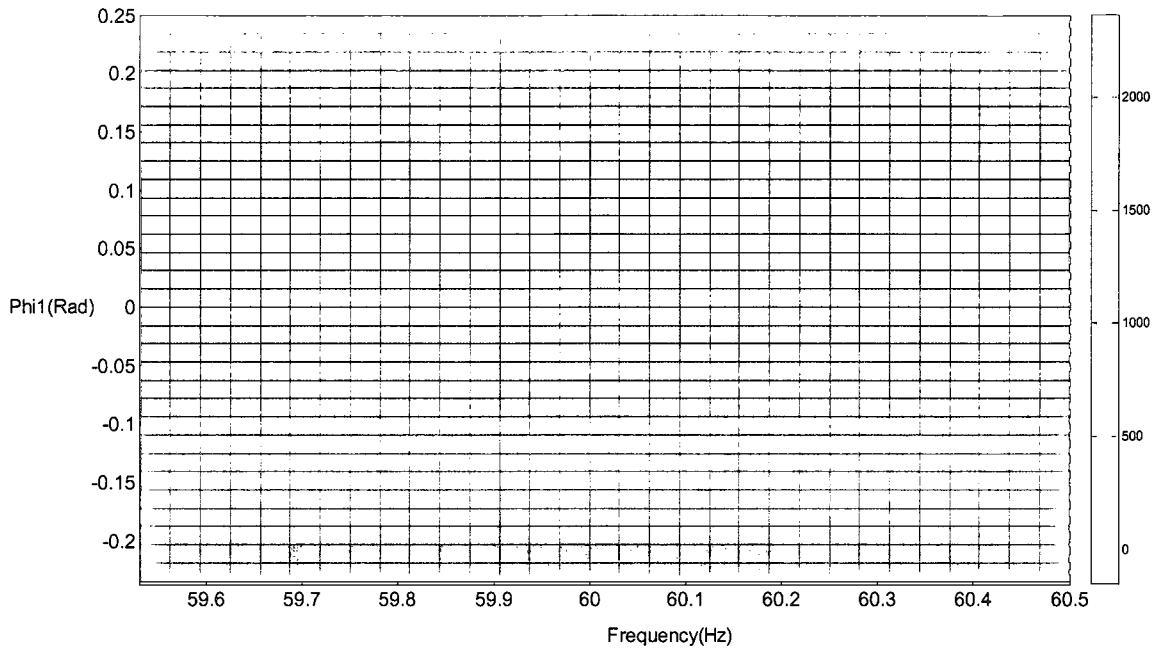


Fig. 2-23 Changes in P1(W) as the system's frequency and the first source's phase angle change

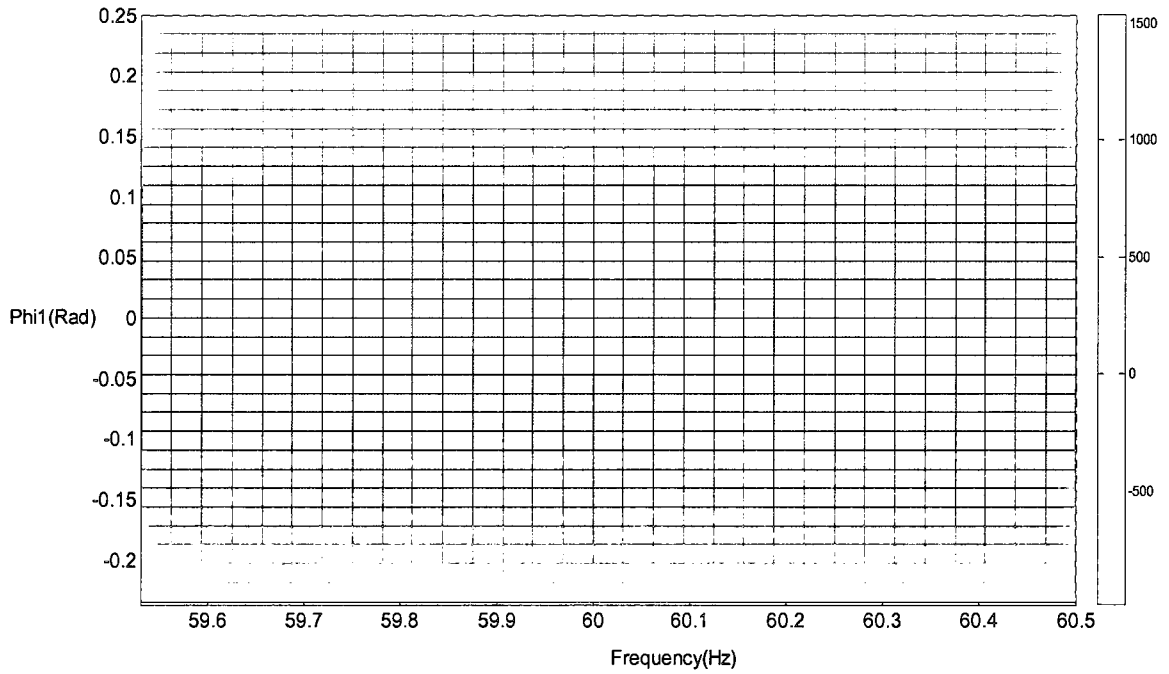


Fig. 2-24 Changes in P2(W) as the system's frequency and the first source's phase angle change

Figure 2-25 demonstrates the changes in P1 & P2(W) as the system's frequency and the first source's phase angle change.

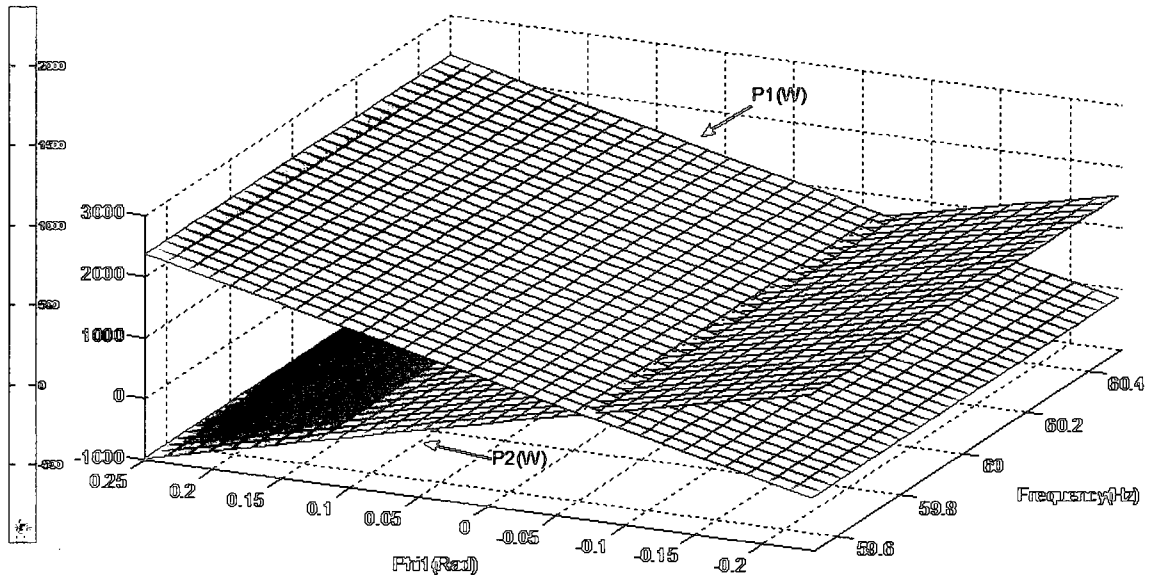


Fig. 2-25 Changes in P1 & P2(W) as the system's frequency and the first source's phase angle change

It has been observed in this subsection that the steady state frequency doesn't have any considerable effect on the P & Q sharing but as it was seen in the subsection 2.2.2.1, the transient state frequencies have effects on power sharing since the difference of the sources' phase angles is the integral of the difference of the sources transient state frequencies, in other terms  $(\phi_1 - \phi_2)_{(t)} = \Delta\phi_0 + (2\pi \int_{t_0}^t (f_1 - f_2) dt)$  where  $(t \geq t_0)$ ,  $t_0$  is a time in the stability period at which the difference between the sources' phase angles is  $\Delta\phi_0$ , and the time interval of  $[t_0, t]$  can include the transient state.

### 2.3. BASIC DROOP LOOP

In some papers' droop systems, the sources' voltage magnitudes ( $|\vec{E}_i|$ ) are made dependent on the source output real powers ( $P_i$ ); and the sources frequencies ( $\omega_i$ ) are made dependent on the source output reactive power ( $Q_i$ ), via linear equation with the droop coefficients [18]. In this scheme, there will be good Q sharing but not good P sharing. In some other papers' droop schemes, the  $|\vec{E}_i|$  is made related to  $Q_i$ ; and the  $\omega_i$  is made related to  $P_i$ , using basic linear droop equations [19]. For this scheme, there will be good P sharing but not good Q sharing. Both schemes are implementable for islanded microgrids, but the latter is better since good controlled P sharing is important for the control of the states of the charge of the sources' energy saving elements (such as batteries).

In this chapter this kind of basic droop scheme is used. The droop equations are:

$$|\vec{E}_i| = E_{0i} - m_i Q_i \quad (2-6)$$

$$\omega_i = \omega_{0i} - n_i P_i \quad (2-7)$$

Note that  $E_{0i}$  and  $\omega_{0i}$  are respectively the no reactive load voltage magnitude and the no active load source frequency. Also  $m_i$  and  $n_i$  are droop coefficients.

As it was seen in figures 2-14 & 2-15, by increment in the voltage magnitude  $|\vec{E}_i|$  the reactive power ( $Q_i$ ) will increase; so that in (2-6) the negative sign creates a negative feedback to help the system stability. Also Fig. 2-9 shows that increment in the  $\phi_1 (= \int_0^t (\omega_1 - 120\pi) dt)$  will increase  $P_1$ . So the negative sign in (2-7) makes negative feedback in the system to help its stability. Also notice that in the droop equations, the frequency is used instead of the phase angle even though the phase angle has a lot of effect in power equations (2-4) & (2-5) since each source doesn't know the initial phase

angle of the other sources [20] and one can just measure each source frequency at a time. Also frequency works as the intersources communication signal.

For the same system as described at the beginning of section 2.2, the droop coefficients are obtained as below:

$$m_1 = \frac{\Delta E_{\max}}{2 \cdot Q_{\max 1}} = \frac{12 \cdot \sqrt{2} V}{2 \cdot 1400 \cdot 0.6 \text{ VAR}} \rightarrow m_1 = 0.0102 \frac{V}{\text{VAR}} \quad (2-8)$$

Note that  $\Delta E_{\max}$  is 10% of the rated voltage magnitude [21].

$$E_{01} = 120 V \cdot \sqrt{2} = 169.7 V \quad (2-9)$$

Note that for the case that  $|\vec{E}_i| = E_{0i}$ , there is no Q, though there might be maximum P which causes the maximum voltage drop at the load; so that if the source provides the rated (or even close to rated) P & Q, the load voltage will be too low. That's one of the disadvantages of the basic droop system which will be solved by adding the "Voltage Drop Factor" in the proposed system in the next chapter.

$$m_2 = \frac{\Delta E_{\max}}{2 \cdot Q_{\max 2}} = \frac{12 \cdot \sqrt{2} V}{2 \cdot 700 \cdot 0.6 \text{ VAR}} \rightarrow m_2 = 0.0204 \frac{V}{\text{VAR}} = 2m_1 \quad (2-10)$$

$$E_{02} = 120 \cdot \sqrt{2} = 169.7 V = E_{01} \quad (2-11)$$

$$n_1 = \frac{\Delta \omega_{\max}}{P_{\max}} = \frac{0.1 \text{ Hz} \cdot 2\pi}{1400 \cdot 0.8} \approx 0.00056 \frac{\text{Rad}}{\text{S.W}} = \frac{n_2}{2} \quad (2-14)$$

$$\omega_{01} = \omega_{02} = 2\pi \cdot 60.05 \frac{\text{Rad}}{\text{S}} \quad (2-15)$$

Note that the allowed ranges of voltage magnitude and frequency changes in previous equations are in harmony with IEEE 1547 standard.

According to the simulation results in section 3.3.2, by increment in  $\Delta \omega_{\max}$ , (or equivalently parameters ns), the system will be slower and will become unstable at some

point. This feature and other behaviors of the system will be addressed in detail in section 3.3.2.

Also note that according to (2-7)

$$P_i = \frac{\omega_0 - \omega_i}{n_i} \quad (2-16)$$

Besides, the inverters have the same steady state and no load frequencies, and according to the basic droop scheme

$$S_1 * n_1 = S_2 * n_2 \quad (2-17)$$

where S is the apparent rated power of the inverter; thus

$$\frac{P_1}{P_2} = \frac{S_1}{S_2} \quad (2-18)$$

Which shows very good P sharing; But since the steady state voltage magnitudes of the inverters ( $|\vec{E}_i|$ ) are not necessarily identical or not even very close, (especially in the case of non-identical apparent rated powers or different feeders' impedances), if the droop parameters  $m_s$  are chosen as in (2-8) & (2-10), it will not result in good Q sharing.

## 2.4 SYSTEM TRANSIENT AND STEADY STATE BEHAVIOR

The following simulation's results are obtained by SIMULINK software. The power system parameters are the same as the ones in Table 2-1 and the beginning of section 2.2.

The power system schematic is shown in Fig. 2-26.

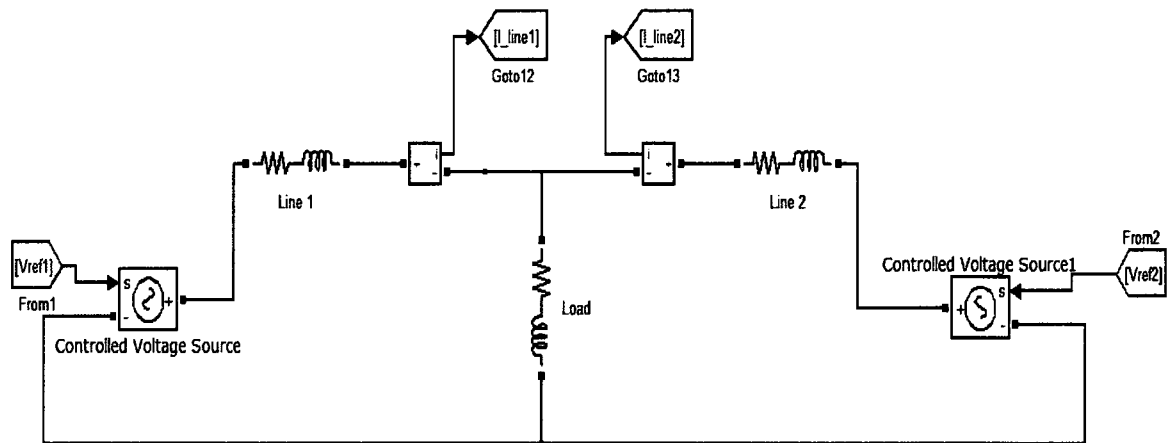


**Fig. 2-26** Power system schematic

Also the control system schematic is shown on Fig. 2-27.

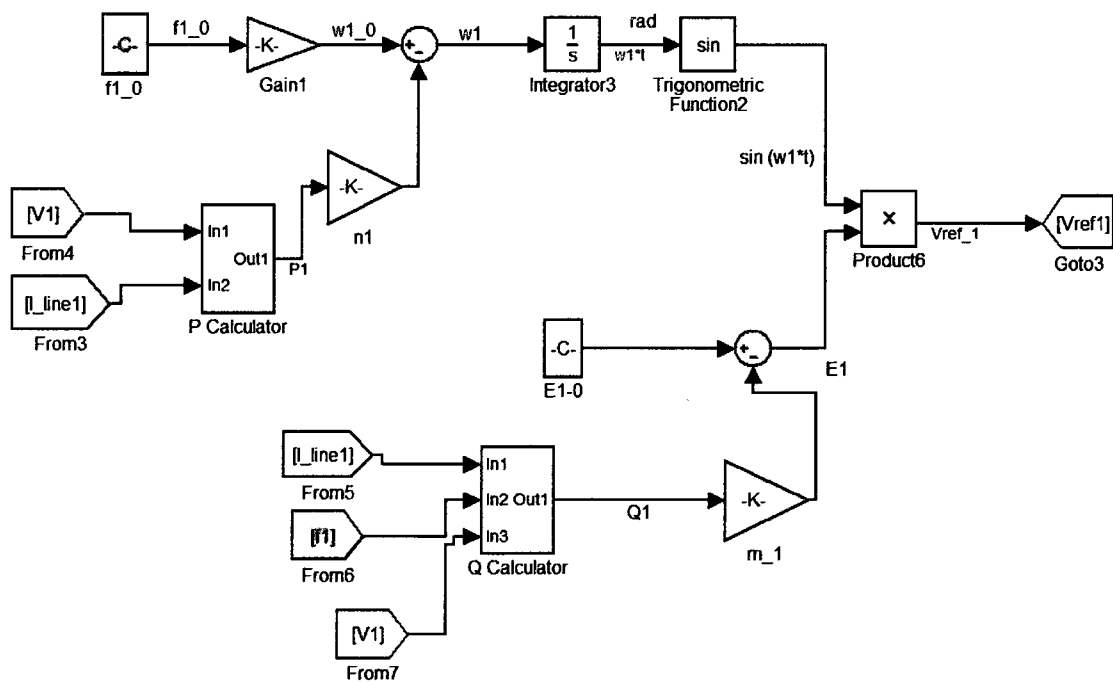


**Fig. 2-27** Control system schematic

Figure 2-28 shows the system sources' powers when there is full load (before load change), and also after 20% decrement in the load at  $t=0.8s$ .

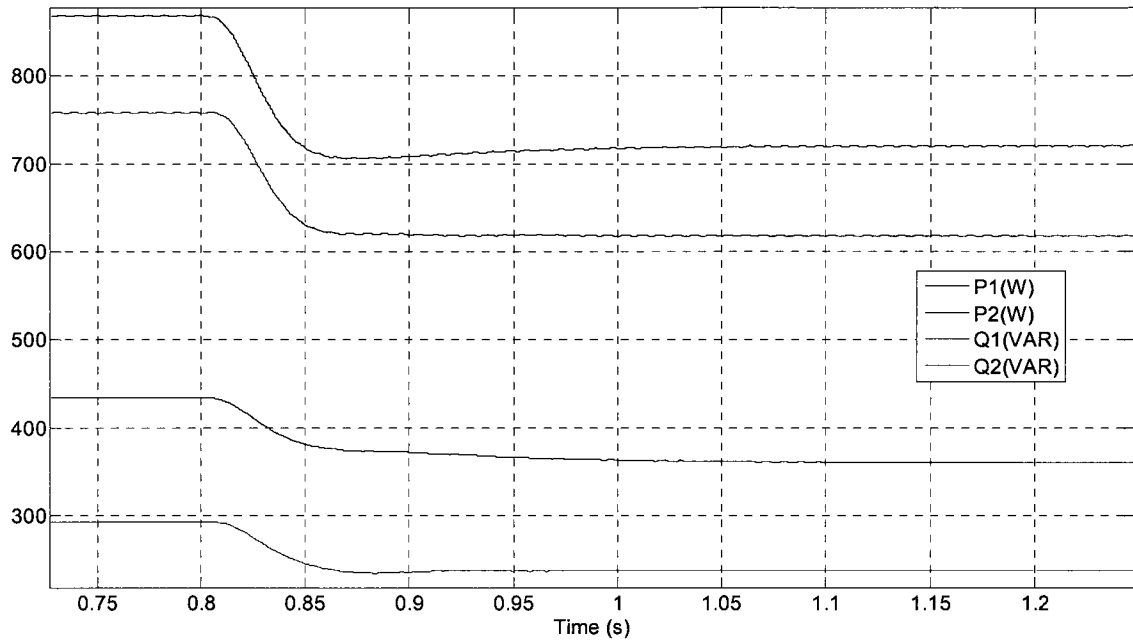


**Fig. 2-28** System powers changes as the load decreases by 20% at  $t=0.8s$

(waveform's order from the top to the bottom: P1, Q1, P2, Q2)

The steady state values of the system's powers on Fig. 2-28 will be shown in Table 2-2 to evaluate the system's power sharing quality.

It can be seen in Fig. 2-29 that load voltage regulation is not good since the load voltage is less than the minimum of  $120V \cdot 0.95 = 114V$ . This problem will be eliminated in the proposed system in next chapter. The small ripples are due to the oscillations caused by the multipliers in the power calculator units (shown in Fig. 2-27) and also due to the RMS calculator blocks in SIMULINK.

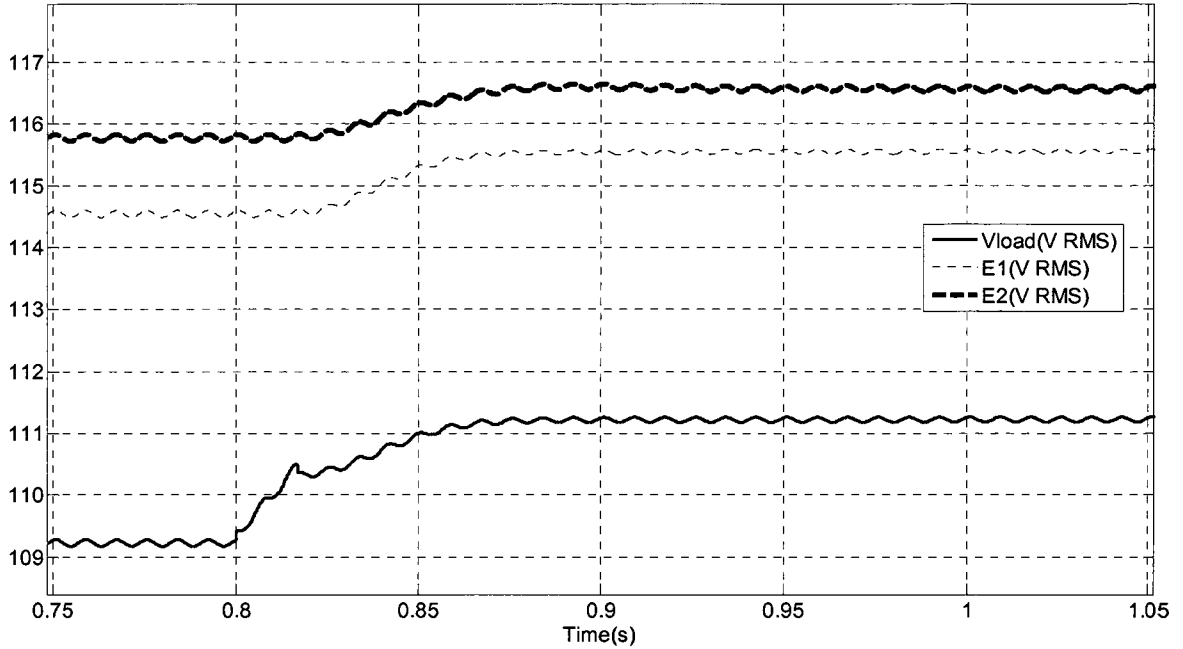


**Fig. 2-29** System voltages' changes as the load decrease by 20% at t=0.8s

The area between the two frequency curves in Fig. 2-30 is the phase angle difference between the sources ( $\phi_1 - \phi_2$ ) which is effective on sources' active and reactive powers.

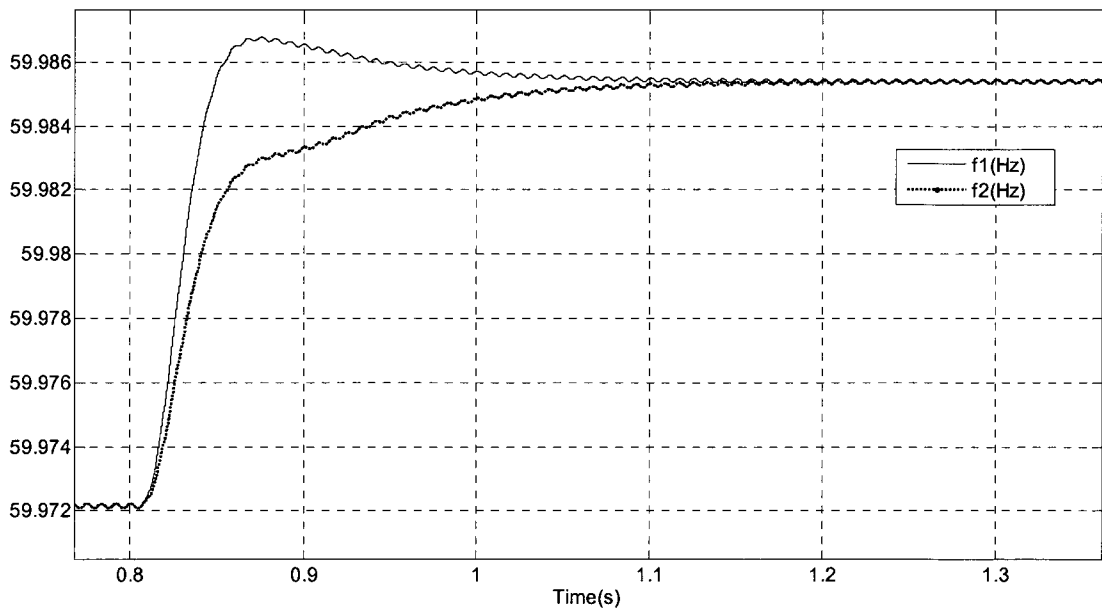


**Fig. 2-30** Sources' frequencies' changes as the load decreases by 20% at t=0.8s

In Table 2-2, the steady state results are for the full load case before load change, and the transient results are for the transient case state after 20% decrement in the load at  $t=0.8s$ . It could be seen in this table that the Q sharing is not good since its value is not even close to the desired value of 2; but the P sharing is good. Good Q sharing will be achieved in the proposed system in chapter three by changing the way of the determination of m & n parameters. Also frequency regulation is acceptable in Table 2-2. (According to [21])

**TABLE 2-2** Steady state results (before load change) and some transient state results

Q1 (VAR)	Q2 (VAR)	Q1/Q2	P1=2P2 (W)	E <sub>1</sub> (V <sub>RMS</sub> )	E <sub>2</sub> (V <sub>RMS</sub> )	V <sub>load</sub> (V <sub>RMS</sub> )	φ1-φ2 (Deg)	Steady state Frequency (Hz)	Ts (s)	Over shoot (%)
757	293	2.58	868	114.6	115.8	109.2	-1.02	59.972	0.4	10.6

## 2.5 CONCLUSION

In this chapter the exact power equations were used to attain the relationships between the system's parameters and the system's powers. It was observed that the sources' voltage's magnitudes and phase angles have significant effects on the system's powers. On the other hand, the system's steady state frequency doesn't have such effect on system's powers. The design of the basic conventional droop system was considered using these power relationships. It was explained why the sources' voltages' parameters have been made dependent on the sources' powers in the specific manner in (2-6) & (2-7). It was also discussed how the droop system makes negative feedback to help the system stability.

The disadvantages of the basic droop system were determined to be Q sharing and load voltage regulations problems with the help of the mathematical equations and also the bench mark system simulation results. These disadvantages of the basic droop system will be resolved in the proposed droop system in the next chapter using the “Voltage Drop Factors”, and “Correction Factors”.

# CHAPTER 3

## PROPOSED DROOP SYSTEM

---

### 3.1 INTRODUCTION

In this chapter a novel droop strategy is proposed which provides both desired P & Q sharing and also acceptable load voltage regulation. This is done in section 3.2 by modifying the basic droop system used in chapter 2 which includes adding the voltage drop factors and correction factors to the system.

In section 3.3, the effects of each droop coefficient on system's steady state results such as the active and reactive powers and their ratios, sources' voltages' magnitudes and phase angles, load voltage's magnitude, and system's frequency are evaluated. Also, the effects of the droop coefficients on system's stability and system's transient state results like overshoot, and speed are considered. Then the optimum droop coefficients are obtained from those results to have a solution for the best Q sharing, highest speed, and least overshoot; and also to have the load voltage's magnitude and system's frequency within their allowed ranges.

The same method has been used in section 3.4 to obtain the optimum droop coefficients for different cases (with different values of the sources' apparent powers and feeders' lengths).

### 3.2 THE STRUCTURE OF THE PROPOSED DROOP SYSTEM

One starts with the values below from the benchmark model used in chapter 2.

**TABLE 3-1** Power system Characteristics

	Source 1	Source 2
Power rating (VA)	1400	700
Line impedances ( $\Omega$ )	$(0.20 + j\omega * 0.00154)$	$3*(0.20 + j\omega * 0.00154)$

Full load impedance=  $(5.99 + j\omega * 0.0119)$  ( $\Omega$ ) and also  $V_{\text{rated}} = 120V_{\text{RMS}}$ .

Like in section 2-2 the general droop equations are:

$$E = E_0 - mQ \quad (3-1)$$

$$\omega = \omega_0 - nP \quad (3-2)$$

But now another method is used to determine the values of n and m as following:

$$\begin{aligned} \text{The reference } m_1 = m_{01} &= \frac{\Delta E_{\text{max\_source}}}{2 * Q_{\text{max}1}} \approx \frac{\Delta E_{\text{max\_load}}}{2 * Q_{\text{max}1}} * \left| \frac{Z_{\text{load\_eq\_min}1}}{Z_{\text{load\_eq\_min}1} + Z_{\text{line}1}} \right|^{-1} = \\ &= \frac{12 * \sqrt{2}V}{2 * 1400 * 0.6\text{VAR}} * \left| \frac{1.5 * [(5.99 + j\omega * 0.0119)]}{1.5 * [(5.99 + j\omega * 0.0119)] + (0.20 + j\omega * 0.00154)} \right|^{-1} \\ &\rightarrow m_{01} \approx 0.0100 * 1.0457 \approx 0.0105 \frac{V}{\text{VAR}} \end{aligned} \quad (3-3)$$

Note that the voltage drop factor  $1 = V_{\text{DF}1} = 1.0457$  and its counterpart in the second inverter, modify the conventional droop coefficients values to have good load voltage regulation.

For the full load condition there would be a too low load voltage because of the voltage drop in the feeders, that's why the  $V_{\text{DF}s}$  are multiplied into the rated voltages for calculation of  $E_{0s}$ .

$$E_{01} = 120 * \sqrt{2} * V_{DF_1} = 169.7 * 1.0457V \approx 177.5V \quad (3-4)$$

Also, the reference  $m_2 = m_{02} = \frac{\Delta E_{max\_source}}{2 * Q_{max2}} \approx \frac{\Delta E_{max\_load}}{2 * Q_{max2}} * \left| \frac{Z_{load\_eq\_min2}}{Z_{load\_eq\_min2} + Z_{line2}} \right|^{-1} =$

$$\frac{12 * \sqrt{2} V}{2 * 700 * 0.6 VAR} * \left| \frac{3 * [(5.99 + j\omega * 0.0119)]}{3 * [(5.99 + j\omega * 0.0119)] + 3 * (0.20 + j\omega * 0.00154)} \right|^{-1}$$

$$\rightarrow m_{02} \approx 0.0204 * 1.0689 \approx 0.0218 \frac{V}{VAR} \quad (3-5)$$

$$E_{02} = 120 * \sqrt{2} * V_{DF_2} = 169.7 * 1.0689 \approx 181.4V \quad (3-6)$$

$$\text{Where } Z_{load\_eq\_min1} = \frac{J+1}{J} Z_{load\_min} = 1.5 * (5.99 + j\omega * 0.0119) \quad (3-7)$$

$$Z_{load\_eq\_min2} = (J + 1) Z_{load\_min} = 3 * (5.99 + j\omega * 0.0119) \quad (3-8)$$

Where  $J = \frac{S_1}{S_2} = 2$  is the ratio between the sources' apparent powers.

The equivalent load impedances ( $Z_{load\_eq\_1,2}$ ) are obtained by splitting the joint load impedance into a combination of parallel equivalent loads. Each equivalent load represents the load seen by the correspondent inverter. The ratios of the impedance magnitudes are the reverse of the correspondent sources' apparent powers' ratios. Using these equivalent loads one can divide the system with a joint load to some systems, each with a source and a load.

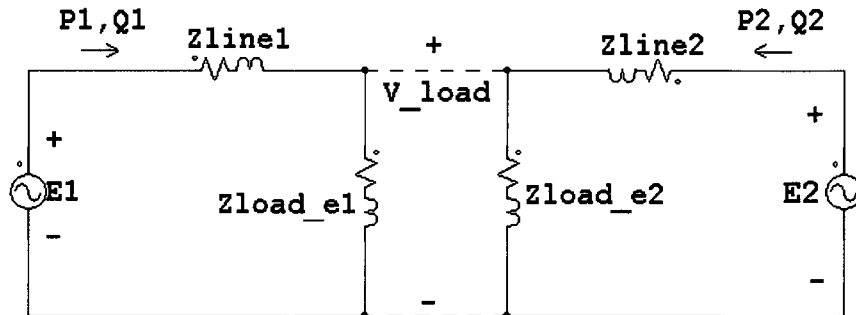


**Fig. 3-1** Simplified split system's circuit using the equivalent loads

$$\text{The reference } n_1 = n_{01} = \frac{\Delta\omega_{\max}}{P_{\max}} = \frac{1 \cdot 2\pi}{1400 \cdot 0.8} \approx 0.0056 \frac{\text{Rad}}{\text{s.W}} = \frac{n_{02}}{J} \quad (3-9)$$

$$f_{01} = f_{02} = 60.5\text{Hz} \quad (3-10)$$

Final values of the droop coefficients are

$$n_1 = n_{01} * \alpha \quad (3-11)$$

$$n_2 = \alpha * (J * n_{01}) \quad (3-12)$$

$$m_1 = m_{01} * \beta * CF_1 \quad (3-13)$$

$$m_2 = m_{02} * \beta * CF_2 \quad (3-14)$$

$$\text{where } \alpha \leq 1 \quad (3-15)$$

$$\beta \leq 1 \quad (3-16)$$

$$\text{and CFs (correction factors)} \leq 1 \quad (3-17)$$

(The maximum values of  $\alpha = 1$  corresponds to the frequency range of

$59.5\text{Hz} \leq f \leq 60.5\text{Hz}$  and  $\beta = 1$  corresponds to the  $120 \cdot 0.95V_{\text{RMS}} < V_{\text{load}} < 120 \cdot 1.05V_{\text{RMS}}$ ).

By using this droop strategy there will be good P sharing and one needs modified droop coefficients for obtaining appropriate Q sharing as it will be done by using the “Correction Factors” later in this chapter.

### **3.3 EVALUATION OF THE EFFECTS OF DROOP PARAMETERS ON SYSTEM TRANSIENT AND STEADY STATE BEHAVIOR**

In this section, the system power parameters are the same as the ones in the section 3.2. Overshoots are measured from the frequency waveforms. Also note that in the following simulations, for now, the both correction factors are kept equal to 1; but they might be decreased later to create better Q sharing.

As an example of system behavior, one can see in Fig. 3-2, the system powers when  $\alpha = 0.2$ ,  $\beta = 0.7$ .

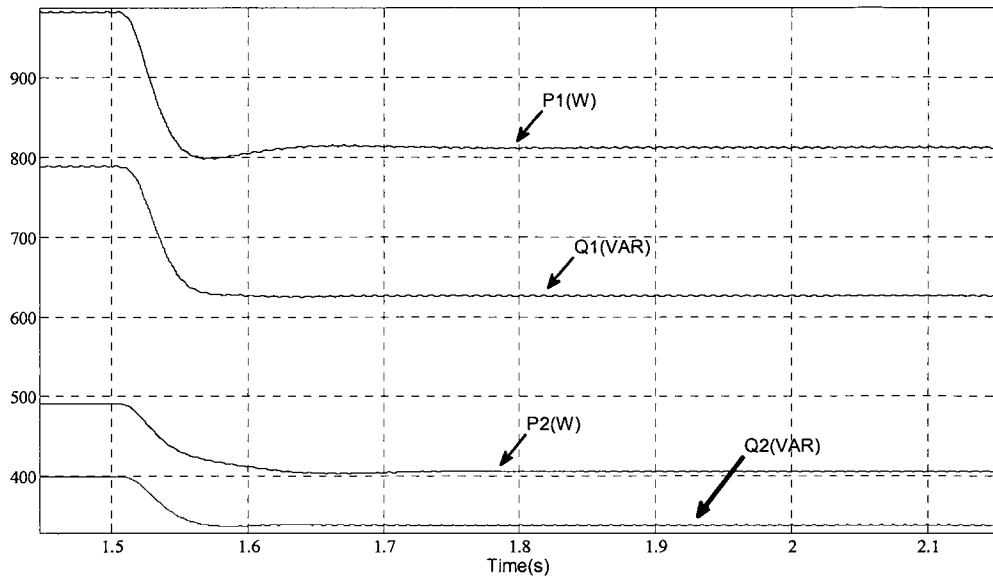


**Fig. 3-2** System's powers as the load decreases by 20%

Table 3-2 shows the values obtained for several system parameters from simulations conducted with different values of  $\beta$  while keeping the other parameters constant (e.g.  $\alpha = 0.2$ ,  $CF1 = CF2 = 1$ ). Notice that the steady state results are for the 100% load and the transient results are for the transient state after 20% decrement in the load at  $t = 1.5s$ .

**Table 3-2** Effects of  $\beta$  on system's behavior

$\beta$	Q1 (VAR)	Q2 (VAR)	Q1/Q2	P1=2P2 (W)	E <sub>1</sub> (V)	E <sub>2</sub> (V)	E <sub>1</sub> -E <sub>2</sub> (V)	Vload (RMS)	Delta $\phi$ (Deg)	Steady state freq. (Hz)	Ts (s)	Over shoot (%)
<b>0.1</b>	829	428	1.937	1039	176.6	180.5	-3.9	119.4	-0.763	60.315	0.46	7.1
<b>0.3</b>	815	417	1.954	1019	174.9	178.7	-3.8	118.2	-0.772	60.318	0.46	7.7
<b>0.5</b>	802	407	1.971	1000	173.3	177.0	-3.7	117.1	-0.777	60.322	0.47	8
<b>0.7</b>	788	399	1.975	982	171.7	175.3	-3.6	116.1	-0.781	60.325	0.47	7.9
<b>0.8</b>	781	395	1.977	973	170.9	174.5	-3.6	115.6	-0.782	60.327	0.47	8.4
<b>0.9</b>	774	391	1.980	964	170.2	173.7	-3.5	115	-0.784	60.3280	0.46	8.5
<b>1</b>	<b>768</b>	<b>387</b>	<b>1.984</b>	<b>956</b>	<b>169.4</b>	<b>172.9</b>	<b>-3.5</b>	<b>114.5</b>	<b>-0.785</b>	<b>60.330</b>	<b>0.46</b>	<b>8.7</b>

As it can be seen in the Table 3-2, by increment in  $\beta$  (m),  $(E_1-E_2)$  increases, which will result in increment in  $Q1/Q2$  (in accordance with figure 2-14 & 2-15) and will make this reactive power ratio closer to the desired value of 2 as it can be seen in Fig. 3-5.

Since both  $E_1$  and  $E_2$  decrease by increment in  $\beta$ , the load voltage and the real powers decrease too;  $P1$  decreases since  $E_1$  and  $\varphi_1$  decrease (as shown on Fig. 2-9), so the droop system decreases  $E_2$  enough to decrease  $P2$  adequately to keep the constant ratio between the real powers.

Moreover, as seen in the Table 3-2, by increment in  $\beta$  (m), the steady state frequency increases, since the real power decreases and these two are related reversely via the droop equation (3-2). Note that  $\beta$  (m) has effect on the difference between the phases of sources even though it is not linked directly to the system frequency in the droop system. Also pay attention that  $\beta$  (m) has very small effects on the settling time.

Figures 3-3 to 3-5 demonstrate the effects of  $\beta$  on system's behavior.

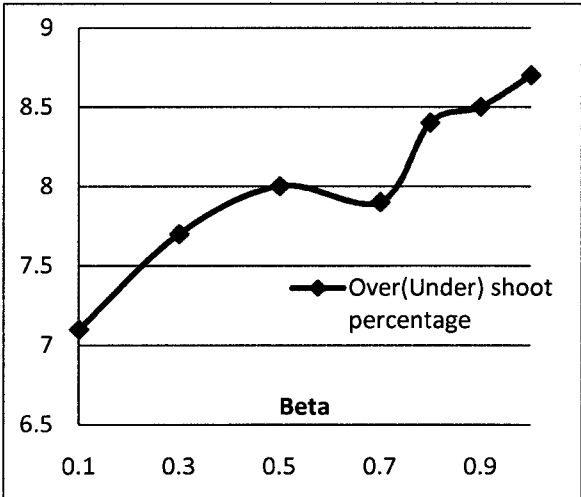


**Fig. 3-3** Effect of  $\beta$  on system over shoot

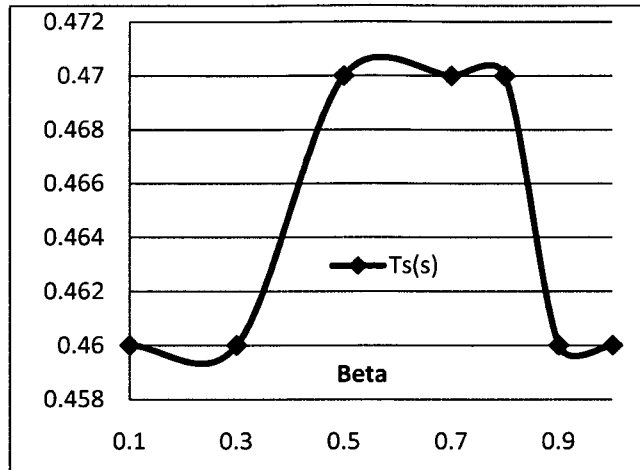


Fig. 3-4 Very small changes in settling time vs. changes in  $\beta$

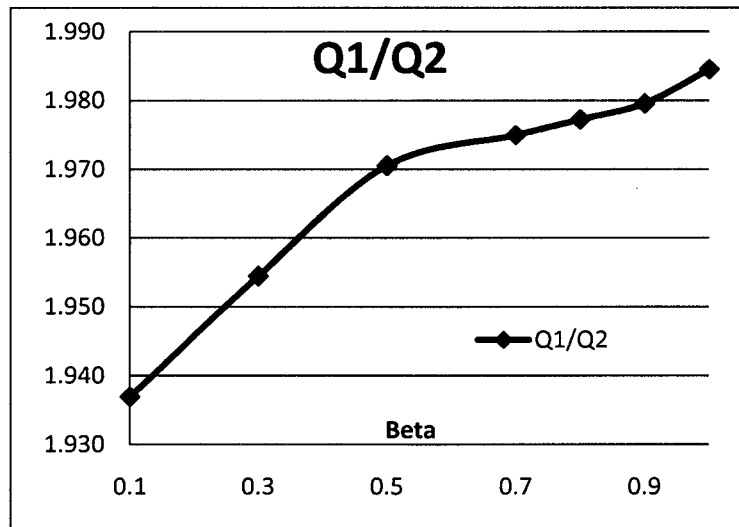


Fig. 3-5 Effect of  $\beta$  on reactive power sharing

The best point here is chosen to be for  $\beta=1$  since in this case there are the best Q sharing and settling time.

Then, the values of  $\beta$  as well as the CFs are kept constant to 1; and now  $\alpha$  (n) is changed to see its effects on system behavior. The results are shown in Table 3-3.

**TABLE 3-3** Effects of  $\alpha$  on system's behavior

$\alpha$	Q1 (VAR)	Q2 (VAR)	Q1/Q2	P1= 2P2 (W)	E1 (V)	E2 (V)	E1-E2 (V)	Vload (RMS)	Delta $\phi$ (Deg)	Steady state freque. (Hz)	Ts (s)	Over shoot (Max) (%)
0.1	769	387	1.987	955	169	173	-3.6	114.5	-0.785	60.4149	0.48	11.2
0.2	<b>768</b>	<b>387</b>	<b>1.984</b>	<b>956</b>	<b>169</b>	<b>173</b>	<b>-3.5</b>	<b>114.5</b>	<b>-0.785</b>	<b>60.3295</b>	<b>0.46</b>	<b>8.7</b>
0.3	768	387	1.984	957	169	173	-3.6	114.5	-0.785	60.244	0.7	7.4
0.4	769	387	1.987	958	169	173	-3.6	114.5	-0.784	60.1583	1	10
0.6	771	388	1.987	957	169	173	-3.6	114.5	-0.784	59.987	4.1	22.4
0.8	Unstable							Unstable				
1	Unstable							Unstable				

The effects of  $\beta$  on settling time, overshoot, and stability is less than the effects of  $\alpha$ (n) on them as the results of comparison of Tables 3-1 & 3-2.

The effects of  $\alpha$  on system's transient state behavior are shown on figures 3-6 and 3-7.

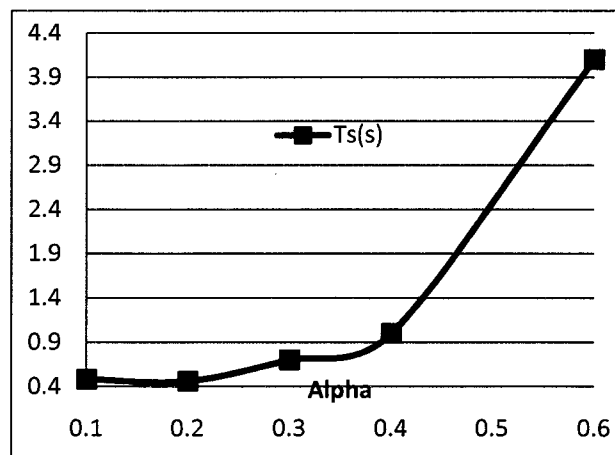


**Fig. 3-6** Changes in settling time vs. changes in  $\alpha$

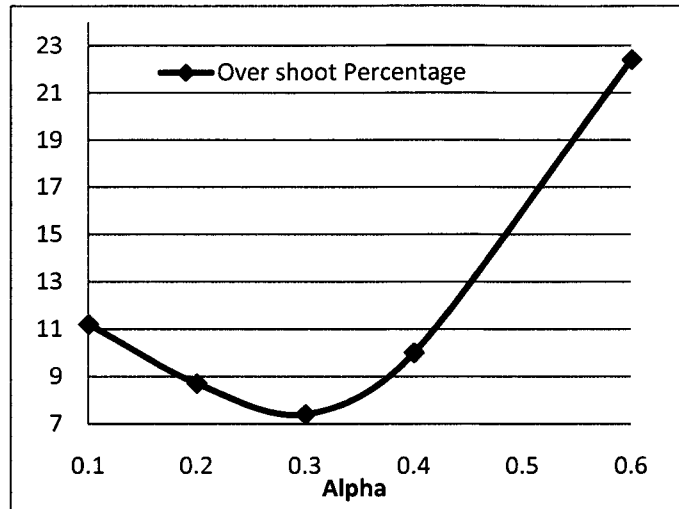


**Fig. 3-7** Effect of  $\alpha$  on system over shoot

It can be seen that in Table 3-3 that  $\alpha$  (n) has almost no effect on the source voltages' magnitudes and phases, and therefore no effect on sources powers but it has remarkable effects on the system steady state frequency and transient behavior, even more than  $\beta$  (m). One can see in figures 3-6 and 3-7 that the best transient state can be achieved at around  $\alpha=0.2$  (the best speed and smallest overshoot). This value of  $\alpha$  has been verified before as the selected value, so that no more iteration is needed and finally the values of  $\alpha=0.2$  and  $\beta=1$  have been chosen as the optimum droop coefficients.

Moreover, since  $\frac{Q_1}{Q_2} = 1.98 \approx 2$ , there is no need to change the correction factors ( $CF_1$  and  $CF_2$ ) and they will remain equal to 1.

### 3.4 OPTIMUM DROOP COEFFICIENTS FOR DIFFERENT SYSTEM TYPES

#### 3.4.1 SYSTEM BEHAVIOR (LENGTH2 = (LENGTH1), S1=S2)

One starts with the simplest case in which the sources have the same rated apparent power and feeder impedance.

**TABLE 3-4** Power system Characteristics

	Source1	Source2
Power rating (VA)	1050	1050
Line impedances	(0.20 +jω* 0.00154)	(0.20 +jω* 0.00154)

The calculated droop parameters are:

$$\rightarrow m_{01} \approx 0.0134 * 1.034 \approx 0.0139 \frac{V}{VAR} \quad (3-18)$$

$$E_{01} = 120 * \sqrt{2} * V_{DF1} = 169.7 * 1.034 \approx 175.5V \quad (3-19)$$

$$\rightarrow m_{02} \approx 0.0134 * 1.034 \approx 0.0139 \frac{V}{VAR} \quad (3-20)$$

$$E_{02} = 120 * \sqrt{2} * V_{DF1} = 169.7 * 1.034 \approx 175.5V \quad (3-21)$$

$$n_{01} = n_{02} = \frac{\Delta\omega_{max}}{P_{max}} = \frac{1*2\pi}{1050*0.8} \approx 0.0075 \frac{Rad}{S.W} \quad (3-22)$$

$$f_{01} = f_{02} = 60.5Hz \quad (3-23)$$

Note that in the following simulations  $\alpha=0.15$ ,  $\beta=1$ ,  $CF_1=CF_2=1$ . In this specific case which has completely symmetric power stage, if the sources have the same initial phases, there will be no transient frequency difference; also there will be equal Qs no matter how much  $\alpha$  and  $\beta$  are. So to have some better evaluation of system the initial phase difference is applied. ( $\phi_2=\phi_1+0.03$  (Radians))

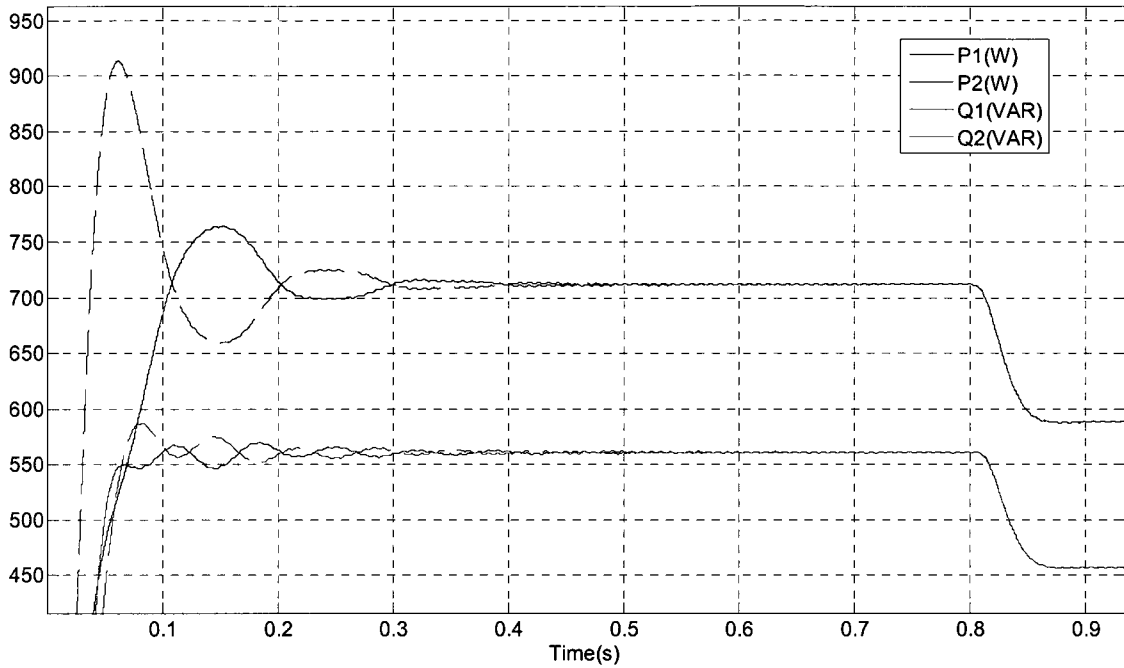


**Fig. 3-8** System frequencies response as the load decreases by 20% at t=1s (the order of the waveform from the top to the bottom (at t=0.15) P1, P2, Q2, Q1)

As it can be seen on the figure 3-8, the initial phase difference makes transient frequency difference; but for changes in load in the steady state, there will not be any transient frequency difference.

When  $\alpha = 0.15$ ,  $CF_1 = CF_2 = 1$  results are shown in Table 3-5.

**TABLE 3-5** The effects of  $\beta$  on system behavior

$\beta$	Vload (RMS)	$f_{st}$ (Hz)	$T_s$ (s)	Over shoot (%)
<b>0.2</b>	118.88	60.3630	0.06	0.0
<b>0.4</b>	117.74	60.3665	0.07	0.1
<b>0.6</b>	116.69	60.3679	0.07	0.2
<b>0.8</b>	115.65	60.3703	0.08	0.5
<b>1</b>	<b>114.68</b>	<b>60.3725</b>	<b>0.08</b>	<b>0.9</b>

As mentioned before for any value of  $\beta$  there will be great Q sharing. Also as it can be seen in the previous table, the overshoot just changes a little as  $\beta$  changes, so that it doesn't make such an advantage if a small value of  $\beta$  is chosen to have just a little bit less overshoot. On the other hand, in reality, because of the system feeders and LPFs are not ideal, there are always differences in the equivalent line impedances (sum of the feeder impedance and the LPF output impedance); so that it is better to use the value of  $\beta=1$  which works for the non balanced feeders cases too. By increment in  $\beta$ , load voltage decreases. Moreover the steady state frequency increases since the real power decreases.

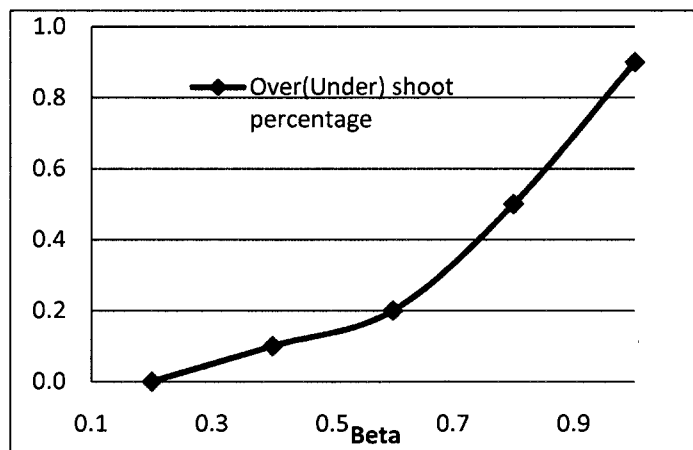


**Fig. 3-9** Effect of  $\beta$  on system's over(under)shoot

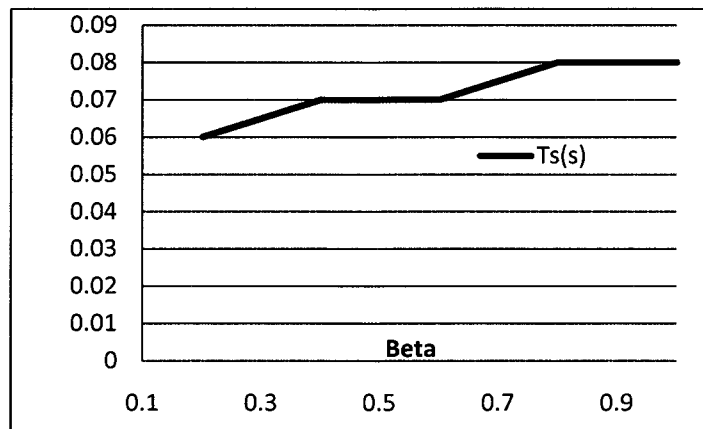


**Fig. 3-10** Effect of  $\beta$  on system's settling time

When the values of  $\beta$ ,  $CF_1$ , and  $CF_2$  are kept constant to 1,  $\alpha$  (n) is changed to see its effects on system behavior which are presented on Table 3-6.

**TABLE 3-6** Effects of  $\alpha$  on system's behavior

$\alpha$	Vload (RMS)	Steady state frequency (Hz)	Ts(s)	Over shoot (Max) (%)
0.1	114.68	60.4150	0.08	0.7
0.15	114.68	60.3725	0.08	0.9
0.2	114.68	60.3299	0.08	1.4
0.3	114.68	60.2446	0.08	1.5
0.4	Unstable			

Figure 3-11 shows the effects of  $\alpha$  on system's overshoot percentage.

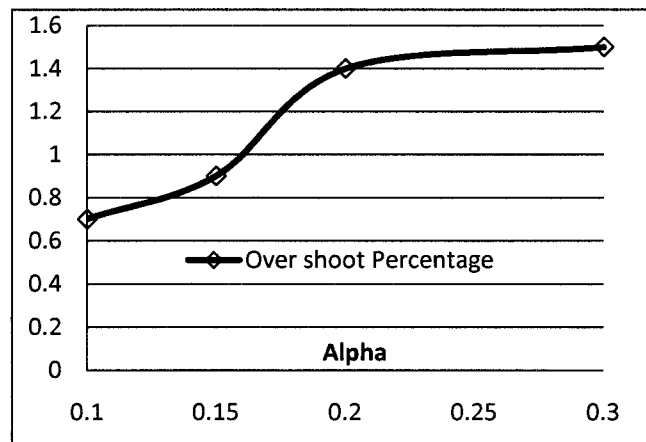


**Fig. 3-11** Effects of  $\alpha$  on system's overshoot percentage

It can be seen that  $\alpha$  (n) has almost no effect on the sources' voltages' magnitudes and phase angles, and therefore no effect on sources' powers. Also it has almost no effect on the settling time. But it has some small effects on the system steady state frequency and overshoot. One can concluded by results in Table 3-6 and Fig. 3-11 that the best case can be achieved at  $\alpha=0.1$  which has smallest overshoot.

So finally the values of  $\alpha=0.1$  and  $\beta=1$  have been chosen as the optimum droop parameters. Also since the Q sharing is already achieved the traditional values of  $CF_1=CF_2=1$  will be kept.

### 3.4.2 SYSTEM WITH (LENGTH2 = LENGTH1, S1=2S2)

The system apparent powers and feeder impedances are shown in Table 3-7.

**TABLE 3-7** Power system Characteristics

	Source1	Source2
Power rating (VA)	1400	700
Line impedances	(0.20 +j $\omega$ * 0.00154)	(0.20 +j $\omega$ * 0.00154)

Similarly as in section 3.3 the calculations are done. The results follow.

$$m_{01} \approx 0.0100 * 1.0457 \approx 0.0105 \frac{V}{VAR} \quad (3-24)$$

$$m_{02} \approx 0.0204 * 1.0457 \approx 0.0213 \frac{V}{VAR} \quad (3-25)$$

$$E_{02} = E_{01} = 120 * \sqrt{2} * V_{DF1} = 169.7 * 1.0457V \approx 177.5V \quad (3-26)$$

$$\text{Also the reference } n_1 = n_{01} = \frac{\Delta\omega_{max}}{P_{max}} = \frac{1*2\pi}{1400*0.8} \approx 0.0056 \frac{Rad}{S.W} = \frac{n_{02}}{J} \quad (3-27)$$

$$f_{01} = f_{02} = 60.5Hz \quad (3-28)$$

As an example of system behavior, one can see the system frequencies in Fig. 3-12 when  $\alpha = 0.2, \beta = 0.5$ .

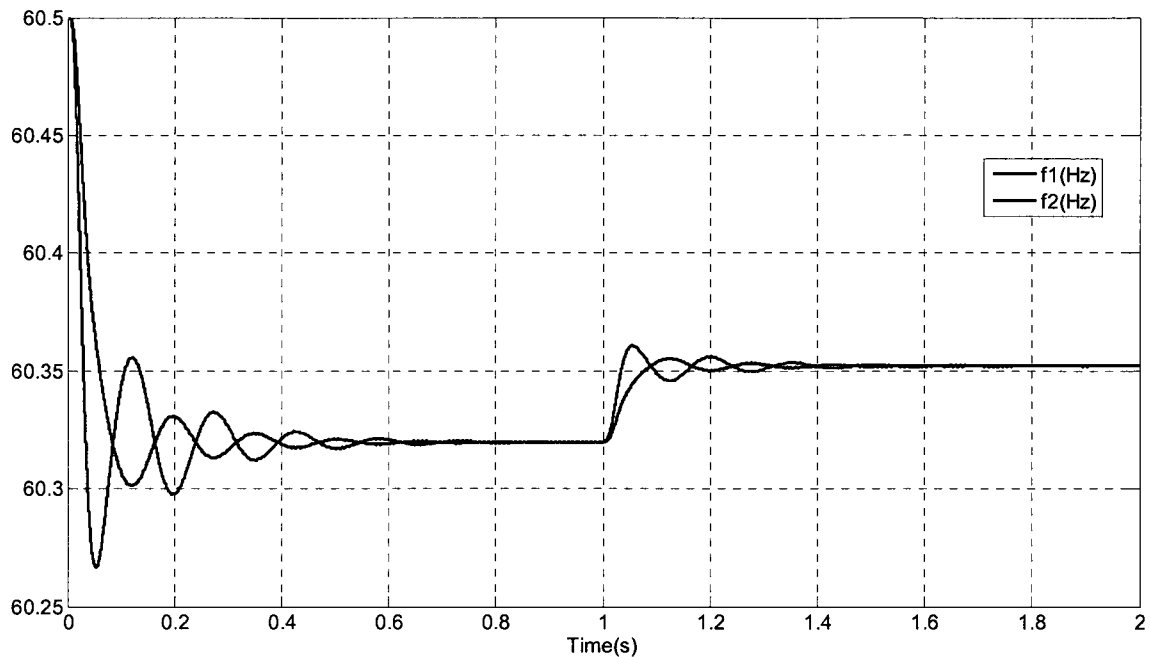


**Fig 3-12** System frequencies response as the load decreases by 20% (f2 has more initial undershoot ( $0 < t < 0.15s$ ) and more overshoot ( $1s < t < 1.15s$ ) than f1)

With  $\alpha = 0.2, CF_1 = CF_2 = 1$  results are as shown in Table 3-8.

**TABLE 3-8** System simulation results when  $\beta$  changes

$\beta$	Q1 (VAR)	Q2 (VAR)	Q1/Q2	Vload (RMS)	f <sub>st</sub> (Hz)	Ts (s)	Over shoot (%)
<b>0.1</b>	598	649	0.921	120.7	60.312	0.91	29.5
<b>0.3</b>	651	570	1.142	119.4	60.315	0.97	26.6
<b>0.5</b>	673	524	1.284	118.2	60.32	0.98	26.2
<b>0.7</b>	683	492	1.388	117.1	60.3230	0.98	25.2
<b>0.8</b>	<b>685</b>	<b>480</b>	<b>1.427</b>	<b>116.6</b>	<b>60.325</b>	<b>0.98</b>	<b>24.6</b>
<b>0.9</b>	686	469	1.463	116.1	60.3262	1	24.1
<b>1</b>	686	459	1.495	115.6	60.328	1.15	23.9

As it can be seen in the previous table and following diagrams, by increment in  $\beta$  (m) there would be increment in Q1/Q2 and better Q sharing (since  $S_1 = 2S_1$ ).

By increment in  $\beta$ , load voltage decreases. Moreover the steady state frequency increases since the real power decrease.

Figures 3-13 to 3-15 show the effects of  $\beta$  on system's transient behavior and Q sharing ratio.

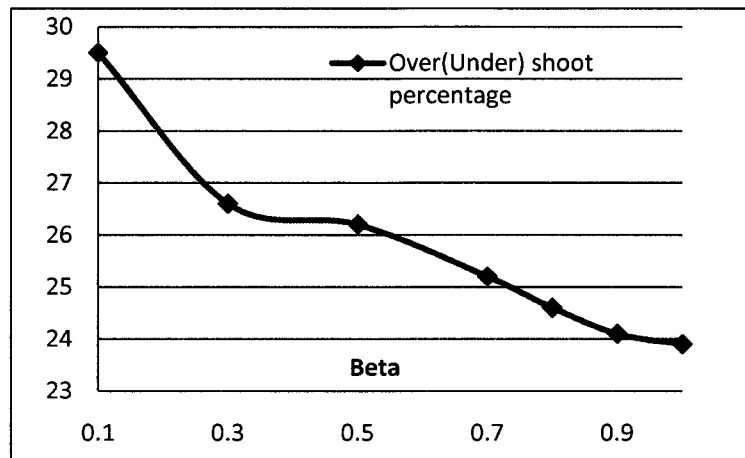


**Fig 3-13** Effects of  $\beta$  on system's over(under)shoot

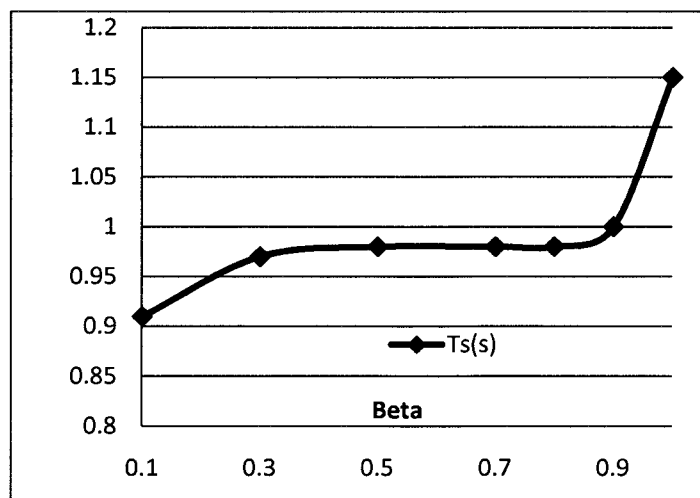


**Fig 3-14** Effects of  $\beta$  on system's settling time

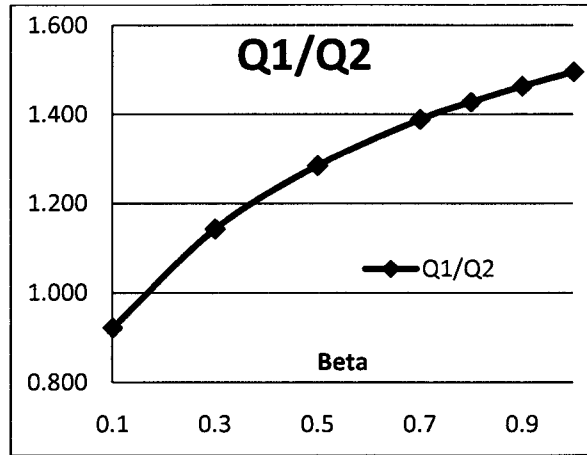


Fig 3-15 Effects of  $\beta$  on system's Q sharing ratio

Also note that increment in  $\beta$  (m) has very small effects on overshoot and increases the settling time a bit. According to the previous results the  $\beta=0.8$  has been chosen which has small settling time and rather good Q sharing.

The value of  $\beta$  is kept constant to 0.8, also  $CF1= CF2 =cte=1$ ; Now  $\alpha$  (n) is changed to see its effects on system behavior. The results are shown in Table 3-9.

TABLE 3-9 Effects of  $\alpha$  on system behavior

$\alpha$	Q1 (VAR)	Q2 (VAR)	Q1/Q2	Vload (RMS)	f <sub>st</sub> (Hz)	Ts(s)	Over shoot (%)
<b>0.05</b>	685	480	1.427	116.6	60.4562	0.5	35.1
<b>0.1</b>	685	480	1.427	116.6	60.4122	0.53	30.1
<b>0.15</b>	685	480	1.427	116.6	60.3686	0.61	29.6
<b>0.2</b>	<b>685</b>	<b>480</b>	<b>1.427</b>	<b>116.6</b>	<b>60.3247</b>	<b>0.98</b>	<b>24.6</b>
<b>0.25</b>	685	480	1.427	116.6	60.2807	1.8	23.1
<b>0.3</b>	685	480	1.427	116.6	60.237	4.5	22.8
<b>0.4</b>	Unstable						
<b>0.6</b>	Unstable						
<b>0.8</b>	Unstable						
<b>1</b>	Unstable						

Figures 3-16 and 3-17 show the effects of  $\alpha$  on the system's settling time and overshoot percentage respectively.

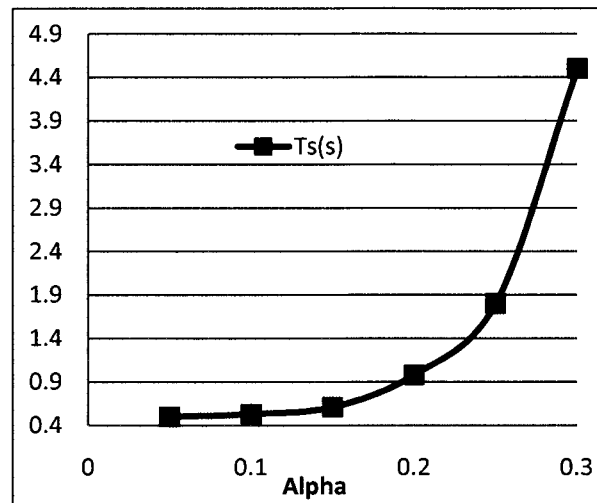


**Fig 3-16** Effects of  $\alpha$  on the system's settling time

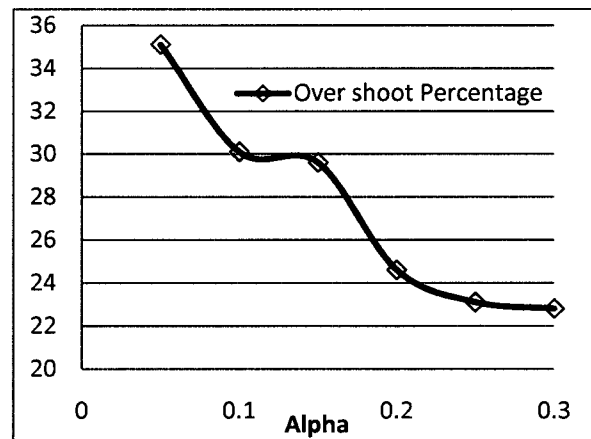


**Fig 3-17** Effects of  $\alpha$  on the system's overshoot percentage

It can be seen that  $\alpha$  (n) has almost no effect on the source voltages magnitudes and phases, and therefore no effect on sources powers but it has remarkable effects on the system steady state frequency and transient behavior even more than  $\beta$  (m). One can see in figures 3-16 and 3-17 that the trade-off point can be achieved at around  $\alpha = 0.2$  which rather small settling time and overshoot. So finally the values of  $\alpha = 0.2$  and  $\beta = 0.8$  have been chosen as the optimum droop parameters.

When one keeps the values of  $\alpha = 0.2$  and  $\beta = 0.8$ ,  $CF_2=1$  constant and varies the values of  $CF_1$  to see its effects on the system behavior, the results can be seen in Table 3-10.

**TABLE 3-10** Effects of the correction factor1 on the system behavior

$CF_1$	$P1=2P2(W)$	$Q1$ (VAR)	$Q2$ (VAR)	$Q1/Q2$	$V_{load}$ ( $V_{RMS}$ )	Steady state frequen. (Hz)	$T_s$ (s)	Overshoot (%)
0.4	1010	812	387	2.10	118.18	60.3198	1.3	16.4
0.7	995	743	437	1.7	117.32	60.3224	1.05	21
1	983	685	480	1.427	116.60	60.3247	0.98	24.6

Figure 3-18 demonstrates the effects of  $CF_1$  on the system's settling time and Q sharing ratio. The intersection of the two curves on top has a real part which is the exact desired

$CF_1$  at which  $\frac{Q1}{Q2} = 2$ .

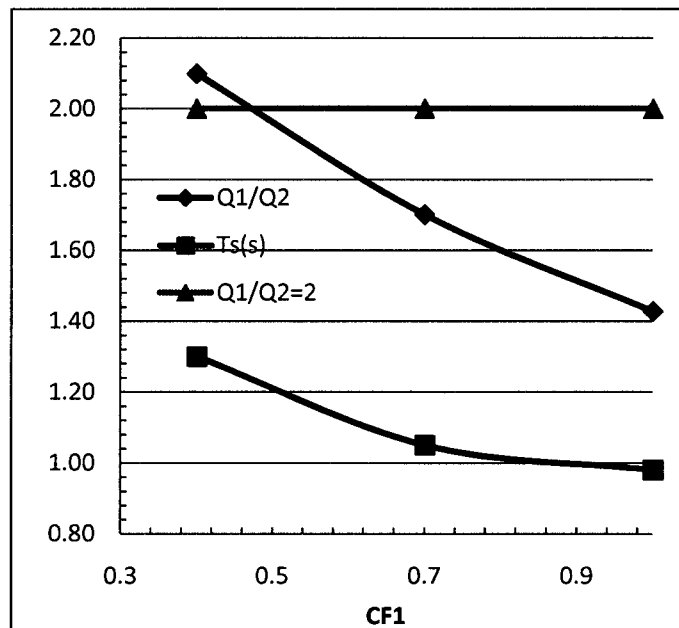


**Fig 3-18** The effects of  $CF_1$  on the system's settling time and Q sharing ratio

As one can see in the previous table, by decrement in the  $CF_1$  starting from 1 (conventional value), the real powers and load voltage increase. During the course of decrement of  $CF_1$ , the steady state frequency decreases since  $P$  increases; meanwhile the settling time increases a bit and overshoot decreases. So the value of  $CF_1=0.45$  has been chosen since it results in good reactive power sharing.

### 3.4.3 SYSTEM WITH LENGTH2 = (LENGTH1)/3, S1=2S2

Now the system is changed to have the power characteristics as shown in Table 3-11 as another case.

**TABLE 3-11** Power system characteristics

	Source1	Source2
Power rating (VA)	1400	700
Line impedances	$(0.20 + j\omega * 0.00154)*3$	$(0.20 + j\omega * 0.00154)$

Like the previous systems the calculations were done:

$$\rightarrow m_{01} \approx 0.0100 * 1.140 \approx 0.0114 \frac{V}{VAR} \quad (3-29)$$

$$E_{01} = 120 * \sqrt{2} * V_{DF1} = 169.7 * 1.40V \approx 193.4V \quad (3-30)$$

$$\rightarrow m_{02} \approx 0.0204 * 1.0457 \approx 0.0213 \frac{V}{VAR} \quad (3-31)$$

$$E_{02} = 120 * \sqrt{2} * V_{DF1} = 169.7 * 1.0457V \approx 177.5V \quad (3-32)$$

$$\text{The reference } n1 = n_{01} = \frac{\Delta\omega_{max}}{P_{max}} = \frac{1*2\pi}{1400*0.8} \approx 0.0056 \frac{\text{Rad}}{\text{S.W}} = \frac{n_{02}}{2} \quad (3-33)$$

$$f_{01} = f_{02} = 60.5\text{Hz} \quad (3-34)$$

As an example of system behavior, one can see in figure 3-19 the system's voltages when  $\alpha = 0.2$ ,  $\beta = 0.8$ ,  $CF_1 = CF_2 = 1$ .

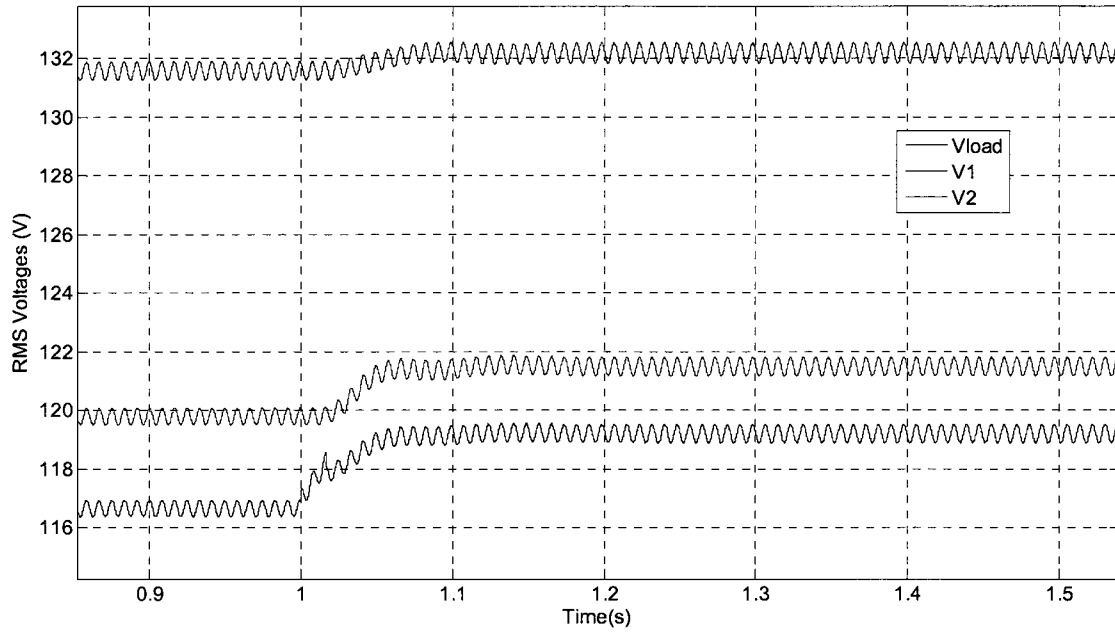


**Fig. 3-19** System voltages as the load decreases by 20% at  $t=1s$

When  $\alpha = 0.2$ ,  $CF_1 = CF_2 = 1$ , and  $\beta$  changes, simulation results are shown in Table 3-12.

**TABLE 3-12** Simulation results as  $\beta$  changes

$\beta$	Q1 (VAR)	Q2 (VAR)	Q1/Q2	Vload (RMS)	$f_{st}$ (Hz)	$T_s$ (s)	Over shoot (%)
<b>0.1</b>	818	557	1.469	121.21	60.3057	0.68	91.5
<b>0.2</b>	821	540	1.520	120.5	60.3080	0.67	91.5
<b>0.4</b>	812	491	1.654	117.88	60.3162	0.66	104.6
<b>0.8</b>	804	474	1.696	116.68	60.3198	0.65	91.3
<b>1</b>	<b>795</b>	<b>459</b>	<b>1.732</b>	<b>115.51</b>	<b>60.3234</b>	<b>0.65</b>	<b>90.9</b>

It can be concluded from the simulation results that by increment in  $\beta$  (m) there would be increment in Q1/Q2 and better Q sharing. Also by increment in  $\beta$ , load voltage decreases. Moreover the steady state frequency increases since the real power decreases.

Figures 3-20 and 3-21 show respectively the influences of  $\beta$  on system's settling time and Q sharing ratio for this case.

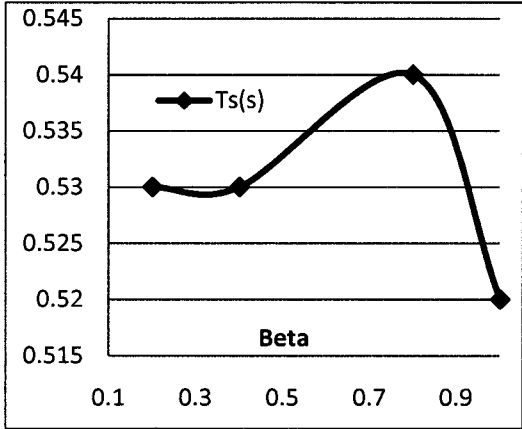


**Fig. 3-20** The influence of  $\beta$  on system's settling time

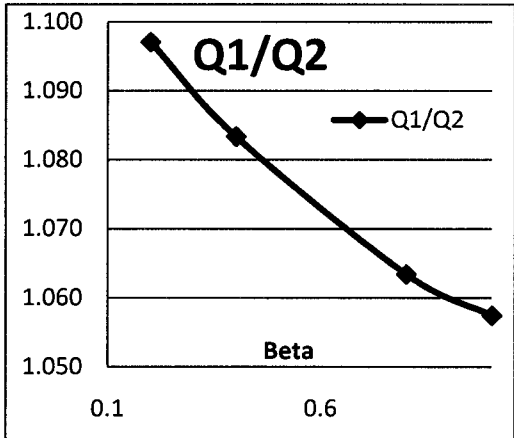


**Fig. 3-21** The influence of  $\beta$  on system's Q sharing ratio

Also note that increment in  $\beta$  (m) has small effects on overshoot and increases the settling time a bit. The  $\beta = 1$  has been chosen which has small settling time and overshoot and also good Q sharing.

Now the value of  $\beta$  is kept constant to 1 ( $CF_1=1$ ,  $CF_2=1$ ), and  $\alpha$  (n) is changed. The results are in Table 3-13.

**TABLE 3-13** System's results as  $\alpha$  is changed

$\alpha$	Q1 (VAR)	Q2 (VAR)	Q1/Q2	Vload (RMS)	f <sub>st</sub> (Hz)	Ts(s)	Over shoot (%)
<b>0.05</b>	795	459	1.732	115.5	60.4559	0.9	98.6
<b>0.1</b>	<b>795</b>	<b>459</b>	<b>1.732</b>	<b>115.5</b>	<b>60.4118</b>	<b>0.4</b>	<b>97.9</b>
<b>0.15</b>	795	459	1.732	115.5	60.3676	0.43	92.1
<b>0.2</b>	795	459	1.732	115.5	60.3234	0.65	90.9
<b>0.3</b>	795	459	1.732	115.5	60.2347	1.1	87.0
<b>0.5</b>	795	459	1.732	115.5	60.0562	2.8	85.5
<b>0.7</b>	Unstable						

Figures 3-22 and 3-21 show the effects of  $\alpha$  on the system's settling time and overshoot percentage respectively.

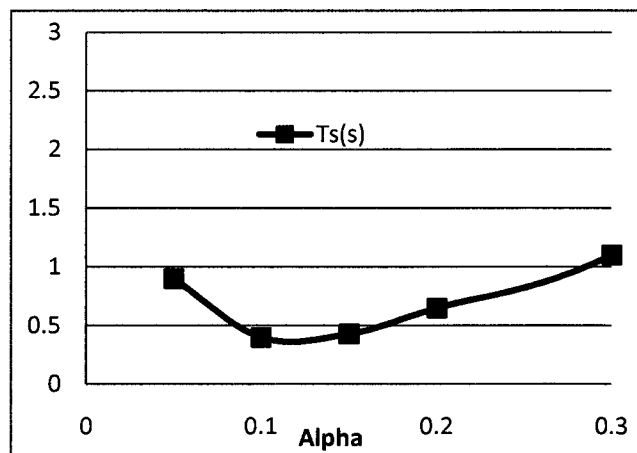


**Fig. 3-22** Effect of  $\alpha$  on the system's settling time

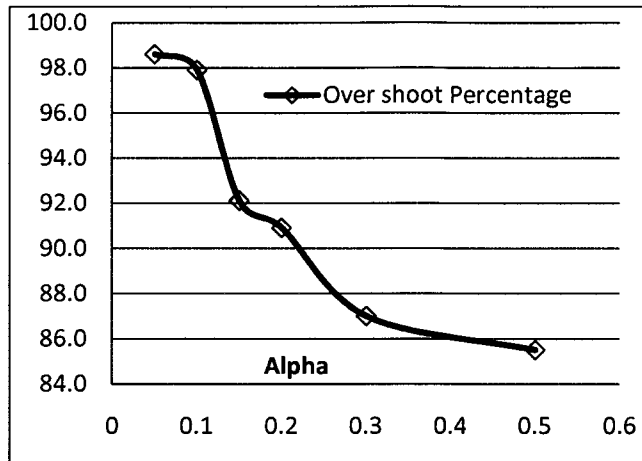


**Fig. 3-23** Effect of  $\alpha$  on the system's overshoot percentage

One can see in figures 3-22 and 3-23 that the trade-off point transient state can be achieved at around  $\alpha = 0.15$  which has small settling time and rather small overshoot. If one repeats the first procedure to change  $\beta$  again this time for  $\alpha$  of 0.15 instead of 0.2 one will get a table close to the table for with  $\alpha = 0.2$  (even exactly the same results for system powers), and the value of  $\beta = 1$  will be chosen again since it has the best Q sharing. So finally the values of  $\alpha = 0.15$  and  $\beta = 1$  have been chosen as the optimum droop parameters.

Then, one keeps the values of  $\alpha = 0.15$  and  $\beta = 1$ ,  $CF_2=1$  constant and varies the values of  $CF_1$ , the results are presented on Table 3-14.

**TABLE 3-14** System's behavior when  $CF_1$  varies

$CF_1$	Q1 (VAR)	Q2 (VAR)	Q1/Q2	Qline1 (VAR)	Qline2 (VAR)	Qline1/Qline2	Qload1 (VAR)	Qload2 (VAR)	Qload1/Qload2	Vload (V <sub>RMS</sub> )
<b>0.75</b>	847	426	1.99	173	18	9.61	674	408	1.65	116.19
<b>0.8</b>	836	433	1.93	171	18	9.50	665	415	1.60	116.05
<b>1</b>	795	459	1.73	165	19	8.68	630	440	1.43	115.50

As one can see in Table 3-14, by decrement in  $CF_1$  starting from 1 (conventional value) the load voltage increases. Also note that since the length of feeder1 is 3 times that

of the feeder2 and also the apparent power (current) of source1 is twice of source2, P and Q consumed in feeder1 are much larger than those in feeder2. As it can be assessed in this table, the ratios of the reactive powers consumed in the feeders, loads, and overall are different. The Q sharing is based on the last ratio (4<sup>th</sup> column above from left). The value of  $CF_1=0.75$  has been chosen since it results in good total Q sharing.

### 3.4.4 SYSTEM WITH (LENGTH2 = (LENGTH1)/3, S1=S2)

The new values for power stage for this case are presented in Table 3-15.

**TABLE 3-15** Power system characteristics

	Source1	Source2
Power rating (VA)	1050	1050
Line impedances	$(0.20 + j\omega * 0.00154)*3$	$(0.20 + j\omega * 0.00154)$

The calculated droop parameters are:

$$\rightarrow m_{01} \approx 0.0134 * 1.104 \approx 0.0148 \frac{V}{VAR} \quad (3-36)$$

$$E_{01} = 120 * \sqrt{2} * VDF_1 = 169.7 * 1.104V \approx 187.3V \quad (3-37)$$

$$\rightarrow m_{02} \approx 0.0134 * 1.034 \approx 0.0139 \frac{V}{VAR} \quad (3-38)$$

$$E_{02} = 120 * \sqrt{2} * VDF_1 = 169.7 * 1.034 \approx 175.5V \quad (3-39)$$

$$n_{01} = n_{02} = \frac{\Delta\omega_{max}}{P_{max}} = \frac{1*2\pi}{1050*0.8} \approx 0.0075 \frac{Rad}{S.W} \quad (3-40)$$

$$f_{01} = f_{02} = 60.5Hz \quad (3-41)$$

When  $\alpha = 0.1$ ,  $CF_1=CF_2=1$ , and  $\beta$  changes, the results are shown in Table 3-16.

**TABLE 3-16** Effects of  $\beta$  on system's behavior

$\beta$	Q1 (VAR)	Q2 (VAR)	Q1/Q2	Vload (RMS)	Steady state frequency (Hz)	Ts (s)	Over shoot (%)
<b>0.2</b>	667	608	1.097	118.8	60.4074	0.53	39.2
<b>0.4</b>	650	600	1.083	117.65	60.4091	0.53	39.4
<b>0.8</b>	621	584	1.063	115.48	60.4125	0.54	42.1
<b>1</b>	<b>608</b>	<b>575</b>	<b>1.057</b>	<b>114.46</b>	<b>60.4140</b>	<b>0.52</b>	<b>38.9</b>

As it can be seen in this table and following diagrams, by increment in  $\beta$  (m) there would be decrement in Q1/Q2 and better Q sharing. Also, by increment in  $\beta$ , load voltage decreases; moreover, the steady state frequency increases since the real power decreases.

The influences of  $\beta$  on the system's overshoot percentage, settling time, and Q sharing ratio are shown in the figures 3-24 to 3-26 respectively.

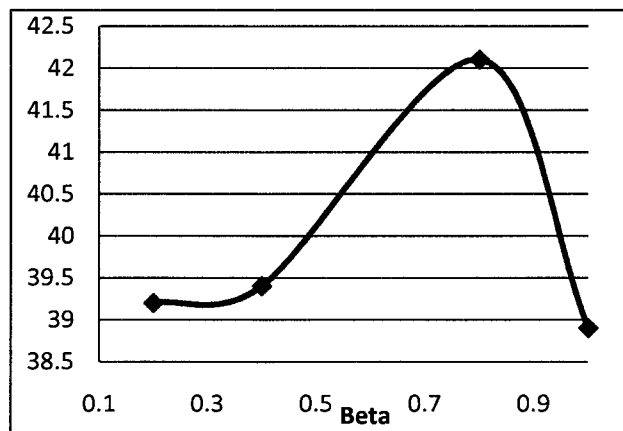


**Fig. 3-24** System's frequency's overshoot percentage as  $\beta$  changes

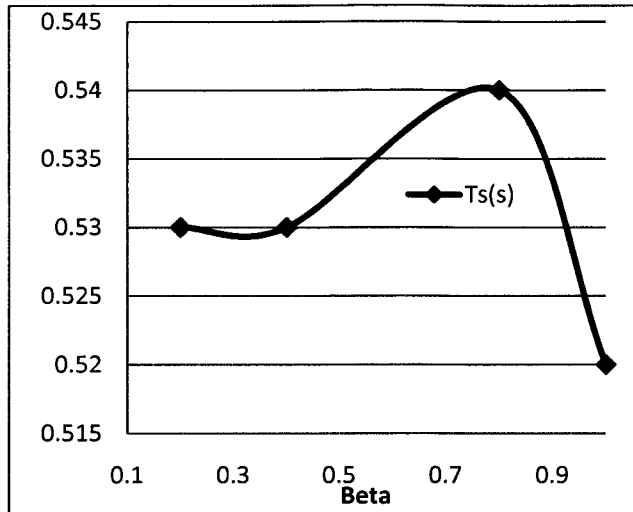


**Fig. 3-25** System's settling time as  $\beta$  changes

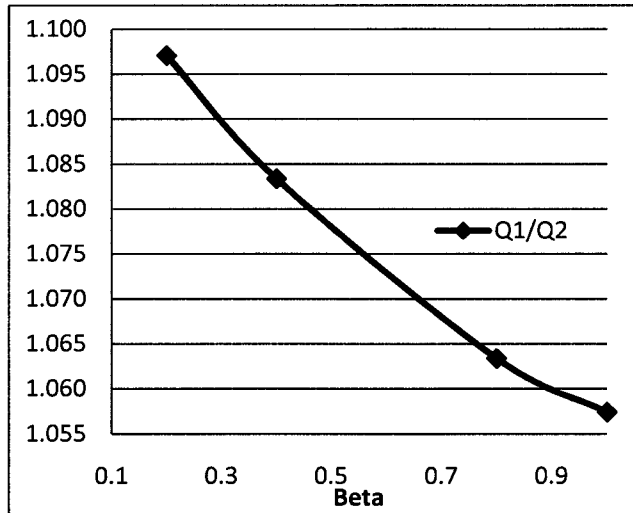


**Fig. 3-26** System's Q sharing ratio as  $\beta$  changes

Note that increment in  $\beta$  (m) has small effects on overshoot and settling time.

According to the results above the  $\beta = 1$  has been chosen which ends to smallest settling time and overshoot and also the best possible Q sharing.

The values of  $\beta$ ,  $CF_1$  and  $CF_2$  are kept constant to 1 and now  $\alpha$  ( $n$ ) is changed to see its effects on system behavior in Table 3-17.

**TABLE 3-17** Effects of changes in  $\alpha$  on system behavior

$\alpha$	Q1 (VAR)	Q2 (VAR)	Q1/Q2	$V_{load}$ (RMS)	Steady state frequency(Hz)	Ts(s)	Over shoot (%)
0.1	608	575	1.057	114.5	60.4140	0.52	38.9
0.15	608	575	1.057	114.5	60.3710	0.45	37.2
0.2	608	575	1.057	114.5	60.3279	0.49	35.9
0.3	608	575	1.057	114.5	60.2415	0.64	34.7
0.5	608	575	1.057	114.5	60.0682	1.8	31.2
0.7	Unstable						

Also the influences of  $\alpha$  on the system's settling time and overshoot percentage are shown in the figures 3-27 and 3-28 respectively.

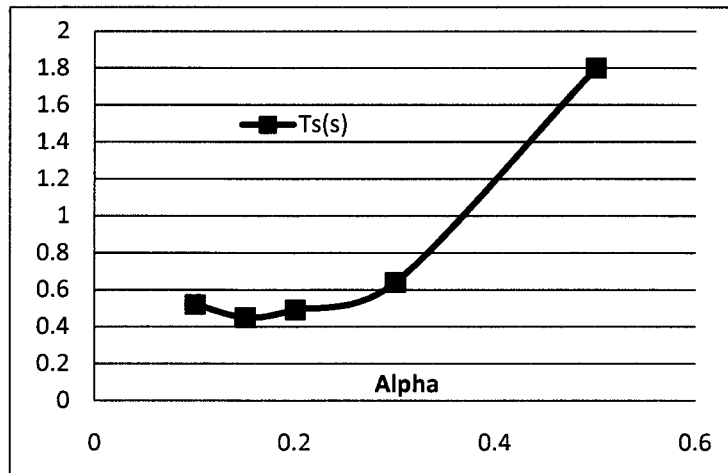


**Fig. 3-27** The influences of  $\alpha$  on the system's settling time

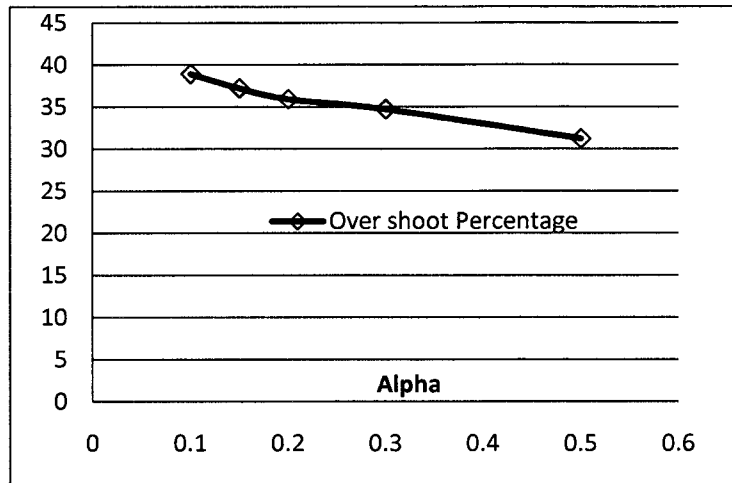


**Fig. 3-28** The influences of  $\alpha$  on the system's overshoot percentage

One can see in figures 3-27 and 3-28 that the trade-off point transient state can be achieved at  $\alpha = 0.15$  with smallest settling time and rather small overshoot. So finally the values of  $\alpha = 0.15$  and  $\beta = 1$  have been chosen as the optimum values.

When one keeps the values of  $\alpha = 0.15$  and  $\beta = 1$ ,  $CF_1 = 1$  constant and varies the values of  $CF_2$ , the following results are obtained in Table 3-18.

**TABLE 3-18** Effects of  $CF_2$  on the system's Q sharing and load voltage

$CF_2$	Q1 (VAR)	Q2 (VAR)	Q1/Q2	Vload (RMS)
0.85	589	603	0.98	114.91
0.9	595	593	1.00	114.78
1	608	575	1.06	114.46

As one can see in this table, by decrement in the  $CF_2$  from 1, the load voltage increases and Q1/Q2 decreases. The value of  $CF_2 = 0.9$  has been chosen since it results in good total Q sharing.



### 3.5 CONCLUSION

In this chapter the effects of different system's parameters on the P & Q sharing were considered. It was seen that by correct control of the sources' voltages' magnitudes, phase angles, and steady state frequency, one can have any desired power sharing. Based on the obtained relations of the sources' voltages' magnitudes and phase angles with sources' powers, the proposed droop strategy was designed.

The proposed droop system includes correction factors which make good Q sharing. This droop system also includes the voltage drop factors to guarantee desired load voltage regulation. The details of droop system design were elaborated and the effects of each droop parameter on system transient and steady state behaviors were evaluated.

The design of the droop system and evaluation of the droop parameters' effects on system's nonlinear behaviors were generalized for different cases of the power system with different ratios of the sources' apparent powers and different ratios of feeders' lengths.

Having compared the relevant figures for different power systems, it was observed that by increment in  $\beta(m)$ , the ratio of  $Q1/Q2$  gets close to  $S1/S2$  in all the cases; also by this increment, the sources' voltages' magnitudes and consequently load voltage magnitude and sources' produced powers decrease. Besides, system's frequency increases. Also as  $\beta$  changes between 0 & 1, it makes rather small changes on system's settling time & overshoot.

For all the cases,  $\alpha(n)$  doesn't have any effect on the sources' voltage's magnitudes and phase angles, and consequently no effect on the load voltage's magnitude and sources' P & Q. But it has huge effect on the system's stability, steady state frequency, speed, and overshoot, which is more than  $\beta(m)$  effects. For all the considered states, by increment in  $\alpha(n)$ , the system's steady state frequency decreases. Besides, for all the cases (except the ideal symmetric one), for small values of  $\alpha(n)$  the settling time doesn't change a lot and after that as  $\alpha$  increases, settling time increases significantly till the system becomes unstable at some point.

Decrement in a correction factor (while the other one is 1), makes its relevant source produce more Q than the other one (with CF=1) to adjust the Q sharing. This decrement in CF value also increases its pertinent source's voltage's magnitude and consequently the load voltages' magnitude and sources' Ps, which makes slight decrement in system's frequency.

As a comprehensive approach to choose droop parameters for any power system, the droop parameters  $m_{0s}, n_{0s}, E_{0s},$  &  $f_{0s}$  should be designed as in (3-3) to (3-10).  $\beta=1$  can be a good choice for all the cases but in the cases similar to the one in subsection 3.4.2 (which have almost equal feeders' impedances but one source larger than the other one), it is better to use  $\beta \approx 0.8$  to make the system faster.  $0.1 \leq \alpha \leq 0.2$  can be used for all the cases to have small oscillations and proper speed. Also, the correction factor of the source which needs to provide more Q should be decreased. The more the  $i$ th source needs to provide  $Q_i$  (Larger  $\frac{S_i}{S_j}$  and/or larger  $\frac{Z_{line_i}}{Z_{line_j}}$ ), the more decrement in  $CF_i$  should be implemented.

## CHAPTER 4

# SYSTEM WITH COMPLETE BENCHMARK AND CONTROL ELEMENTS

---

### 4.1 INTRODUCTION

In this chapter the simulation results for the benchmark model with complete control system are presented. The power stage of the system is a laboratory scale version of a real Canadian system. Compared to the power systems in chapters 2 & 3, the ideal dependent AC power sources (as in Fig. 2-1) have been replaced by DC sources (representing the combination of RES and storage unit), unipolar single-phase ( $1\phi$ ) sinusoidal pulse width modulated (SPWM) inverters which are controlled by the proposed control system, and finally second order LC low pass filters (LPF) for attenuating the switching harmonics.

Also in chapters 2 & 3, the voltage control stage was not included, with the inverters being represented by dependent voltage sources for the sake of simplicity of control system and faster simulations; but in this chapter the voltage control stage is added to the control system to see the effect of that in transient and steady state results.

The steps of the design of power stage and voltage control stage are also explained.

## 4.2 POWER ELEMENTS

The system has the following characteristics.

$S_{load}= 2100VA$  ;  $V_{rated}=120V$  which is used at the low voltage level in North America;

$$I_{rated\_load} = \frac{S_{load}}{V_{rated}} = 17.5 \text{ A} \quad (4-1)$$

The base impedance of the scaled down system is

$$Z_{base-benchmark} = \frac{V_{rated}}{I_{rated\_load}} \approx 6.86\Omega \quad (4-2)$$

In a real system in Canada (information obtained by Natural Resources Canada),  $R_{line}=0.0305 \Omega$ , and  $L_{line}=235\mu H$  (for 100 meters of used feeder1) and  $R_{load}=0.914 \Omega$ ,  $L_{load}=1.816mH$ ,  $PF=0.8$  lagging ; and for this real system  $V_{rated}=240V_{RMS}$  and  $S_{load}=55$  kVA. So that for the mentioned 240 V system implemented in Canada

$$Z_{base-real\ model} = \frac{V_{base}^2}{S_{base}} = 1.047 \text{ ohm} \quad (4-3)$$

So the line and load parameters in the benchmark scaled down (120V) system will be  $R_{line1} = \frac{R_{line2}}{3} = 0.2 \Omega$ , and  $L_{line1} = \frac{L_{line2}}{3} = 1.54mH$ ,  $R_{load}=5.99 \Omega$ ,  $L_{load}=11.9mH$  obtained by using the same per unit line and load values for the two systems. Note that feeder2 is three times longer than feeder1.

In the power system, there are two DC voltage sources (representing the RES and storage unit) which are connected to two PWM unipolar 1 $\phi$  inverters; and the inverters are connected to two LC second order low pass filters (LPFs) on the AC side.

Figure 4.1 shows the power stage of the system. The 3 RL (Resistive-Inductive) elements at the middle of Fig. 4-1 are the same as the ones in Fig. 2-1. The  $E_1$  and  $E_2$  (shown in Fig 2-1) are the outputs of the two LC low pass filters which are connected to two sets of switches on the other ends.

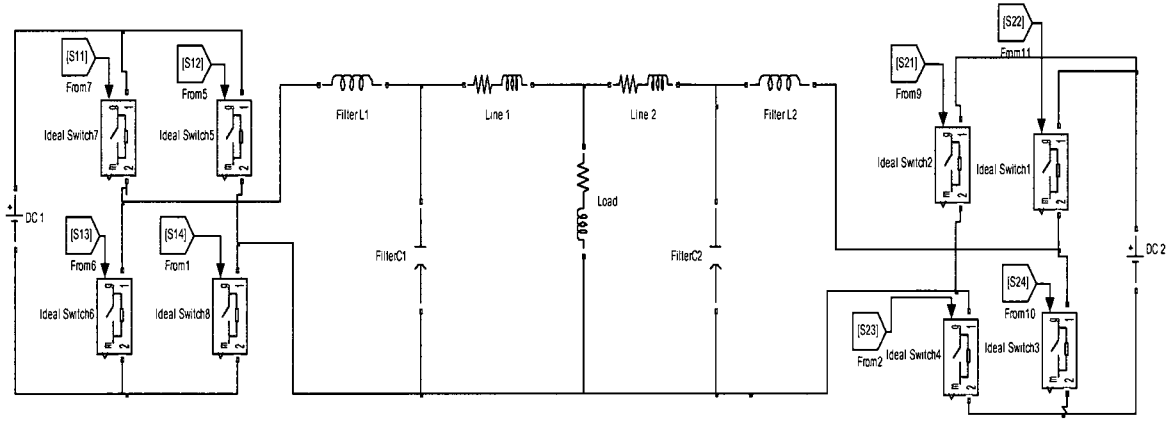


Fig. 4-1 Power stage of the system

The switching frequency is  $f_{sw} = 20$  kHz, and LPF inductor is  $L_{fil} = 2$  mH (with parasitic resistance of  $0.174 \Omega$ ), LPF capacitor is  $C_{fil} = 20$   $\mu$ F (with parasitic resistance of  $0.04 \Omega$ ) which will produce the LPF output voltage transfer function's cut-off frequency of around  $1300$  Hz  $= 6.5\% * f_{sw}$  as it could be seen in Fig. 4-2. The small percentage of  $6.5\%$  assures the small harmonics in the LPFs' output voltages.

Using the equivalent loads mentioned in section 3.2, The LPF<sub>1</sub> output voltage's first (main) harmonic ( $E_{1_{h1}}$ ) transfer function is

$$\frac{E_{1_{h1}}}{V_{ref_{h1}}} = \frac{[(Z_{load_{eq}} + Z_{line1}) || Z_{Cfil}]}{[(Z_{load_{eq}} + Z_{line1}) || Z_{Cfil}] + Z_{Lfil}} (s) = \frac{20 (s + 1.25e006) (s + 480.7)}{(s + 452) (s^2 + 137.2s + 2.696e007)} \quad (4-4)$$

Where  $V_{ref_{h1}}$  is the first (main) harmonic of the inverter reference signal (output of voltage controller for a PWM inverter), and  $Z_{Lfil}$  and  $Z_{Cfil}$  are respectively the LPF's inductor's and capacitor's impedances including their parasitic resistances. The order of this transfer function is three since for an isolated inverter circuit using the equivalent loads (as in Fig. 3-1), only the series combination of equivalent load and line's R & L are considered so that there will be two inductors and one capacitor in each separated power circuit, which are totally three storage elements.

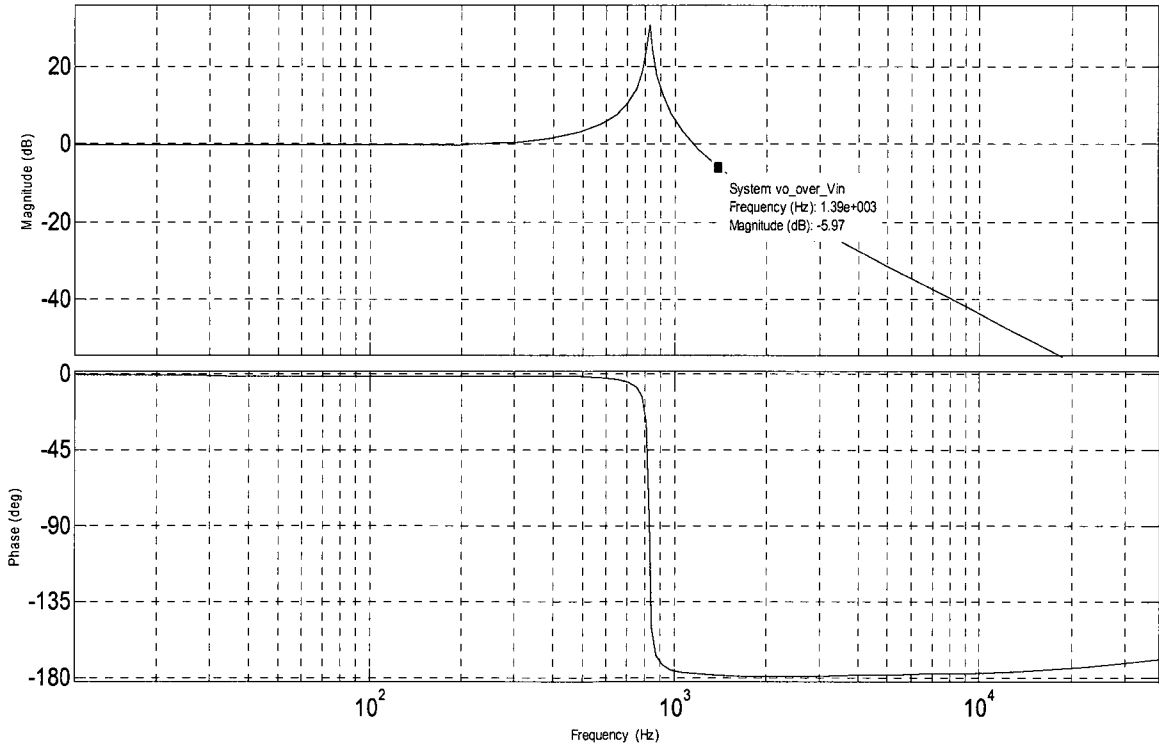


**Fig. 4-2** Magnitude (on top) and phase (at the bottom) of the LPF's output voltage's main harmonic's transfer function

It can be seen in Fig. 4-2 that the power system has a resonant frequency of about 830Hz (the diagram's peak) whose voltage harmonics should be eliminated by correct design of the voltage controller.

### 4.3 CONTROL ELEMENTS

The source1 control system's scheme is shown in Fig. 4-3. The second source control scheme has the same scheme but it has different values for the droop parameters. As it can be seen in this figure, the measured line voltage and current, and system frequency are used to calculate P & Q. The details of the power calculation are addressed in subsection 4.3.5. Droop system uses these calculated P & Q to make the required amount of voltage magnitude and frequency for the source voltage reference. Then the output of the voltage controller goes to the gating system to be commanded to the inverter. Details of the gating system follow.

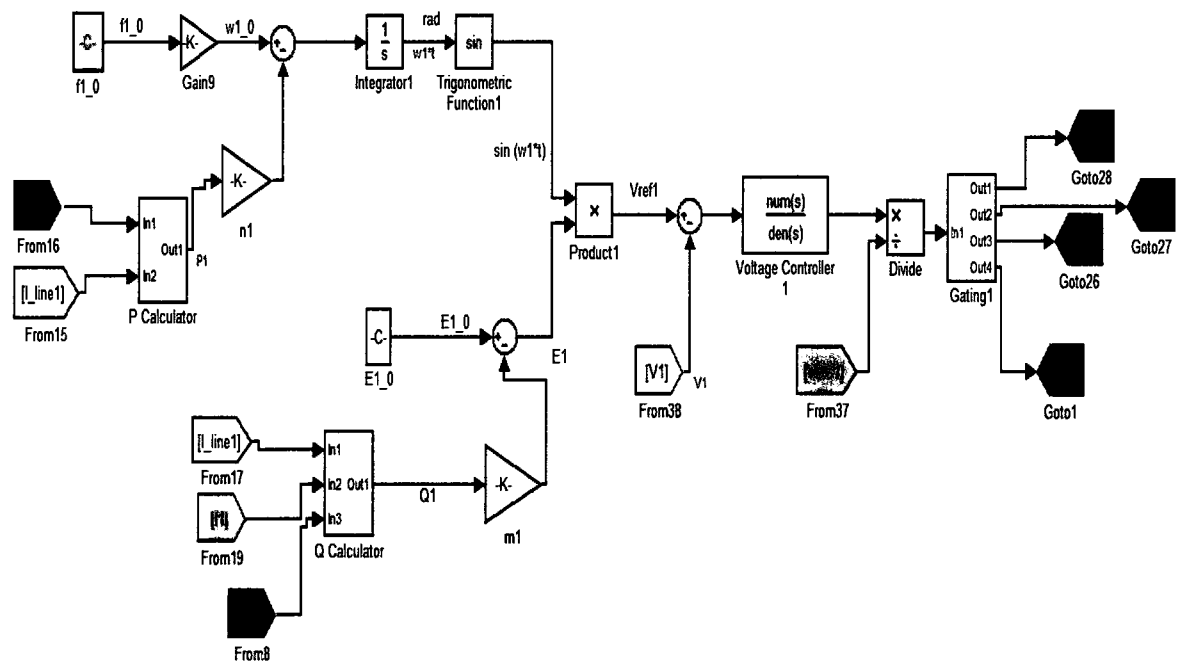


Fig. 4-3 Schematic diagram of control system

### 4.3.1 GATING SYSTEM

Gating system uses 20kHz sawtooth waveform to be compared to the control signal (In1 of the gating1 box in Fig. 4-3) to make unipolar gating signals of the inverter (4 outputs of gating1 box). This circuit first receives the output of the voltage controller; then it divides that by the source voltage ( $V_{DC1}$  in Fig. 4-3) to generate the control signals. This division makes the inverters capable of working with variable DC bus voltages as they have always the constant ratio of 1 between their fundamental components of reference voltages and the their output voltages by proper selection of  $K_{PWM}$  which is equal to  $\frac{1}{V_{DC}}$  (division of the voltage controller's output by  $V_{DC}$ ).

$$\left(\frac{V_{out_{h1}}}{V_{ref}} = \frac{V_{DC}}{V_{st}} * K_{PWM} = 1\right) \quad (4-5)$$

where  $V_{DC}$ ,  $V_{st}$ , &  $K_{PWM}$  are respectively the DC bus voltage, maximum saw tooth waveform magnitude (= 1), and PWM gating gain. Notice that the variations in  $V_{DC}$  should be much slower than sawtooth variations (20kHz) to have good modulation and small harmonics in the power system's sources' voltages. Also  $V_{DC}$  should be greater than the peak of the reference voltage of inverters all the time; otherwise there will be some low order harmonics in the system's sources' voltages or even instability due to overmodulation in the inverters.

### 4.3.2 CURRENT LOOP

A controller can be used which facilitates the design of voltage controller. The current controller would be used when it is hard to design the voltage controller directly. In such a case the current loop is used as the inner loop and the reference current is the

output of voltage controller. The current controller should be about 10 times faster than voltage controller as in basic cascaded control loops scheme.

In the simulations in this chapter, the current controller is not useful because it is not necessary to be included since one can design the voltage controller directly. In this case the control system would be simpler and cheaper too. This current controller elimination has been done in some publications such as [19, 22].

### **4.3.3 VOLTAGE LOOP**

A PR controller [23] is used to have sinusoidal voltage waveforms with very small distortions and zero error in the steady state, following a step variation. A proportional resonant (PR) controller such as the one in (4-6) consists of two conjugate purely imaginary roots (though it might include some other poles in the left hand side of the s-plane). Also the order its numerator should be equal or less than that of the denominator. The purely imaginary conjugate roots are to amplify the desired frequency of the reference signal. The other details are explained in the coming subsection.

#### **4.3.3.1 DESIGN OF THE VOLTAGE CONTROLLER**

The Bode diagram and root and zero loci of the voltage loop transfer function (VLTF) (product of the LPF output voltage and voltage controller transfer functions), and the Bode diagrams of the closed voltage loop transfer function (CVLTF) are shown in Fig. 4-3. The open loop transfer function was presented in (4-4).

The voltage controller needs two imaginary roots ( $S = \pm j377$ ) on 60Hz to make a huge amplification of the main frequency of the reference voltage in that region around 60Hz, and attenuate the effect of the power system's internal resonance at around 830 Hz dramatically. PI controller can't do this great attenuation since it has limited gain around 60Hz.

Controller's three zeros are chosen to make appropriate PM for VLTF, and the phase margin (PM) is designed to be  $43 \approx 100 \times$  damping factor [24].

As it can be seen in Fig. 4-4, the real controller's root ( $s = -14610$ ) makes a slope between  $-40 \frac{\text{dB}}{\text{dec}}$  and  $-20 \frac{\text{dB}}{\text{dec}}$  at high frequencies (around switching frequency and its multiples) in the VLTF and consequently CVLTF to help attenuating the switching's high frequency harmonics. The gain is adjusted to make a proper open loop transfer function cut-off frequency of  $1280\text{Hz} = 6.4\% * f_{\text{sw}}$  (consequently low cut-off frequency of around  $2500\text{kHz} = 12.5\% * f_{\text{sw}}$  in the CVLTF) which helps the appropriate attenuation of switching's high frequency harmonics in the LPF's output voltages too.

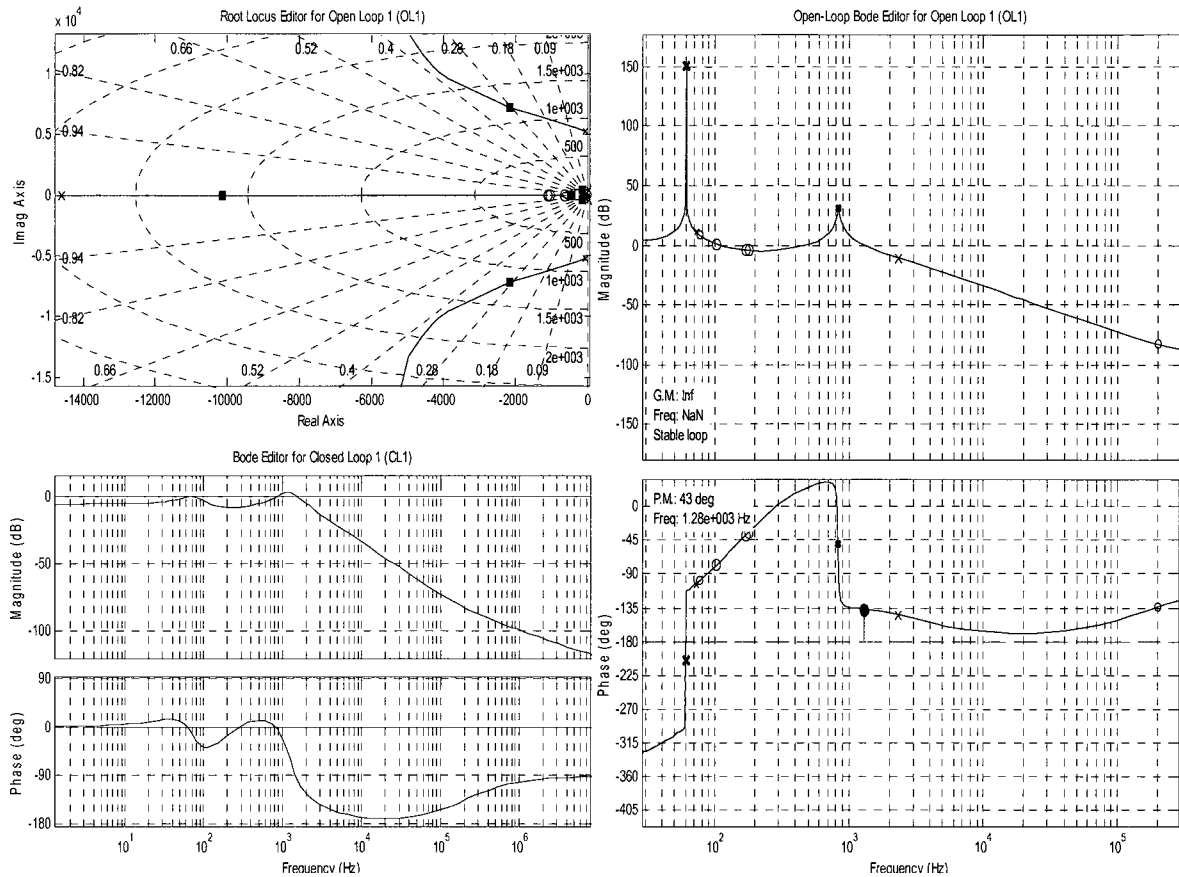


**Fig. 4-4** Voltage open and closed loop control systems characteristics

So finally the PR controller transfer function is achieved:

$$C_v(s) = \frac{3.0676 (s+1058) (s+1118) (s+639.7)}{(s+14610) (s^2 + 142100)} \quad (4-6)$$

The two sources' references and real voltages' waveforms can be seen in Fig. 4-5. The  $V_{ref2}$  has been increased from  $96V_{RMS}$  to  $120V_{RMS}$  at the time  $t=0.04s$ . It can be seen in this figure that there are very small harmonics in the system steady state voltages, and also the voltage controller can restore the desired voltage fast after the change its reference signal. The settling time for the voltage loop is about 15ms which shows a very proper speed.

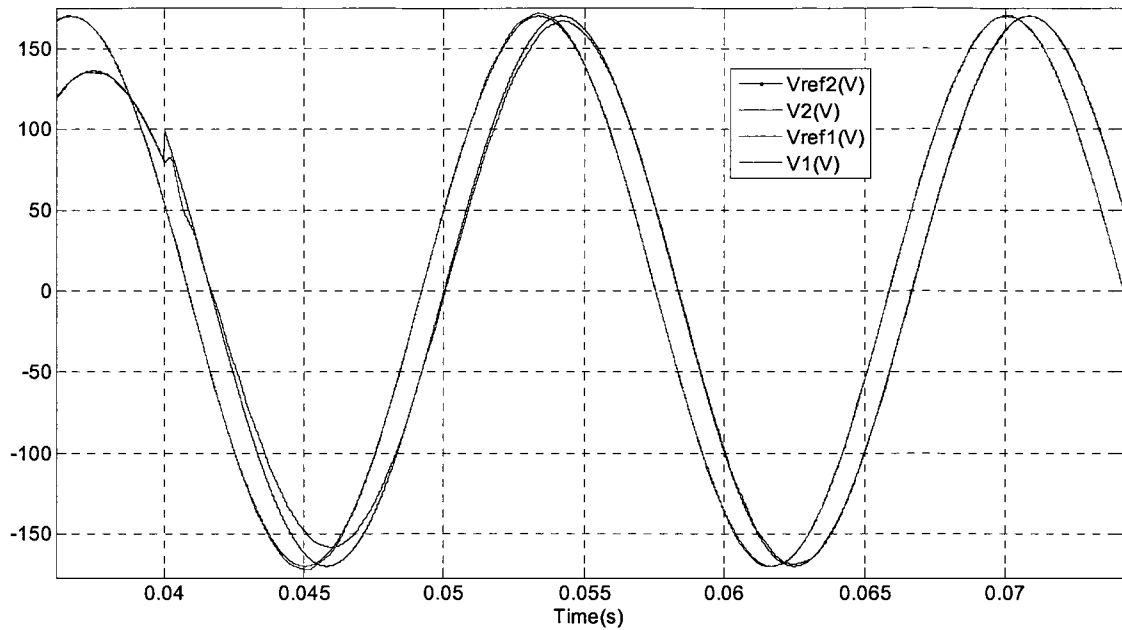


**Fig. 4-5** Sources' reference and actual voltages before and after a change in  $V_{ref1}$

Figure 4-6 shows the difference between the reference and real voltages (voltage ripple (error)), before and after the change in  $V_{ref2}$ . The maximum momentary steady state voltage ripple is 1.4V which is 0.8% of nominal peak voltage. This small value shows the desired accuracy of the voltage controller. This ripple can be reduced by decreasing the simulation step size since a portion of the error is due to the simulation software calculations approximations in each time step.

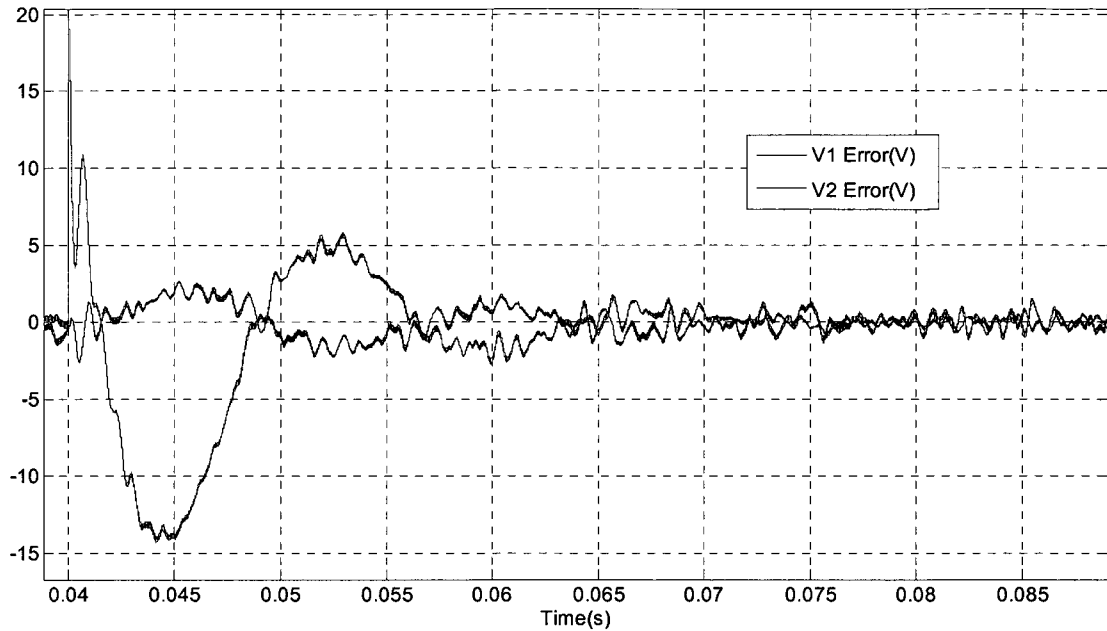


**Fig. 4-6** Sources' output voltages' ripple (V2 ripple (error) has more initial variations)

#### **4.3.4 DROOP LOOP**

The droop system makes the reference of the voltage controller using the measured P and Q and also droop parameters. The values of the droop parameters are the same as ones used in section 3.2. The detailed design of the droop loops is also elaborated in that section.

#### **4.3.5 POWER CALCULATORS**

Figure 4-7 shows the scheme of a P calculator. The Q calculator unit is the same as P calculator except  $I_{in1}$  which is shifted by  $90^\circ$  [18]. The product of the inverter's output voltage and current has the DC desired value and a harmonic around 120Hz which should be attenuated by control system's LPFs. That's why two second order LPFs with the cut-off frequency of 20Hz have been used in the power calculator units. If the cut-off frequency of the control LPFs decreases, the system will be slower to respond to changes

in load (as in [18]), but there will be less ripple in the system steady state voltages' magnitudes and frequency, and also measured Ps & Qs. In the other hand these LPFs are the slowest units in the whole control system, so the solution would be two LPFs in series with a rather high cut-off frequency such as 20Hz which maintains good system speed and control stage simplicity while they attenuate the harmonics of around 120Hz sufficiently.

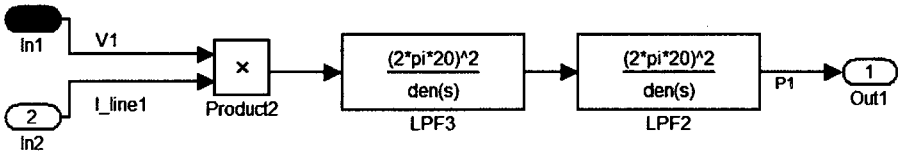


**Fig. 4-7 Active Power Calculator**

**4.4 SIMULATION RESULTS FOR THE COMPLETE SYSTEM**

By changing the control system in section 4.3.3, the reference voltage is now put to be the output of the droop system. The power system feeders, and droop system in section 3.3 are the same as the ones in the all the simulations in this section.

Note that because of the complexity of the complete system, high switching frequency, required rather long simulation time, and limitations of RAM and CPU of the available computers, one has been forced to use PSIM instead of SIMULINK for this step of the simulation which makes almost no change in the results.

### 4.4.1 TWO SOURCES WITH A LINEAR LOAD WHICH CHANGES

In the following simulations, the linear load (the same as the one used in section 3.3) has decreased by 20% at the time  $t=0.6s$ . Fig 4-8 shows the steady state system's results before the load change.

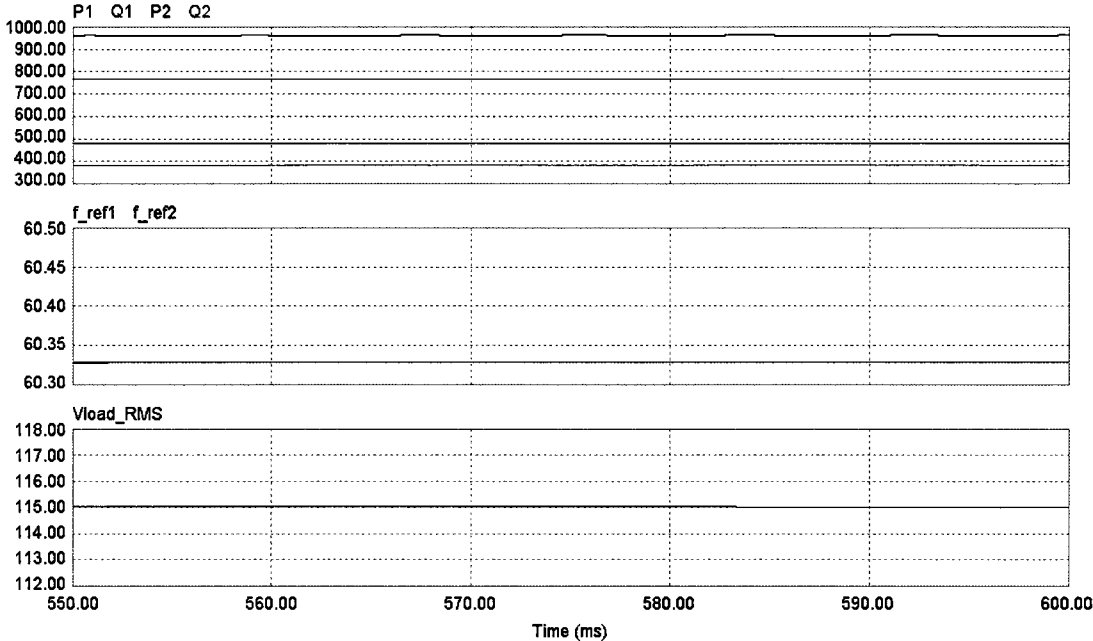


**Figure 4-8** Steady state system results before the load's change (for the graph on top, the order of the waveforms from the top to the bottom: P1, Q1, P2, Q2)

The values of the power system parameters measures taken in steady state before the load's change (at  $t=0.596s$ ) are shown on Table 4-1 which demonstrate system's appropriate P & Q sharing, and frequency and load voltage regulation.

**Table 4-1** Power system's steady state parameters' values

Time	0.596s
P1	961W
P2	480W
P1/P2	2.00
Q1	768 VAR
Q2	385VAR
Q1/Q2	1.99
System Frequency	60.3Hz
RMS Load Voltage	115.0V

The transient waveforms after the 20% load decrement are shown in Fig. 4-9. According to the waveforms in this figure, settling time is 0.48s and the frequency overshoot is 9.2% which show system's proper speed and transient response.

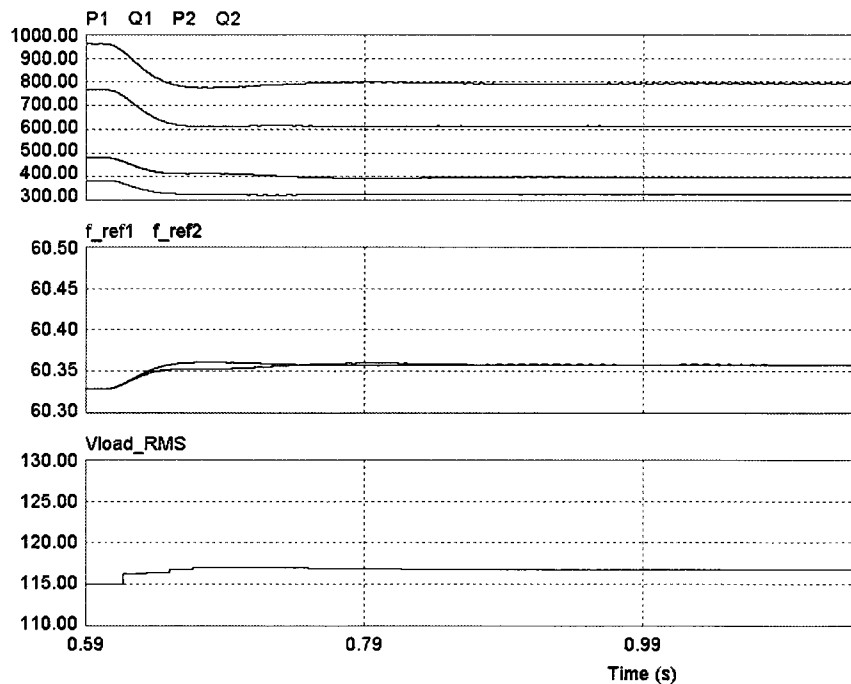


**Figure 4-9** System's transient behavior after the 20% load decrement (for the graph on top, waveforms from the top to the bottom: P1, Q1, P2, Q2), (for the graph at the middle:

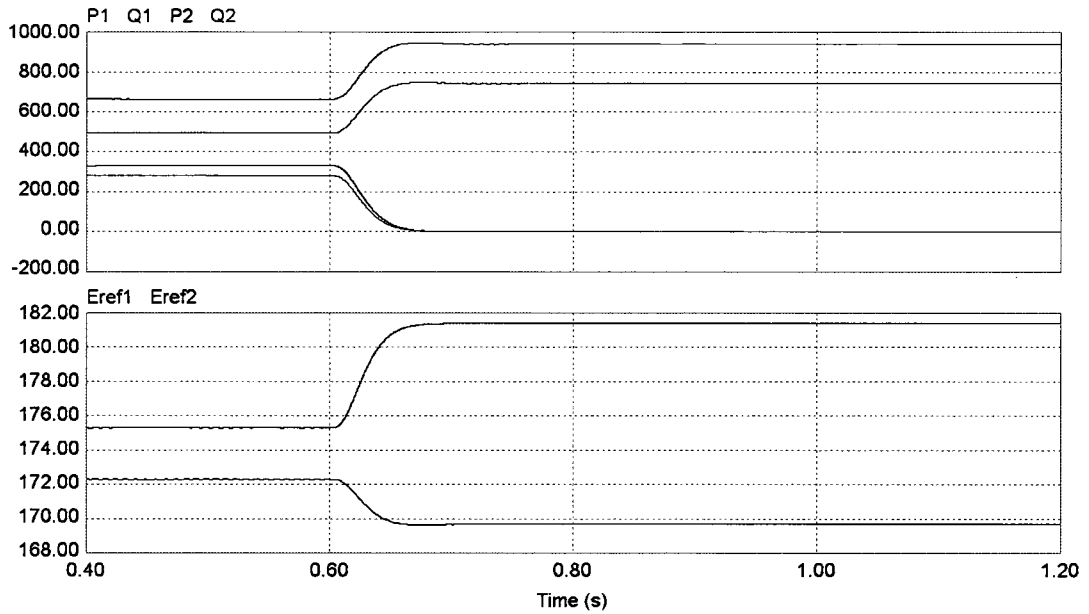
$f_{ref1}$  has overshoot and  $f_{ref2}$  has undershoot at the beginning)

Steady state and transient results are close to the ones obtained in section 3.3 (without voltage controller or LPFs and with ideal sources) since they have the same main power and control parameters. The very slight difference is due to the difference in switches' models and the simulation calculations procedure in SIMULINK and PSIM, and also addition of the voltage control stage to the control system.

#### **4.4.2 DISCONNECTION OF ONE SOURCE FROM THE NETWORK**

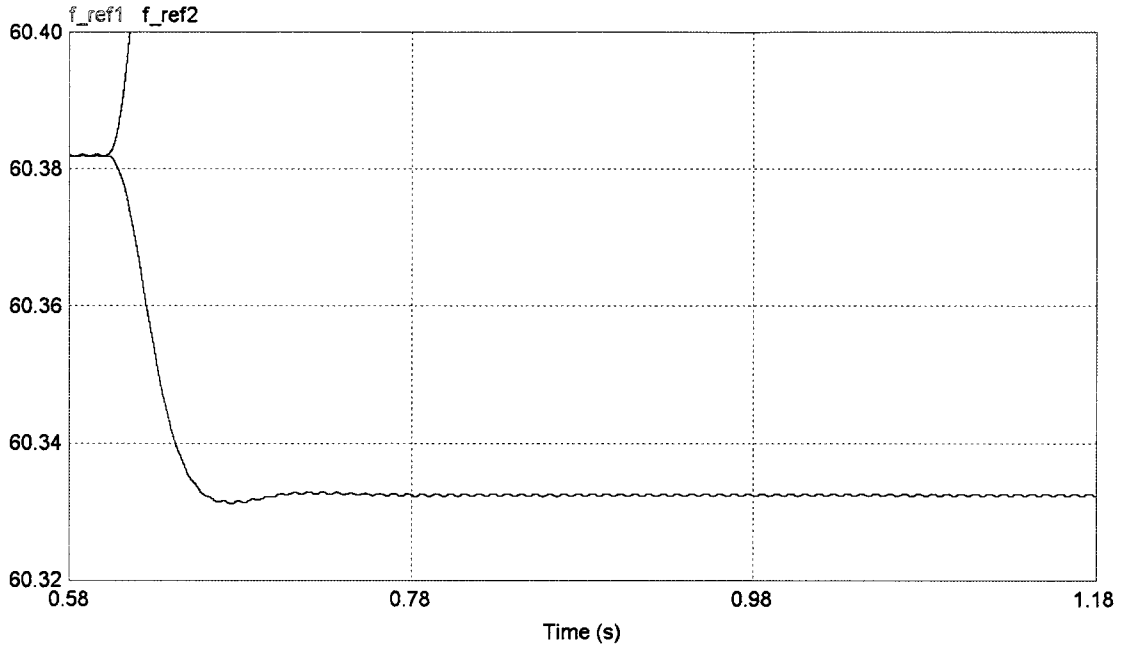
Now the joint load is 65% full load compared to the initial load in the previous subsection. (i.e.  $R_{load} = \frac{5.99}{0.65} \Omega$ ,  $L_{load} = \frac{11.9}{0.65} \text{ mH}$ ) at the beginning and then at  $t = 0.6 \text{ s}$  the second source goes out of the network (e.g. because of the operation of circuit breakers as a result of a short circuit in the sources' terminals). Also notice that the other control and power system's elements have been kept constant to the previous subsection's values.

Fig. 4-10 shows the system's power and sources' voltage's peaks before and after the disconnection of source2 from the network. Since the load is small enough, the first source can deliver the whole power to the load without exceeding the nominal powers (current) after the disconnection of the source2.



**Fig. 4-10** System's powers (on top) and sources' voltage's peaks (at the bottom) before and after the disconnection of source2 from the network (for the graph on top, waveforms from the top to the bottom: P1, Q1, P2, Q2), (the graph at the middle: Eref1 is lower than Eref2)

Also since the droop parameters are designed correctly, the first source frequency would remain in the allowable range (59.5 Hz to 60.5Hz) after the other sources' disconnection as it can be seen in Fig 4-11. Also note that since source 2 has been disconnected, its post disconnection ( $t > 0.6$ ) frequency value should be disregarded.



**Fig. 4-11** System's sources' frequencies

Sinusoidal wave forms of the sources' output voltages and load voltage and also feeders' currents can be observed on Fig. 4-12.

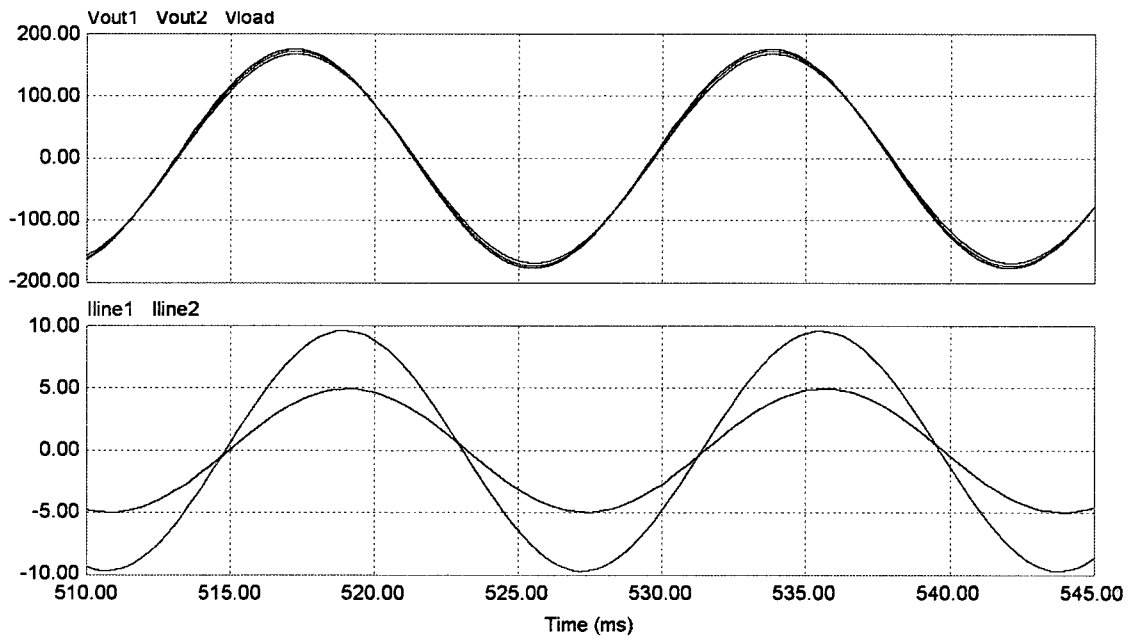


**Fig. 4-12** Sources' output voltages and load voltage (on top) and also feeders' currents (at the bottom) ( $|I_{line1}| > |I_{line2}|$ )

The variations of the peak value of the load voltage can be seen in Fig. 4-13. It can be observed in this figure that since the load is small enough, and the droop parameters are designed correctly, the load voltage's peak remains in the desired range (161.2V to 178.2V) after the disconnection of the other source.

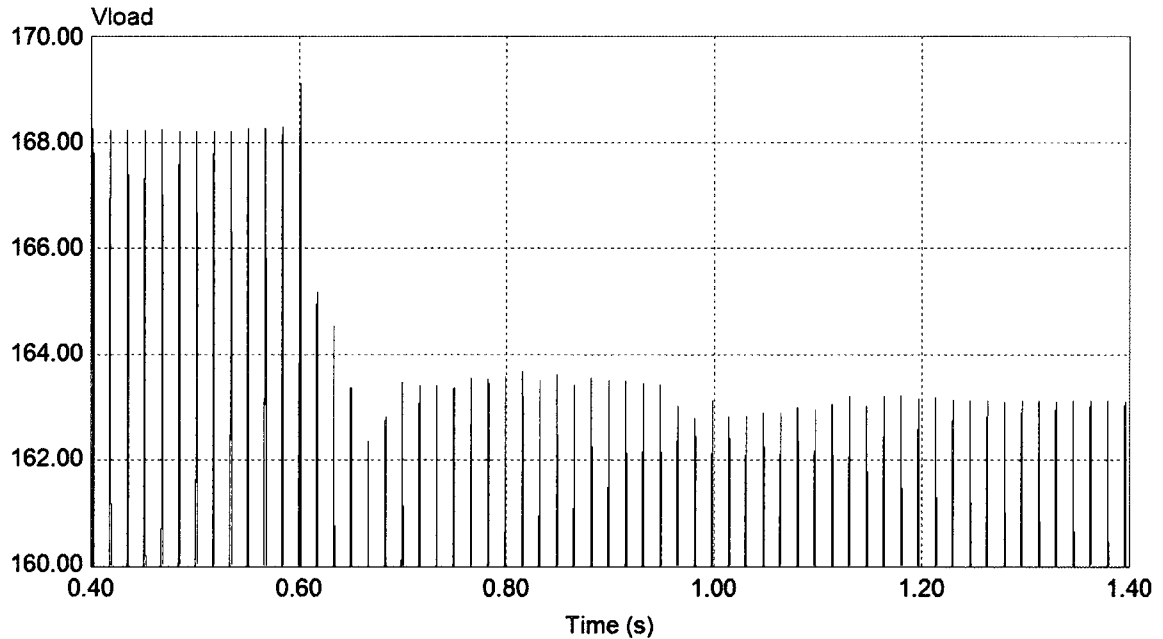


**Fig. 4-13** The variations of the peak value of the load voltage

### **4.4.3 SYSTEM WITH A RESISTIVE-INDUCTIVE (RL) NONLINEAR LOAD**

The system has the same system's parameters as the ones in section 4.4.1 except the load, which consists of a linear portion which is 80% of the initial load in 4.4.1; and a nonlinear load (20% of the initial load in 4.4.1) which is connected to the linear load through a full diode bridge).

Fig. 4-14 shows the load and feeders' currents and also sources' output voltages as well as the load voltage. It can be seen that since the load has a nonlinear portion, the feeder's currents and the load voltage have some harmonics (the load voltage is zero during the current commutation period [25]). Consequently the nonlinear load even makes some small harmonics in the linear load's current and in the sources' output voltages after the LPFs. But the control system is still capable of controlling the system's voltage and stability and the sources share the load current.

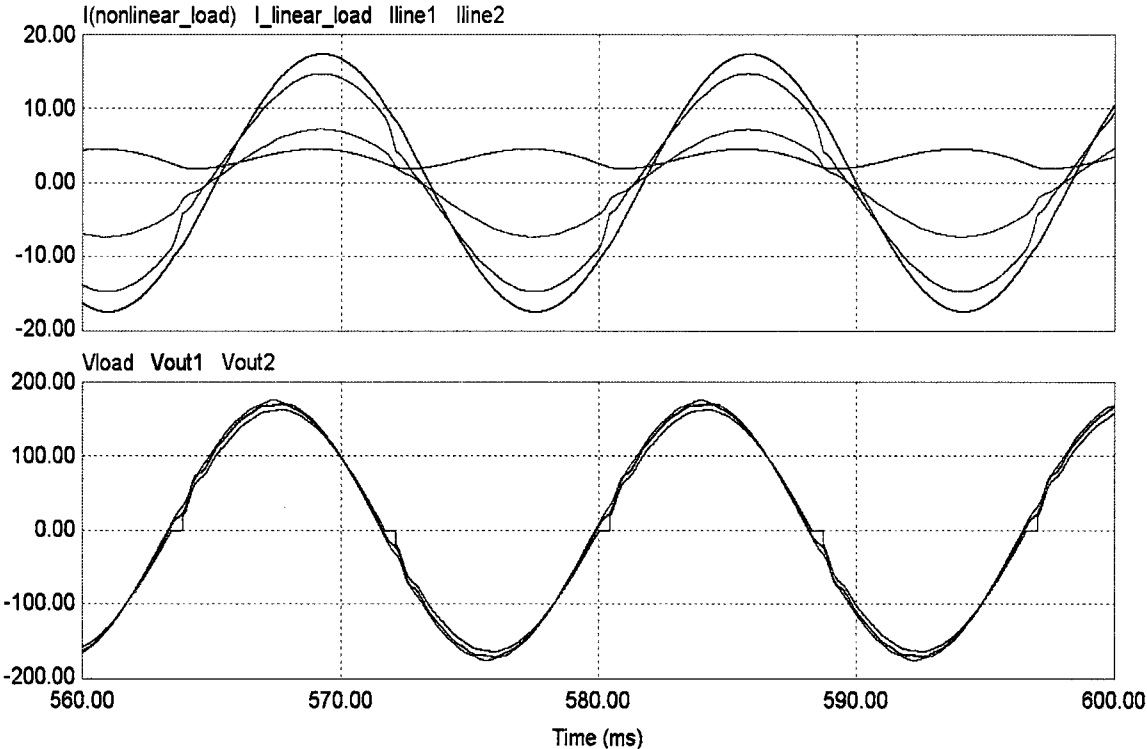


**Fig. 4-14** Load and feeders' currents (on top) and also sources output and load voltages (at the bottom)

## 4.5 CONCLUSION

The system in this chapter has been a more complete version of those used in chapters 2 & 3. That means, the DC sources, power stage LPFs, voltage controllers, and gating systems have been added to the system.

The control system and its different stages were discussed. Also the design of the LPFs, voltage controllers, active and reactive power calculators, and gating systems' elements were addressed. The proper accuracy of the PR voltage controllers was shown.

The simulation results for the benchmark with more complete control stage (after addition of voltage controller stage) were presented for a system with same load, feeder, and droop elements as in section 3.3. It was observed that those results were close to those of the simpler system in section 3.3.

Finally, the simulations have been performed for the case when one source is disconnected from the network, and also for the cases when the power system has a resistive-inductive nonlinear load. It was observed the control system is capable of controlling the system in all mentioned cases.

# CHAPTER 5

## CONCLUSION

---

### 5.1 SUMMARY

This thesis proposes a new droop system for very proper power sharing between some energy sources which are integrated in a low voltage isolated microgrid. This droop system also provides desired load voltage regulation for such an integrated system. The system uses its frequency as the intercommunication signal so that there is not any intercommunication cable cost or any problem with the electromagnetic interference with the intercommunicating signal.

Proper P sharing has been achieved by making the frequency of each inverter dependent on its measured P; appropriate Q sharing has been achieved by using new parameters called “Correction Factors” inserted in the calculations of the droop parameters “ms”; and desired load voltage regulation has been obtained by inserting the “Voltage Drop Factors” into the calculations of the droop parameters “ms” and “E<sub>0s</sub>.” The last two features are the main advantages of the proposed droop scheme over the basic conventional one.

Also for the first time, the exact effects of the sources’ voltages’ characteristics (i.e. their magnitudes, phase angles, and frequency) on the system active and reactive powers flows have been elaborated by means of 3 dimensional graphs, which finally explain the way the droop equations are derived from these power relationships. So the

droop system is designed in a way to make negative feedbacks for the power system to help the system stability.

Then, the optimum droop coefficients ( $m_s$  and  $n_s$ ) were obtained by defining the new parameters ( $\alpha$ ,  $\beta$ ,  $V_{DF1}$ ,  $V_{DF2}$ ,  $CF_1$ ,  $CF_2$ ) and adding them to the basic ones ( $m_s$ ,  $n_s$ ,  $f_{0s}$ , and  $E_{0s}$ ) and verification of their effects on the system's steady state behavior (i.e. reactive power sharing ratio, load voltage, and system frequency magnitudes), system's transient behavior (i.e. overshoot, settling time), and system's stability.

The correction factors make good Q sharing and the voltage drop factors are used to guarantee desired load voltage regulation.

The design of the droop system and evaluation of the droop parameters' effects on system's nonlinear behaviors were generalized for different cases of the power system with different ratios of the sources' apparent powers and different ratios of feeders' lengths.

Having compared the relevant figures for different power systems, it was observed that by increment in  $\beta(m)$ , the ratio of  $Q_1/Q_2$  gets close to  $S_1/S_2$  in all the cases; Also as  $\beta$  changes between 0 & 1, it makes rather small changes on system's settling time & overshoot.

For all the cases,  $\alpha(n)$  doesn't have any effect on the load voltage's magnitude and sources' P & Q. But it has huge effect on the system's stability, steady state, speed, and overshoot, which is more than  $\beta(m)$  effects. For all the cases, (except the ideal symmetric one), for small values of  $\alpha(n)$  the settling time doesn't change a lot; and after that, as  $\alpha$  increases, settling time increases significantly till the system becomes unstable at some point.

Decrement in a correction factor (while the other one is 1), makes its relevant source produce more Q than the other one (with CF=1) to adjust the Q sharing.

As a comprehensive approach to choose droop parameters for any power system, the droop parameters ( $m_0s, n_0s, V_{DFS}, E_0s, \& f_0s$ ) should be designed as in (3-3) to (3-10).  $\beta=1$  can be a good choice for all the cases but in the cases similar to the one in subsection 3.4.2 (which have almost equal feeders' impedances but one source larger than the other one), it's better to use  $\beta \approx 0.8$  to make the system faster.  $0.1 \leq \alpha \leq 0.2$  can be used for all the cases to have small oscillations and proper speed. Also, the correction factor of the source which needs to provide more Q, should be decreased. The more the  $i$ th source needs to provide  $Q_i$  (Larger  $\frac{S_i}{S_j}$  and/or larger  $\frac{Z_{line_i}}{Z_{line_j}}$ ), the more decrement in  $CF_i$  should be applied.

In the inner part of control system, the current loop was eliminated to make the system faster and simpler. Besides, the design of a proportional resonant voltage controller was addressed. This controller results in a smaller voltage's steady state error compared to PI type controllers. Besides, this controller can attenuate switching frequency multiples harmonics and specially the power stage internal resonant frequency harmonic very well.